

# Bridging Microscopic Constructions and Continuum Topological Field Theory of Three-Dimensional Non-Abelian Topological Order

Yizhou Huang<sup>1, \*</sup>, Zhi-Feng Zhang<sup>1, \*</sup>, Qing-Rui Wang<sup>3, †</sup> and Peng Ye<sup>1, ‡</sup>

<sup>1</sup>Guangdong Provincial Key Laboratory of Magnetoelectric Physics and Devices,  
State Key Laboratory of Optoelectronic Materials and Technologies,  
and School of Physics, Sun Yat-sen University, Guangzhou, 510275, China

<sup>2</sup>Max Planck Institute for the Physics of Complex Systems, Nöthnitzer Straße 38, Dresden 01187, Germany

<sup>3</sup>Yau Mathematical Sciences Center, Tsinghua University, Haidian, Beijing, China

(Dated: Thursday 25<sup>th</sup> December, 2025)

Topological orders in three and higher spatial dimensions host spatially extended topological excitations, such as loops, whose fusion and shrinking processes encode essential topological data beyond those of two-dimensional anyon systems. Recent advances based on twisted  $BF$ -type topological field theories have established a unified continuum field-theoretical framework for the topological data of three-dimensional topological orders, including braiding, fusion, and shrinking, together with diagrammatic representations and stringent consistency relations required for anomaly-free topological orders. However, an explicit microscopic construction of these field-theoretical principles has remained an open challenge, and it has been unclear whether the diagrammatic representations and consistency relations derived in continuum field theories remain valid and complete in microscopic lattice models. Here we provide a microscopic lattice construction of excitations, fusion, and shrinking in a non-Abelian topological order by studying the three-dimensional quantum double model. We explicitly construct lattice operators that create, fuse, and shrink particle and loop excitations, systematically derive their fusion and shrinking rules, and demonstrate that non-Abelian shrinking channels can be controllably selected through internal degrees of freedom of loop operators. Most importantly, we show that the lattice shrinking rules obey the fusion–shrinking consistency relations predicted by twisted  $BF$  field theory, providing solid evidence for the validity of field-theoretical principles developed over the past years. In particular, we compute the full set of excitations, fusion, and shrinking data at the microscopic lattice level and verify exact agreement between the microscopic  $\mathbb{D}_4$  quantum double lattice model and the continuum  $BF$  field theory with an  $AAB$  twist and  $(\mathbb{Z}_2)^3$  gauge group, thereby placing the latter field theory, originally discovered in 2018 in connection with Borromean-ring braiding, on a solid microscopic footing. Our results bridge continuum topological field theory and exactly solvable lattice models, elevate fusion–shrinking consistency from a continuum field-theoretical principle to a genuine topological phenomenon defined at the microscopic lattice scale, and provide a concrete microscopic foundation for experimentally engineering higher-dimensional non-Abelian topological orders in controllable quantum simulators, such as trapped-ion systems.

## CONTENTS

I. Introduction	2	C. Example of non-Abelian fusion rules	16
II. Field-theoretical consistency conditions and diagrammatics of fusion and shrinking rules	4	V. Shrinking rules and fusion-shrinking consistency	16
A. Consistent fusion and shrinking rules	4	A. General consideration	16
B. Diagrammatics	6	B. Example of Abelian shrinking rules	19
III. Excitation creation	7	C. Example of non-Abelian shrinking rules	19
A. Hamiltonian on a lattice	8	D. Controlling non-Abelian shrinking channels	21
B. Particle excitations	10	E. Microscopic verification of consistency relations between fusion and shrinking	22
C. Loop excitations	11	VI. Microscopic construction of the $BF$ field theory with an $AAB$ twist	22
IV. Fusion rules	14	A. Overview	22
A. General consideration	14	B. Microscopic construction	23
B. Example of Abelian fusion rules	15	C. $BF$ field theory with $AAB$ twisted term as a Borromean-Rings topological order	26
		D. Matching between microscopic construction and continuum field theory	27
* These authors contributed equally.		VII. Summary and outlook	27
† wangqr@mail.tsinghua.edu.cn		A. Summary	27
‡ yepeng5@mail.sysu.edu.cn			

\* These authors contributed equally.

† wangqr@mail.tsinghua.edu.cn

‡ yepeng5@mail.sysu.edu.cn

B. Outlook	28
Acknowledgments	29
A. Diagrammatics, pentagon and hexagon equations	29
B. Details about basic operators	31
1. Proof of Eq. (37)	31
2. Proof of Eqs. (38), (39) and (40)	32
3. Proof of Eqs. (46), (47) and (48)	33
4. Proof of Eq. (49)	33
5. The commutation relations between $B_p$ and $L_M^c$	33
6. The commutation relations between $A_v$ and $L_M^c$	34
7. Proof of Eqs. (61), (62), (63) and (64)	34
C. Irreducible Representations of Quantum Double	36
References	37

## I. INTRODUCTION

Since the discovery of the fractional quantum Hall effect, 2d<sup>1</sup> topological phases of matter characterized by long-range entanglement [1] have attracted sustained attention over the past few decades. A salient property of 2d topological orders is the existence of point-like topological excitations—anyons—whose fusion rules and braiding statistics are central to topological quantum computation. A quantum computer must both encode information and implement gates. A canonical example of robust quantum information storage is the toric code [2], whose ground-state degeneracy encodes quantum information. However, being Abelian, the toric code supports only phase braiding, which is insufficient for universal quantum computation without auxiliary modules such as magic-state injection [3], lattice surgery [4, 5], or extrinsic defects [6, 7]. In contrast, non-Abelian anyons carry internal degrees of freedom; braiding operations act as noncommuting unitary transformations on the associated Hilbert spaces. Information encoded in these spaces can be manipulated by braiding, and certain non-Abelian theories (e.g., Fibonacci anyons) already support universal quantum computation without additional resources. So far, topological data of 2d topological orders—such as fusion rules and braiding statistics—have been systematically developed within category theory [8], Chern-Simons

field theory—a typical type of topological quantum field theory (TQFT) [9–13], and exactly solvable lattice models [2, 14–16].

In higher dimensions the landscape broadens substantially: in 3d topological orders and beyond, point particles are restricted to bosons or fermions [17], while topological excitations generically include spatially extended objects such as loops. A powerful field-theoretical framework for 3d topological orders is provided by untwisted and twisted (3+1)D *BF* theories, which also capture gauged symmetry-protected-topological (SPT) responses [18–28]. The action contains a *BF* term,  $BdA$  with  $B$  a 2-form and  $A$  a 1-form gauge field, plus twisted terms such as  $AAAdA$ ,  $AAAA$ ,  $AAB$ ,  $dAdA$ , and  $BB$ . These terms give rise to a rich variety of higher-dimensional topological phenomena, including particle-loop braiding [29–33], multi-loop braiding [21, 34–42], particle-loop-loop Borromean-rings braiding [25], emergent fermionic statistics [22, 27, 43, 44], and nontrivial topological responses [18, 20, 28, 45–49]. Within the field-theoretical framework, fractionalization of global symmetry on loop excitations has been analyzed in Refs. [50–52], where mixed three-loop braiding formed by external symmetry fluxes and internal loop excitations (i.e., dynamical gauge fluxes) plays a key role in classifying higher-dimensional SET (symmetry-enriched topological) phases. Not all braiding processes coexist: certain combinations of twisted terms violate gauge invariance. By excluding such terms, Ref. [26] enumerates all legitimate combinations of braiding processes.

Beyond braiding, twisted *BF* theories reveal a new class of topological data absent in 2d topological orders, namely *shrinking rules*, which describe how spatially extended excitations can continuously contract into lower-dimensional ones. Given an  $n$ -dimensional excitation, one may shrink it to several  $k$ -dimensional excitations with  $k < n$ . For instance, a loop in 3d topological order can shrink to a point which is a particle excitation. In our previous work [53], such shrinking processes were systematically analyzed within (3+1)D twisted *BF* theories, demonstrating that certain twisted terms can induce non-Abelian fusion and shrinking rules even for Abelian gauge groups.

Lifting to 4d topological order, topological excitations include particles, loops, and membranes. Within (4+1)D twisted *BF* theories [54, 55] there are two *BF* structures,  $CdA$  and  $\tilde{B}dB$ , where  $A$  is a 1-form,  $C$  is a 3-form, and  $B$  and  $\tilde{B}$  are distinct 2-form gauge fields. Corresponding twisted terms include  $AAAAA$ ,  $AAAdA$ ,  $AdAdA$ ,  $AAC$ ,  $AAAB$ ,  $BBA$ ,  $AdAB$ ,  $AAdB$ , and  $BC$ . It was shown in Ref. [55] that  $BBA$ ,  $AAAB$ ,  $AAC$ ,  $AAAAA$ , and  $AAAdA$  lead to non-Abelian shrinking. Furthermore,  $BBA$  and  $AAAB$  produce *hierarchical* shrinking: a membrane can shrink to loops that subsequently shrink to particles.

Importantly, by deriving fusion and shrinking rules in twisted *BF* field theories, one can verify that, in 3d topological order, the shrinking rules are consistent with

<sup>1</sup> In this paper, “ $(n+1)$ D” refers to  $(n+1)$ -dimensional spacetime with  $n$ -dimensional real space. We avoid to use “ $n$ D” or “ $(n)$ D” unless otherwise specified. When referring specifically to spatial dimensions, we use “ $nd$ ”, e.g., 3d ground state, 3d topological order, 3d cubic lattice and 1d closed string.

fusion: fusing first and then shrinking yields the same outcome as shrinking first and then fusing. In 4d topological order, hierarchical shrinking rules are consistent with fusion, but in general shrinking and fusion need not commute. These consistency requirements motivate *diagrammatic representations* [56] for hierarchical shrinking and fusion, from which algebraic constraints such as *fusion pentagon relations* and *(hierarchical) shrinking–fusion hexagon relations* emerge, pointing toward underlying higher-categorical structures.

While these results establish a coherent and predictive continuum framework, their microscopic construction on lattices remains a crucial open problem, especially in the context of condensed matter systems and quantum simulators where lattice regularization is an inevitable step. Especially, motivated by the systematic field-theoretical diagrammatics of fusion and shrinking [53, 55, 56], we ask whether shrinking processes and their associated rules can be microscopically constructed in an exactly solvable three-dimensional lattice model, and whether the fusion–shrinking consistency relations derived in continuum field theory persist at the lattice level. Moreover, the field-theoretical analysis allows us to identify the *allowed shrinking channels*, but it remains unclear whether a specific channel can be selected—or even controlled—microscopically during a shrinking process. Specifically, the *BF* field theory with an *AAB* twist has been proposed and studied since Ref. [25], where an exotic braiding dubbed “Borromean rings braiding” among particle and two loop excitations is discovered purely from the field-theoretical analysis. However, the microscopic construction of such field theory as well as the underlying non-Abelian topological order remains an open question.

In this work, we address these questions through constructing particle and loop excitations, fusion and shrinking processes. We derive the corresponding fusion and shrinking rules. We further demonstrate that non-Abelian shrinking channels can be selectively controlled by tuning internal degrees of freedom of loop operators. We show that the lattice shrinking rules are fully consistent with the fusion rules. Furthermore, by establishing an isomorphism between the excitations in the 3d  $\mathbb{D}_4$  quantum double model and those in the (3+1)D *BF* field theory with an *AAB* twist with  $G = (\mathbb{Z}_2)^3$  [25, 53], we conclude that the former is exactly the microscopic construction of the latter. This work thus provides the first concrete microscopic verification of the fusion–shrinking correspondence predicted by continuum field theory and its diagrammatic formulation [56]. Our results establish a direct bridge between topological field theories and exactly solvable lattice models and lay a microscopic foundation for controlling extended excitations in higher-dimensional quantum matter. Concretely, this work is composed by the following parts.

- **Excitation creation.** In 3d topological orders, topological excitations include both particles and loops, which are represented by Wilson operators

(e.g., Wilson loops and Wilson surfaces) in continuum topological field theory [44, 53–55]. In the microscopic construction—specifically, the 3d quantum double model with a finite group  $G$ —the corresponding creation operators for excitations are slightly thickened open membrane operators consisting of a direct part and a dual part. To construct excitation operators, we introduce four basic operators  $T_g^\pm$  and  $L_g^\pm$ . The operators  $T_g^\pm$  act as projectors on edges, while  $L_g^\pm$  modify the group elements on edges. By linearly combining these basic operators, we systematically construct the thickened open membrane operators in Eq. (60) to create topological excitations, which are labeled by pairs  $(C, R)$ , where  $C$  is a conjugacy class and  $R$  is an irreducible representation of the centralizer of a representative element in  $C$ . The labels  $C$  and  $R$  carried by the operators in Eq. (60) are invariant under local operations—namely, the topological flux and charge associated with loops and particles. This explicit lattice operator formalism establishes the foundation for analyzing fusion and shrinking rules in subsequent sections.

- **Fusion rules.** In continuum topological field theory, the fusion rules of topological excitations are encoded in correlation functions of the corresponding Wilson operators [44, 53, 55]. In contrast, in the 3d quantum double model, fusion is governed by the representation theory of the underlying quantum double algebra  $DG$ . Each excitation labeled by  $[C, R]$  is associated with a local Hilbert space  $V_{(C, R)}$ . When two excitations  $[C_1, R_1]$  and  $[C_2, R_2]$  are brought together, their combined local Hilbert space  $V_{(C_1, R_1)} \otimes V_{(C_2, R_2)}$  forms a representation space of a tensor-product representation of  $DG$ . The fusion rules are thus obtained from the decomposition of this tensor-product representation into irreducible representations, as summarized in Eq. (71). As concrete illustrations, we work out all fusion rules for  $G = \mathbb{Z}_N$  and for  $G = \mathbb{D}_3$ , the dihedral group of order 6. During this derivation, the quantum dimensions of topological excitations are also obtained.

- **Shrinking rules.** In continuum topological field theory, the shrinking process of a loop excitation is defined by continuously shrinking the manifold on which the corresponding Wilson operator is supported [53, 55]. By evaluating the correlation function of the Wilson operator after shrinking, one obtains the corresponding shrinking rules. In this work, to realize shrinking processes on a lattice, we consider a thickened cylindrical operator that creates a pair of loop excitations on its two boundary loops. The derivation of shrinking rules relies crucially on the connecting rules of membrane operators. By applying Eq. (81), a thickened cylinder-like membrane operator associated

with a loop excitation can be shrunk to an infinitesimally thin membrane, which effectively becomes a string operator whose endpoints can carry nontrivial charges and thus behave as particle excitations (see Fig. 15). For non-Abelian  $G$ , even a loop excitation with trivial  $R$  in  $(C, R)$  can produce nontrivial charges upon shrinking, thereby realizing non-Abelian shrinking rules. Mathematically, after shrinking, the local Hilbert space  $V_{(C, R)}$  associated with  $[C, R]$  is mapped to  $\mathcal{S}(V_{(C, R)})$ . The shrinking rules are then obtained from the decomposition of  $\mathcal{S}(V_{(C, R)})$ , as summarized in Eq. (87). We derive all shrinking rules explicitly for  $G = \mathbb{Z}_N$  and  $G = \mathbb{D}_3$ . Moreover, by appropriately choosing the internal degrees of freedom of the membrane operator, we demonstrate that the shrinking channel can be controlled to yield a definite particle outcome.

- **Fusion-shrinking consistency.** The algebraic structures of fusion and shrinking rules are not independent; rather, they must satisfy fusion-shrinking consistency conditions, given in Eq. (10), which were previously derived within continuum topological field theory [53, 55] and summarized in a diagrammatic formulation [56]. In this work, by explicitly deriving all fusion and shrinking rules within the 3d quantum double model, we verify that these rules, at the microscopic level, rigorously satisfy Eq. (10). This verification confirms the algebraic structure predicted by continuum topological field theory and establishes a concrete microscopic construction of fusion–shrinking consistency in a lattice setting.
- **Microscopic construction of the  $BF$  field theory with an  $AAB$  twist.** The  $(3+1)$ D  $BF$  field theory with an  $AAB$  twist, which supports nontrivial Borromean-rings braiding [25], provides an important example of a non-Abelian topological order, despite the underlying gauge group  $(\mathbb{Z}_2)^3$  being Abelian. Gauge invariance constrains which twisted terms may appear in the  $BF$  action, implying that Borromean-rings braiding can coexist only with a compatible subset of multi-loop braiding processes [26]. By further analyzing fusion and shrinking processes in this continuum field theory, Ref. [53] derived the corresponding fusion-shrinking consistency conditions. In this work, we establish a microscopic construction of this continuum field theory by constructing an explicit correspondence with the 3d  $\mathbb{D}_4$  quantum double model. By comparing the fusion and shrinking tables of the two theories, we construct an explicit isomorphism that maps each excitation in the  $BF$  field theory with an  $AAB$  twist and gauge group  $G = (\mathbb{Z}_2)^3$  to a corresponding excitation in the  $\mathbb{D}_4$  quantum double model. This isomorphism preserves both fusion and shrinking rules [Eqs. (175) and (176)], thereby conclusively demonstrating that the 3d  $\mathbb{D}_4$  quantum

double model provides a concrete microscopic construction of the  $BF$  field theory with an  $AAB$  twist. In this way, our results bridge the continuum topological field-theoretic description with an exactly solvable microscopic lattice model.

This paper is organized as follows. Sec. II reviews fusion and shrinking rules derived from field theory and formulates their consistency, including a summary of the diagrammatic representations that encode these processes. A more advanced discussion of diagrammatics is presented in the appendices. Sec. III introduces the 3d quantum double model, constructs the ground states on the three-torus, and computes the ground-state degeneracy (GSD). We define four basic operators and assemble excitation operators for particles and loops. Sec. IV derives the fusion rules, where fusing two excitations amounts to taking the tensor product of irreducible representations of  $DG$ , the quantum double of the group  $G$ . In Sec. V, we construct lattice shrinking processes and derive the corresponding shrinking rules, listing all results for  $G = \mathbb{D}_3$  and demonstrating control over shrinking channels. We further confirm that all shrinking rules are consistent with the fusion rules. Sec. VI shows that the 3d  $\mathbb{D}_4$  quantum double model provides a microscopic construction of the  $BF$  field theory with an  $AAB$  twist and gauge group  $G = (\mathbb{Z}_2)^3$ . Finally, Sec. VII provides a brief summary and outlook. Technical details are collected in the appendices.

## II. FIELD-THEORETICAL CONSISTENCY CONDITIONS AND DIAGRAMMATICS OF FUSION AND SHRINKING RULES

In this section, we first briefly review the consistency conditions between the fusion and shrinking rules that were obtained from the field-theoretical framework in our previous series work. Next, we review the construction of diagrammatic representations in which fusion and shrinking processes satisfy stringent consistency conditions. The consistency between the fusion and shrinking will be justified in the microscopic lattice model in Sec. V. Furthermore, we can define different unitary symbols to transform a diagram into another as shown in Appendix A, which eventually leads to a series of algebraic constraints of higher-dimensional topological orders. Any violation of these constraints indicates quantum anomalies, providing a diagnostic tool for identifying such anomalies in theoretical models.

### A. Consistent fusion and shrinking rules

Fusion rules serve as the most fundamental topological data of a topologically ordered phase. Two excitations collectively behave as another excitation when they are brought to the same spatial region and their total topological charge and flux are measured, which is a process

referred to as *fusion*. In general, a fusion rule takes the form

$$\mathbf{a} \otimes \mathbf{b} = \bigoplus_{\mathbf{c}} N_{\mathbf{c}}^{\mathbf{ab}} \mathbf{c}, \quad (1)$$

where  $\mathbf{a}$ ,  $\mathbf{b}$ , and  $\mathbf{c}$  denote topological excitations, and  $N_{\mathbf{c}}^{\mathbf{ab}}$  is a non-negative integer called the *fusion coefficient*. The value of  $N_{\mathbf{c}}^{\mathbf{ab}}$  counts the number of topologically distinct *fusion channels* into  $\mathbf{c}$ . If  $N_{\mathbf{c}}^{\mathbf{ab}} = 0$ , the fusion channel to  $\mathbf{c}$  is forbidden. A fusion process with a single allowed channel is called *Abelian*, while one with multiple possible fusion channels, hence multiple possible outcomes, is *non-Abelian*.

In 3d topological orders, the presence of loop-like excitations introduces new types of topological data known as *shrinking rules* [53, 55, 56], which determine how extended excitations can be continuously contracted into lower-dimensional ones, typically particles. The general form of a shrinking rule reads

$$\mathcal{S}(\mathbf{a}) = \bigoplus_{\mathbf{b}} S_{\mathbf{b}}^{\mathbf{a}} \mathbf{b}, \quad (2)$$

where  $\mathcal{S}$  denotes the shrinking operator,  $\mathbf{b}$  labels particle excitations, and  $\bigoplus_{\mathbf{b}}$  enumerates all possible outcomes. The non-negative integer  $S_{\mathbf{b}}^{\mathbf{a}}$  is the *shrinking coefficient*, representing the number of shrinking channels into  $\mathbf{b}$ . If  $\mathbf{a}$  is already a particle, the shrinking process acts trivially, i.e.,  $\mathcal{S}(\mathbf{a}) = \mathbf{a}$ . Similar to the fusion, a single shrinking channel corresponds to an Abelian shrinking process, while multiple channels indicate a non-Abelian one.

In our previous works [53, 55], we systematically analyzed fusion and shrinking rules using the continuum topological field theory formalism (A brief review of this formalism is provided in the Section 2 of Ref. [56]). Consider a simple untwisted  $BF$  theory with the gauge group  $G = \prod_i \mathbb{Z}_{N_i}$  as an example. The topological action is

$$S = \int \sum_i \frac{N_i}{2\pi} B^i dA^i, \quad (3)$$

where  $A^i$  and  $B^i$  are 1- and 2-form  $U(1)$  gauge fields, respectively. The gauge transformations are

$$A^i \rightarrow A^i + d\chi^i, \quad B^i \rightarrow B^i + dV^i, \quad (4)$$

where  $\chi^i$  and  $V^i$  are 0- and 1-form gauge parameters satisfying  $\int d\chi^i \in 2\pi\mathbb{Z}$  and  $\int dV^i \in 2\pi\mathbb{Z}$ . An excitation  $\mathbf{a}$  in our field theory is represented by a gauge invariant Wilson operator  $\mathcal{O}_{\mathbf{a}}$ . If  $\mathbf{a}$  is a particle carrying  $n_i$  units of gauge charge that is minimally coupled to the  $A^i$  field, the Wilson operator  $\mathcal{O}_{\mathbf{a}}$  is written as

$$\mathcal{O}_{\mathbf{a}} = \exp \left( i \int_{\gamma} n_i A^i \right), \quad (5)$$

where  $\gamma = S^1$  denotes the closed one-dimensional world-line of the particle  $\mathbf{a}$  in (3+1)D spacetime. If  $\mathbf{b}$  is a loop

carrying  $m_j$  units of gauge flux that is minimally coupled to the  $B^j$  field, we have

$$\mathcal{O}_{\mathbf{b}} = \exp \left( i \int_{\sigma} m_j B^j \right), \quad (6)$$

where  $\sigma = S^1 \times S^1$  denotes the closed two-dimensional world-sheet of the loop.

In path integral formalism, one can denote the fusion of two topological excitations  $\mathbf{a}$  and  $\mathbf{b}$  as

$$\langle \mathbf{a} \otimes \mathbf{b} \rangle = \frac{1}{\mathcal{Z}} \int \mathcal{D}[AB] \exp(iS) \times (\mathcal{O}_{\mathbf{a}} \times \mathcal{O}_{\mathbf{b}}), \quad (7)$$

where  $\mathcal{Z}$  is the partition function, and  $\mathcal{D}[AB]$  represents the field configurations. We can further calculate the fusion rules as

$$\begin{aligned} \langle \mathbf{a} \otimes \mathbf{b} \rangle &= \frac{1}{\mathcal{Z}} \int \mathcal{D}[AB] \exp(iS) \times (\mathcal{O}_{\mathbf{a}} \times \mathcal{O}_{\mathbf{b}}) \\ &= \frac{1}{\mathcal{Z}} \int \mathcal{D}[AB] \exp(iS) \times \left( \sum_{\mathbf{c}} N_{\mathbf{c}}^{\mathbf{ab}} \mathcal{O}_{\mathbf{c}} \right) \\ &= \langle \bigoplus_{\mathbf{c}} N_{\mathbf{c}}^{\mathbf{ab}} \mathcal{O}_{\mathbf{c}} \rangle. \end{aligned} \quad (8)$$

A shrinking rule in the path integral formalism is given by

$$\begin{aligned} \langle \mathcal{S}(\mathbf{a}) \rangle &= \langle \lim_{X_1 \rightarrow X_2} \mathcal{O}_{\mathbf{a}} \rangle = \lim_{X_1 \rightarrow X_2} \frac{1}{\mathcal{Z}} \int \mathcal{D}[AB] \exp(iS) \mathcal{O}_{\mathbf{a}} \\ &= \sum_{\mathbf{b}} \frac{1}{\mathcal{Z}} \int \mathcal{D}[AB] \exp(iS) S_{\mathbf{b}}^{\mathbf{a}} \mathcal{O}_{\mathbf{b}} \\ &= \langle \bigoplus_{\mathbf{b}} S_{\mathbf{b}}^{\mathbf{a}} \mathbf{b} \rangle, \end{aligned} \quad (9)$$

where  $X_1$  and  $X_2$  ( $X_2 \subset X_1$ ) are the spacetime trajectories of the excitation  $\mathbf{a}$  before and after the shrinking process.

A systematic analysis shows that for anomaly-free topological orders, fusion and shrinking must satisfy a *consistency condition*. Specifically, in 3d topological order, the condition reads

$$\mathcal{S}(\mathbf{a}) \otimes \mathcal{S}(\mathbf{b}) = \mathcal{S}(\mathbf{a} \otimes \mathbf{b}), \quad (10)$$

meaning that performing fusion before shrinking yields the same result as shrinking first and then fusing. In the language of category, this implies that the shrinking operator is a *tensor functor* that preserves the fusion structure. We will verify that this condition still holds in the lattice model in Sec. V.

If we further lift the spatial dimension to 4d, topological excitations include not only particles and loops but also membrane-like objects. A membrane excitation can undergo a *hierarchical shrinking process*, in which it first shrinks into loops then the loops further shrink into particles. Correspondingly, the consistency condition in 3d (10) is generalized to

$$\mathcal{S}^2(\mathbf{a}) \otimes \mathcal{S}^2(\mathbf{b}) = \mathcal{S}^2(\mathbf{a} \otimes \mathbf{b}), \quad (11)$$

where  $\mathcal{S}^2$  denotes applying the shrinking operation twice in a hierarchical shrinking process.

In this paper, we focus on the consistent fusion and shrinking rules in 3d topological orders. Starting from the consistency condition (10), we can further derive algebraic constraints between the fusion coefficients  $N_c^{ab}$  and the shrinking coefficients  $S_b^a$ . Using Eqs. (1) and (2), one finds

$$\begin{aligned}\mathcal{S}(a \otimes b) &= \mathcal{S}\left(\bigoplus_i N_i^{ab} i\right) = \bigoplus_i N_i^{ab} \mathcal{S}(i) \\ &= \bigoplus_i N_i^{ab} \left(\bigoplus_c S_c^i c\right) \\ &= \bigoplus_c \left(\sum_i S_c^i N_i^{ab}\right) c,\end{aligned}\quad (12)$$

and

$$\begin{aligned}\mathcal{S}(a) \otimes \mathcal{S}(b) &= \left(\bigoplus_i S_i^a i\right) \otimes \left(\bigoplus_j S_j^b j\right) \\ &= \bigoplus_i \bigoplus_j [S_i^a S_j^b (i \otimes j)] \\ &= \bigoplus_i \bigoplus_j \left[S_i^a S_j^b \left(\bigoplus_c N_c^{ij} c\right)\right] \\ &= \bigoplus_c \left(\sum_{i,j} S_i^a S_j^b N_c^{ij}\right) c.\end{aligned}\quad (13)$$

Comparing both equations above, we can find that the consistency between fusion and shrinking rules enforces a key constraint

$$\sum_i S_c^i N_i^{ab} = \sum_{i,j} S_i^a S_j^b N_c^{ij}, \quad (14)$$

where  $a, b, c, i, j$  label all possible excitations. Eq. (14) encodes the algebraic backbone of consistent fusion–shrinking relations and can also be understood through our diagrammatic formulation as shown in Eq. (A6) of Appendix A.

## B. Diagrammatics

The consistency conditions Eqs. (10) and (11) in 3d and 4d topological orders inspire the diagrammatic representations of consistent fusion and shrinking rules [56]. We can define elementary diagrams for fusion and shrinking processes and treat them as vectors in the fusion and shrinking spaces respectively. By combining these elementary diagrams, we can build more complex diagrams, and use a series of unitary operations to transform between them. The legitimate forms of these unitary operations are strongly constrained by pentagon equations and

(hierarchical) shrinking-fusion hexagon equations, which reveal the algebraic structure of the consistent fusion and shrinking rules. In this section, we briefly review the diagrammatic representations of fusion and shrinking rules in 3d. Details about the transformation between different complex diagrams and the derivation of algebraic constraints are collected in Appendix A.

We need to first introduce some notations. We assume that there are only a finite number of topologically distinct excitations in a topological order, and we collect all of them in a set denoted as  $\Phi_0^{\mathcal{D}}$ , where the superscript  $\mathcal{D}$  denotes the spacetime dimension. In this paper, we mainly focus on 3d topological orders and thus  $\mathcal{D} = 3+1$ . If we perform a shrinking operation on all excitations in  $\Phi_0^{3+1}$ , all the possible shrinking results form a subset of  $\Phi_0^{3+1}$ , denoted by  $\Phi_1^{3+1}$ . We can view the shrinking process as a mapping from the set  $\Phi_0^{3+1}$  to its subset  $\Phi_1^{3+1}$ ,

$$\mathcal{S} : \Phi_0^{3+1} \rightarrow \Phi_1^{3+1}. \quad (15)$$

The excitations in the set  $\Phi_i^{3+1}$  have closed fusion rules, i.e., all possible fusion results of fusing two excitations from the set  $\Phi_i^{3+1}$  still form the set  $\Phi_i^{3+1}$  itself. This is a consequence of the finite number of topological excitations and has been verified in (3+1)D twisted *BF* theories [53, 55]. Thus, we can also treat a fusion process as a mapping,

$$\otimes : \Phi_i^{3+1} \times \Phi_i^{3+1} \rightarrow \Phi_i^{3+1}, \quad i = 0, 1. \quad (16)$$

To construct a more generalizable diagrammatics, we consider the cases with fusion multiplicity and shrinking multiplicity. In this section, Latin and Greek letters denote excitations and fusion/shrinking channels, respectively.

Now we can construct the diagrammatics for 3d topological orders. The basic diagram in our 3d diagrammatics is defined as follows. Suppose that the fusion process  $a \otimes b$  has a fusion channel to  $c$ , we can represent the fusion channel diagrammatically in Fig. 1. The solid lines are understood as the spacetime trajectories of the excitations, and here we use double-lines to indicate that  $a, b, c \in \Phi_0^{3+1}$ . One can simply replace the double-lines with single-lines to obtain a fusion diagram that represents the fusion process in the set  $\Phi_1^{3+1}$ . In Fig. 1, we use  $\mu = \{1, 2, \dots, N_c^{ab}\}$  to label different fusion channels to  $c$ , and the fusion diagram can be defined as a vector  $|a, b; c, \mu\rangle$ . The set of orthogonal vectors  $\{|a, b; c, \mu\rangle, \mu = 1, 2, \dots, N_c^{ab}\}$  spans a fusion space  $V_c^{ab}$  with  $\dim(V_c^{ab}) = N_c^{ab}$ .

The basic shrinking diagram is defined as follows. Suppose that  $a \in \Phi_0^{3+1}$  and the shrinking process  $\mathcal{S}(a)$  has a shrinking channel to  $b \in \Phi_1^{3+1}$ , then we define the corresponding shrinking diagram in Fig. 2. We use a triangle to represent the shrinking operation. Note that in a specific diagram, a double-line and a single-line may actually represent the same particle. However, they carry distinct meanings: the double-line means that this particle from  $\Phi_0^{3+1}$  is treated as the input of the shrinking process,

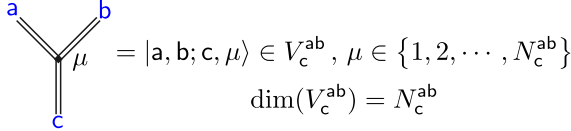


FIG. 1. Elementary fusion diagrams in 3d.  $a, b$  and  $c$  denote excitations and we highlight them in blue.  $\mu = \{1, 2, \dots, N_c^{ab}\}$  labels different fusion channels with the same fusion output  $c$ . Double-lines indicate that  $a, b, c \in \Phi_0^{3+1}$ . If we want to draw a fusion diagram that represents fusion in the set  $\Phi_1^{3+1}$ , we only need to replace all the double-lines with single-lines.

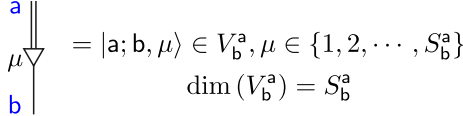


FIG. 2. Shrinking diagram in 3d. The double-line and single-line represent excitations from  $\Phi_0^{3+1}$  and  $\Phi_1^{3+1}$  respectively. Since  $a$  and  $b$  are the input and output of the shrinking process respectively,  $a$  can be a loop or a particle while  $b$  can only be a particle. We use a triangle to represent the shrinking operation. This diagram can be defined as a vector and the orthogonal set  $\{|a; b, \mu\rangle, \mu = 1, 2, \dots, S_b^a\}$  spans the shrinking space  $V_b^a$  with  $\dim(V_b^a) = S_b^a$ .

while the single-line means that this particle from  $\Phi_1^{3+1}$  is the output. We define the shrinking diagram in Fig. 2 as a vector  $|a; b, \mu\rangle$ , where different  $\mu$  label different orthogonal vectors. The set  $\{|a; b, \mu\rangle, \mu = 1, 2, \dots, S_b^a\}$  spans a shrinking space denoted by  $V_b^a$ , whose dimension is given by  $\dim(V_b^a) = S_b^a$ .

We can stack these basic diagrams to construct more complicated diagrams that describe more complicated processes. For example, by stacking two basic fusion diagrams shown in Fig. 1, we construct a fusion diagram that involve three excitations. Consider fusing three excitations  $(a \otimes b) \otimes c$  and there exist legitimate fusion channels to  $d$ , we can draw this process in Fig. 3, which is defined as a vector  $|(a, b); e, \mu\rangle \otimes |e, c; d, \nu\rangle$ , where  $\otimes$  means tensor product. The corresponding space is denoted as  $V_d^{abc}$ , whose dimension is given by

$$\dim(V_d^{abc}) = \sum_e N_e^{ab} N_d^{ec}, \quad (17)$$

because  $V_d^{abc}$  is isomorphic to  $\bigoplus_e V_e^{ab} \otimes V_d^{ec}$ . We can use a similar tensor product construction to incorporate both fusion and shrinking processes in a diagram. Consider  $\mathcal{S}(a) \otimes \mathcal{S}(b)$ , the corresponding diagrams are shown in Fig. 4. This diagram is understood as the vector  $|d, e; c, \lambda\rangle \otimes |b; e, \nu\rangle \otimes |a; d, \mu\rangle$ , where different  $d, e, \mu, \nu$ , and  $\lambda$  label different orthogonal vectors. The diagram shown in Fig. 4 describes the process that  $a$  and  $b$  shrink to  $d$  and  $e$  in the  $\mu$  and  $\nu$  channels respectively first, then  $d$  and  $e$  fuse to  $c$  in the  $\lambda$  channel. This set of orthogonal vectors spans the space denoted as  $V_c^{\mathcal{S}(a) \otimes \mathcal{S}(b)}$ , which is isomorphic to  $\bigoplus_{d,e} V_c^{de} \otimes V_e^b \otimes V_d^a$  due to our tensor

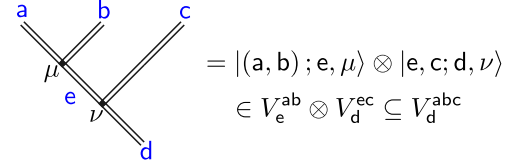


FIG. 3. Fusing three excitations in 3d.  $a, b$ , and  $c$  are ultimately fuse into  $d$ . The bracket “ $(a, b)$ ” is only used to emphasize that  $a$  and  $b$  fuse together first in the whole three-excitation fusion process and it does not change the vectors. The set of vectors  $\{|(a, b); e, \mu\rangle \otimes |e, c; d, \nu\rangle\}$  span the whole space  $V_d^{abc}$ , where different  $\mu, \nu$  and  $e$  label different orthogonal vectors. The space  $V_d^{abc}$  is isomorphic to  $\bigoplus_e (V_e^{ab} \otimes V_d^{ec})$ . The dimension of  $V_d^{abc}$  is given by  $\dim(V_d^{abc}) = \sum_e N_e^{ab} N_d^{ec}$ . Here we only draw the diagram for fusion process in the set  $\Phi_0^{3+1}$ . One can obtain the diagram for subset  $\Phi_1^{3+1}$  by simply replacing all double-lines with single-lines.

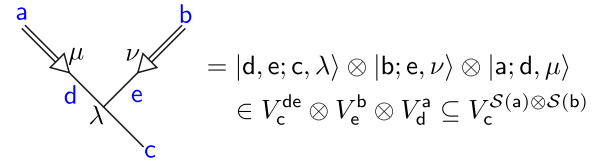


FIG. 4. Incorporating both fusion and shrinking processes in 3d. We stack two basic shrinking diagrams and a basic fusion diagram to describe the process  $\mathcal{S}(a) \otimes \mathcal{S}(b)$ .

product construction. Thus, we have

$$\dim(V_c^{\mathcal{S}(a) \otimes \mathcal{S}(b)}) = \sum_{d,e} N_c^{de} S_e^b S_d^a. \quad (18)$$

The consistency condition Eq. (10) allows us to introduce a series of unitary operations to transform these complicated diagrams. We can derive important algebraic constraints on these unitary operations known as the pentagon equation and shrinking-fusion hexagon equation. Details of these unitary operations and algebraic constraints are shown in Appendix A.

### III. EXCITATION CREATION

In order to make a connection between the field theory and microscopic lattice model, we need to consider a microscopic construction of 3d topological order. The 3d quantum double model serves as an ideal platform. In this section, we consider the 3d quantum double lattice model and design the operators to create topological excitations. We note that topological excitations in 3d differ essentially from their 2d counterparts. While 2d topological orders host point-like anyons that exhibit fractional statistics, point-like particles in 3d are constrained to be either bosons or fermions. Furthermore, spatially extended excitations, i.e., loops, appear in 3d and support nontrivial processes such as fusion and shrinking. Investigating these particles and loops, along with their

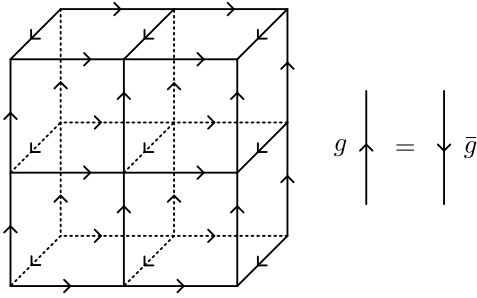


FIG. 5. Local Hilbert space on a cubic lattice. Each edge is assigned with an arrow and a group element  $g \in G$ . Reversing the arrow of an edge changes the group element  $g$  to its inverse  $\bar{g}$ .

fusion and shrinking rules, reveals structures that extend beyond those found in 2d topological orders. These excitations are the cornerstones of the study of fusion and shrinking rules on lattice in Secs. IV and V.

### A. Hamiltonian on a lattice

Consider the 3d quantum double model defined on the cubic lattice with periodic boundary condition. The underlying degrees of freedom are the group elements  $g \in G$  on the edges of the cubic lattice. Each edge is assigned with an orientation (an arrow, see Fig. 5) that can be chosen arbitrarily. Reversing the orientation of an edge changes  $g$  on the edge to its inverse,  $\bar{g}$ . The local state on an edge is denoted as  $|g\rangle$  and we set  $\langle g|h\rangle = \delta_{g,h}$ . The local Hilbert space is spanned by the basis  $\{|g\rangle |g \in G\}$  and its dimension is  $|G|$ , the number of elements in  $G$ . A configuration on the whole lattice is written as  $|g_1\rangle \otimes |g_2\rangle \otimes \dots \otimes |g_N\rangle$ , where  $\otimes$  means tensor product and  $g_i$  labels the group element on the  $i$ -th edge,  $i = 1, 2, \dots, N$ . All possible configurations span the total Hilbert space whose dimension is  $|G|^N$ .

With the local Hilbert space on the edges introduced, we define four basic operators that act on the Hilbert space of an edge. We will see later that the linear combinations of these basic operators give rise to topological excitations. The basic operators (dubbed “T-operators” and “L-operators” hereafter) are

$$T_g^+ = |g\rangle \langle g|, \quad T_g^- = |\bar{g}\rangle \langle \bar{g}|, \quad (19)$$

$$L_g^+ = \sum_{k \in G} |gk\rangle \langle k|, \quad L_g^- = \sum_{k \in G} |kg\rangle \langle k|. \quad (20)$$

The operator  $T_g^+$  ( $T_g^-$ ) acts on  $|h\rangle$  as a test for whether the group element on the edge equals  $g$  ( $\bar{g}$ ), being a projection operator selecting  $h = g$  ( $h = \bar{g}$ ). The operator  $L_g^+$  acts on  $|h\rangle$  as a “left-multiplication” operator,  $L_g^+ |h\rangle = |gh\rangle$ , where the group element on the edge is left-multiplied by  $g$ . While  $L_g^- |h\rangle = |h\bar{g}\rangle$ , where the group element on the edge is right-multiplied by  $\bar{g}$ . We

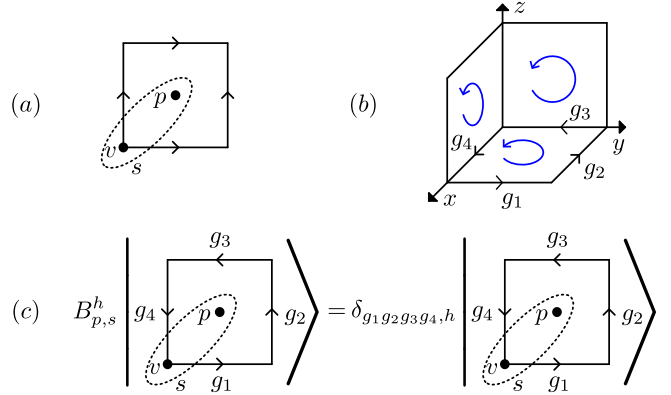


FIG. 6. Action of the plaquette operator  $B_{p,s}^h$ . (a) A site  $s = (v, p)$  is a combination of a vertex  $v$  and a plaquette  $p$ . (b) The blue arrows denote the product order of the group elements on the edges of the plaquette. (c)  $B_{p,s}^h$  projects the ordered product of all group elements on the edges around  $p$ ,  $g_1g_2g_3g_4$ , to  $h \in G$ . Notice that the ordered product depends on the choice of the site  $s = (v, p)$ , i.e., the choice of vertex  $v$ . When  $h = e$ ,  $g_1g_2g_3g_4 = e$  implies  $g_4g_1g_2g_3 = g_3g_4g_1g_2 = \dots = e$ . But for a general  $h$ ,  $g_1g_2g_3g_4 = h$  does not guarantee other ordered product like  $g_4g_1g_2g_3$  is  $h$ .

can verify that the basic operators satisfy the following properties

$$\begin{aligned} T_g^\pm T_h^\pm &= \delta_{g,h} T_h^\pm, & L_g^\pm L_h^\pm &= L_{gh}^\pm, \\ T_g^+ L_h^+ &= L_h^+ T_{\bar{h}g}^+, & T_g^+ L_h^- &= L_h^- T_{\bar{h}g}^+, \\ T_g^- L_h^+ &= L_h^+ T_{\bar{h}g}^-, & T_g^- L_h^- &= L_h^- T_{\bar{h}g}^-, \\ (T_g^\pm)^\dagger &= T_g^\pm, & (L_g^\pm)^\dagger &= (L_g^\pm)^{-1} = L_{\bar{g}}^\pm, \\ [L_g^\pm, L_h^\mp] &= 0, & \sum T_g^\pm &= L_e^\pm = 1. \end{aligned} \quad (21)$$

Before presenting the Hamiltonian of the 3d quantum double model, we first introduce the plaquette operator  $B_{p,s}^h$  acting on the plaquette  $p$  and the vertex operator  $A_v$  acting on the vertex  $v$ .

As shown in Fig. 6, the action of  $B_{p,s}^h$  is to measure whether the ordered product of group elements on the edges around the plaquette  $p$  equals  $h$ . If yes, the state remains intact, otherwise it is annihilated. The site  $s = (v, p)$  defined in Fig. 6(a) determines the order of multiplication in the product, which is important because the group elements are generally non-commutative. Specifically, for a plaquette on the  $xy$ -plane, we set its normal direction as the  $+z$  direction and set the arrows of the edges to form a counterclockwise loop with respect to the normal direction. Then, starting from the vertex  $v$ , we multiply the group elements along the loop direction. For other plaquettes on  $xz$ - and  $yz$ -planes, we set their normal directions as the  $+y$  and  $+x$  directions, the orientations of the arrows of the edges are shown in Fig. 6(b). A plaquette operator  $B_{p,s}^h$  can always be constructed from the basic operators shown in Eq. (19). For

FIG. 7. The action of  $A_v^g$  term.  $A_v^g |g_i\rangle = |gg_i\rangle$  if the arrow points away from  $v$ ,  $A_v^g |g_i\rangle = |g_i\bar{g}\rangle$  if the arrow points towards  $v$ .

example,  $B_{p,s}^h$  in Fig. 6(c) can be written as

$$B_{p,s}^h = \sum_{g_1, g_2, g_3 \in G} T_{\bar{g}_3 \bar{g}_2 \bar{g}_1 h}^+ T_{g_3}^+ T_{g_2}^+ T_{g_1}^+, \quad (22)$$

where  $T_{g_1}^+$ ,  $T_{g_2}^+$ ,  $T_{g_3}^+$ , and  $T_{\bar{g}_3 \bar{g}_2 \bar{g}_1 h}^+$  act on the edges labeled by  $g_1$ ,  $g_2$ ,  $g_3$ , and  $g_4$  respectively. If we take  $h$  as the identity element  $e$ , the action of  $B_{p,s}^h$  is independent of the choice of  $s$ . We denote  $B_{p,s}^e$  as  $B_p$  for simplicity. The  $B_p$  term can be understood as the zero flux condition.

The vertex operator  $A_v^g$  acts on all edges that are attached to the vertex  $v$ . If the arrow of the edge points away from the vertex  $v$ , the group element on the edge is multiplied by  $g$  on the left. Otherwise, the element on the edge is multiplied by  $\bar{g}$  on the right, as shown in Fig. 7. Similar to the plaquette operator, a vertex operator  $A_v^g$  can also be written as a product of the basic operators shown in Eq. (20). As an example, we write the vertex operator  $A_v^g$  in Fig. 7 as

$$A_v^g = L_g^- L_g^+ L_g^+ L_g^- L_g^+ L_g^-, \quad (23)$$

where the three  $L_g^+$  operators act on the edges labeled by  $g_2$ ,  $g_3$ , and  $g_5$ , respectively, while the three  $L_g^-$  operators act on the edges labeled by  $g_1$ ,  $g_4$ , and  $g_6$ , respectively.

The Hamiltonian is given by

$$H = - \sum_v A_v - \sum_p B_p, \quad (24)$$

where

$$A_v = \frac{1}{|G|} \sum_{g \in G} A_v^g. \quad (25)$$

The definition of the  $B_p$  term is given after Eq. (22). By means of  $T$ - and  $L$ -operators shown in Eqs. (19) and (20) as well as the properties shown in Eq. (21), we can verify that  $A_v$ 's and  $B_p$ 's satisfy

$$A_v^g A_v^h = A_v^{gh}, \quad (26)$$

$$A_v A_v = A_v, \quad (27)$$

$$B_p B_p = B_p, \quad (28)$$

$$[A_v^g, A_{v'}^h] = [B_p, B_{p'}] = [A_v, B_p] = 0. \quad (29)$$

which guarantees the exact solvability of the Hamiltonian.

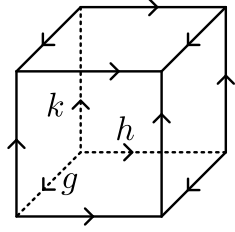


FIG. 8. The simplest 3d lattice on a 3-torus manifold. There are only three independent edges, three independent plaquettes, and one independent vertex. The configuration on this lattice is written as  $|g, h, k\rangle$ .

Any ground state of the Hamiltonian is a state where all  $A_v$ 's and  $B_p$ 's have eigenvalues +1. From the viewpoint of gauge theory,  $A_v = 1$  encodes the gauge invariance and  $B_p = 1$  enforces the zero flux condition. The ground state can be obtained as follows. Starting from a product state  $|\phi\rangle$  that satisfies the zero flux condition ( $B_p$  term has eigenvalue +1) everywhere, i.e.,

$$B_p |\phi\rangle = |\phi\rangle, \quad \forall p, \quad (30)$$

then acting the projector  $\prod_v A_v$  on  $|\phi\rangle$  gives us a ground state

$$|GS\rangle = \prod_v A_v |\phi\rangle. \quad (31)$$

Using Eq. (27) and Eq. (29), we verify that

$$A_{v'} |GS\rangle = A_{v'} \prod_v A_v |\phi\rangle = \prod_v A_v |\phi\rangle = |GS\rangle, \quad (32)$$

$$B_p |GS\rangle = B_p \prod_v A_v |\phi\rangle = \prod_v A_v B_p |\phi\rangle = |GS\rangle. \quad (33)$$

To compute the GSD, we consider the simplest non-trivial case in which the Hamiltonian is defined on a 3-torus. The 3-torus can be represented by a single cube with periodic boundary condition as shown in Fig. 8. A state satisfying the zero-flux condition can be written as  $|g, h, k\rangle$ , where the commuting group elements  $g$ ,  $h$ , and  $k$  denote the three independent group elements on the single cube. The other condition for a ground state is  $A_v |GS\rangle = |GS\rangle$ . Since there is only one vertex in this cube, we have

$$\begin{aligned} |GS_{g,h,k}\rangle &= A_v |g, h, k\rangle = \frac{1}{|G|} \sum_{g_0} A_v^{g_0} |g, h, k\rangle \\ &= \frac{1}{|G|} \sum_{g_0} |g_0 g \bar{g}_0, g_0 h \bar{g}_0, g_0 k \bar{g}_0\rangle. \end{aligned} \quad (34)$$

We can also choose states labeled by other commuting elements  $|g', h', k'\rangle$  to construct other ground states  $|GS_{g',h',k'}\rangle$ . The Burnside's lemma ensures that  $|GS_{g,h,k}\rangle$  and  $|GS_{g',h',k'}\rangle$  are either the same or orthogonal to each

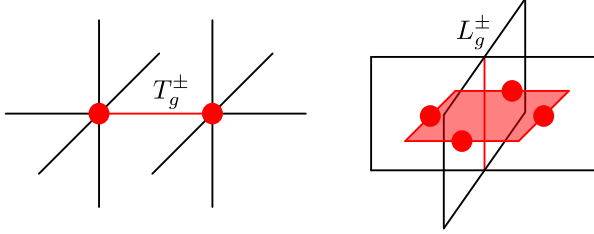


FIG. 9. Acting  $T$ - and  $L$ -operators [Eq. (20)] on a ground state. These basic operators generally do not commute with the vertex terms or plaquette terms in the Hamiltonian. Thus, a  $T_g^\pm$  creates a pair of excited vertices while an  $L_g^\pm$  creates a loop-like excited state.

other. The GSD is given by

$$\text{GSD} = \frac{1}{|G|} \sum_{g_0 \in G} \sum_{\{g, h, k\}} \delta_{g, g_0 g \bar{g}_0} \delta_{h, g_0 h \bar{g}_0} \delta_{k, g_0 k \bar{g}_0}, \quad (35)$$

where  $\{g, h, k\}$  is the triplet of commuting group elements. Here, we give the GSD on a 3-torus for some simple groups. For an Abelian group  $G$ , the GSD is  $|G|^3$ . For  $G = \mathbb{D}_3$  and  $G = \mathbb{D}_4$ , the GSD are 21 and 92, respectively.

## B. Particle excitations

In Sec. III A, we show that a vertex term  $A_v$  and a plaquette term  $B_p$  can be constructed by using several  $L_g^\pm$  terms and  $T_g^\pm$  terms respectively. The ground state condition is  $A_v = B_p = 1, \forall v, p$ . From Eq. (21) we can see that  $T_g^\pm$  generally does not commute with  $L_g^\pm$ , which means that a  $T_g^\pm$  does not commute with the two vertex terms on the endpoints of an edge, and an  $L_g^\pm$  does not commute with the four plaquette terms around the edge. Thus, as shown in Fig. 9, acting a  $T_g^\pm$  on the ground state creates two excited vertices (i.e., violates the condition  $A_v = 1$ ) on the endpoints of the edge, and acting a  $L_g^\pm$  creates four excited plaquettes (i.e., violates the condition  $B_p = 1$ ) whose centers live on a closed loop in the dual lattice. In this sense, the topological excitations in the 3d quantum double model can be particles or loops.  $T_g^\pm$  can be used to construct operators for particles and  $L_g^\pm$  can be used to construct operators for loops. For simplicity, we say that an operator violates vertex terms or plaquette terms when this operator does not commute with them in the following discussion.

We first consider the operators for particles.  $T_L^g$  is defined as an operator that acts on an oriented string  $L$ . If the string  $L$  can be obtained by connecting two shorter strings  $L_1$  and  $L_2$ , we define the connecting rule of  $T_{L=L_1 \cup L_2}^g$  as

$$T_{L=L_1 \cup L_2}^g = \sum_h T_{L_2}^{\bar{h}g} T_{L_1}^h, \quad (36)$$

whose effect is projecting to the state where the product of the group elements on  $L_1$  and  $L_2$  is  $g$ . Note that the operator  $T_{L_1}^h$  in Eq. (36) acts first, we demand that the end of  $L_1$  is also the start of  $L_2$ . In the following discussion, we use  $\partial_0 L$  and  $\partial_1 L$  to denote the start and end of an oriented string  $L$  respectively, and we have  $\partial_1 L_1 = \partial_0 L_2$ . When  $L_1$  is a single edge, then  $T_{L_1}^g = T_g^+$  if the arrow of the edge aligns with the orientation of  $L_1$ , otherwise  $T_{L_1}^g = T_g^-$ .

When we consider connecting more strings as shown in Fig. 10, we expect that the order of connection is irrelevant, i.e.,

$$T_{L_1 \cup (L_2 \cup L_3)}^g = T_{(L_1 \cup L_2) \cup L_3}^g, \quad (37)$$

where the bracket in  $L_1 \cup (L_2 \cup L_3)$  emphasizes that we connect  $L_2$  and  $L_3$  first. Similarly, the bracket in  $(L_1 \cup L_2) \cup L_3$  emphasizes that we connect  $L_1$  and  $L_2$  first. We provide the proof of Eq. (37) in Appendix B.

Another important property of  $T_L^g$  is that it commutes with  $B_p$ 's and  $A_v$ 's, except those  $A_v$ 's at the endpoints of  $L$ . We denote a string by  $L = (v_0, v_1, \dots, v_n)$  that starts at the vertex  $v_0$  and ends at  $v_n$ , where an edge is denoted by  $v_i v_{i+1}$ . Since this operator does not change the group elements on edges ( $T_L^g$  consists of  $T_g^+$  and  $T_g^-$ ), it automatically commutes with all  $B_p$  terms in the Hamiltonian. As for  $A_v$  terms, in Appendix B we prove that

$$A_{v_i}^k T_L^g = T_L^g A_{v_i}^k, \quad (38)$$

where  $k \in G$  and  $i \neq 0, n$ . Since  $A_{v_i} = \frac{1}{|G|} \sum_{k \in G} A_{v_i}^k$ , we conclude that  $[A_{v_i}, T_L^g] = 0$  as long as  $v_i$  is a vertex inside the string  $L$ . However,  $T_L^g$  does not commute with the vertex terms at the endpoints of  $L$ . We first consider the commutation relations between  $A_{v_0}^k$ ,  $A_{v_n}^k$ , and  $T_L^g$ :

$$A_{v_0 = \partial_0 L}^k T_L^g = T_L^{kg} A_{v_0 = \partial_0 L}^k, \quad (39)$$

$$A_{v_n = \partial_1 L}^k T_L^g = T_L^{g\bar{k}} A_{v_n = \partial_1 L}^k, \quad (40)$$

which leads to

$$A_{v_0} T_L^g = \frac{1}{|G|} \sum_k A_{v_0}^k T_L^g = \frac{1}{|G|} \sum_k T_L^{kg} A_{v_0}^k \neq T_L^g A_{v_0}, \quad (41)$$

$$A_{v_n} T_L^g = \frac{1}{|G|} \sum_k A_{v_n}^k T_L^g = \frac{1}{|G|} \sum_k T_L^{g\bar{k}} A_{v_n}^k \neq T_L^g A_{v_n}. \quad (42)$$

Therefore, the operator  $T_L^g$  creates excited vertices at the endpoints of  $L$ , as shown in Fig. 10.

We construct a string operator for particles by linearly combining  $T_L^g$ :

$$W_L(R; i, j) = \sum_g [\Gamma_{ij}^R(g)]^* T_L^g = \sum_g \Gamma_{ij}^{R*}(g) T_L^g, \quad (43)$$

where  $R$  labels the irreducible representation (irrep) of  $G$ ,  $\Gamma$  denotes the matrix of the irrep,  $i, j$  are row and column

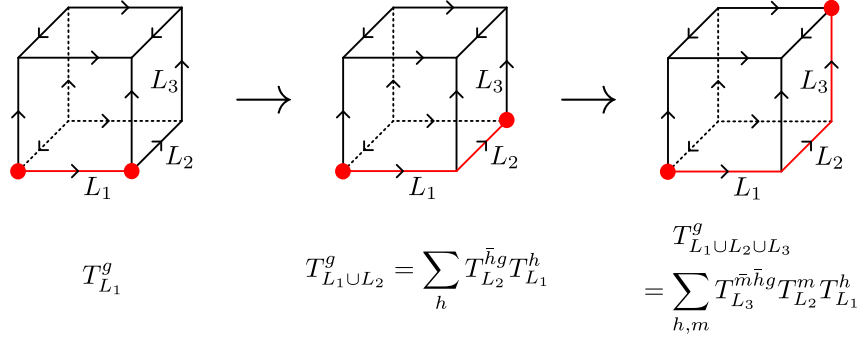


FIG. 10. Connecting three string operators step by step. The red lines and dots denote the string and the excited vertices respectively. This connecting rule allow us to freely move particles.

indices,  $*$  and  $R^*$  denote complex conjugate and complex conjugate representation. In Eq. (43), the particle type is characterized by the irrep  $R$ . The indices  $i$  and  $j$  label some internal degrees of freedom that can be changed by a local action. For a particle living on the vertex  $v$ , an arbitrary local action on this particle can be generated by the local operators  $B_{p,s}^h$  and  $A_v^g$  as

$$\sum_{h,g \in G} n_{h,g} B_{p,s}^h A_v^g, \quad (44)$$

where  $v \in s$ ,  $n_{h,g}$  is a coefficient. Mathematically, Eq. (44) can be viewed as an element of the quantum double algebra  $DG$  with basis  $\{D_{(h,g)} \equiv B_{p,s}^h A_v^g\}$  on a site  $s$ , see Appendix C.

We label the excited state with two particles as

$$|R; i, j\rangle = W_L(R; i, j) |GS\rangle. \quad (45)$$

Acting the local operators  $A_v^g$  and  $B_{p,s}^h$  on the excited state gives

$$A_{v=\partial_0 L}^g |R; i, j\rangle = \sum_k \Gamma_{ki}^R(g) |R; k, j\rangle, \quad (46)$$

$$A_{v=\partial_1 L}^g |R; i, j\rangle = \sum_k \Gamma_{kj}^{R^*}(g) |R; i, k\rangle, \quad (47)$$

$$B_{p,s}^h |R; i, j\rangle = \delta_{h,e} |R; i, j\rangle, \quad \forall (p, s), \quad (48)$$

where the derivations are collected in Appendix B. The local operator  $A_v^g$  changes the row (column) indices of  $\Gamma^R$  when acting on the starting (end) point of the string  $L$ . The particle label  $R$  is invariant under the action of the local operators. The indices  $i$  and  $j$  are related to the internal degrees of freedom of the particles on  $\partial_0 L$  and  $\partial_1 L$ .

Finally, we give the connecting rule of the string operator  $W_{L=L_1 \cup L_2}(R; i, j)$  for the particle as

$$W_{L_1 \cup L_2}(R; i, j) = \sum_k W_{L_2}(R; k, j) W_{L_1}(R; i, k). \quad (49)$$

Since the particles live on the endpoints of the string, the operator  $W_{L_1}(R; i, k)$  creates a pair of particles on vertex

$v_0 = \partial_0 L_1$  and  $v_1 = \partial_1 L_1$  respectively. This connecting rule allows us to move the particle from  $v_1 = \partial_1 L_1$  to  $v_2 = \partial_1 L_2$ . We can similarly move the particle on  $v_0 = \partial_0 L_1$  as well. The proof of Eq. (49) is provided in Appendix B.

### C. Loop excitations

Now we consider membrane operators for loops. Unlike the one-dimensional ribbon operators used for anyons in 2d topological orders, the operator that creates a loop excitation in 3d must be a two-dimensional thickened membrane that consists of a dual part and a direct part. The dual part is formed by dual plaquettes and the boundary of the dual part is related to the flux of the loop. Besides nontrivial flux, a loop can also carry some charge decorations. These charge decorations can freely travel along the boundary of the direct part that is formed by direct plaquettes.

We start by considering the simplest thickened membrane as shown in Fig. 11. The red plaquette is the dual part and cuts the edge  $vv'$ , the blue vertex  $v$  serves as the direct part and can be understood as an infinitesimal direct plaquette  $vv_1v_2v_3$ , where  $v = v_1 = v_2 = v_3$ . Now we consider the action of  $L_{vv'}^h$  on the edge  $vv'$  defined as (see Fig. 11)

$$L_{vv'}^h = \begin{cases} L_h^+, & \text{if } v \rightarrow v' \\ L_h^-, & \text{if } v \leftarrow v' \end{cases}. \quad (50)$$

That means, if the arrow of  $vv'$  points from the direct part to the dual part, i.e., from  $v$  to  $v'$ , we define  $L_{vv'}^h$  as  $L_h^+$  to change the group element on  $vv'$ . Otherwise, we define  $L_{vv'}^h$  as  $L_h^-$ . Since acting  $L_{vv'}^h$  violates  $B_p$  terms around  $vv'$ , we conclude that there exists a loop-like excited state living on the boundary the thickened membrane. To create a spatially larger loop excitation, we need to consider connecting several  $L_{vv'}^h$  terms.

As shown in Fig. 12, consider creating a loop-like excited state on the boundary of an open thickened membrane  $M_\alpha$ , whose dual part cuts  $\alpha$  edges. We set the arrows of edges to point from the direct part to the dual

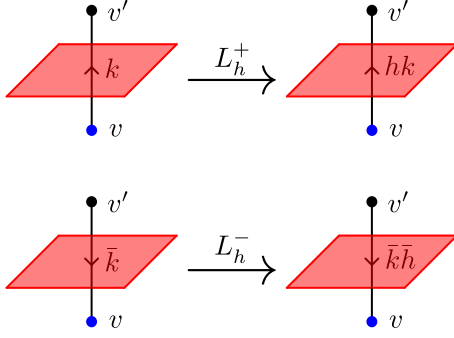


FIG. 11. The action of  $L_{vv'}^h$  on the edge  $vv'$  defined in Eq. (50). The red and blue denote the dual part and the direct part of the thickened membrane respectively. Since  $L_{vv'}^h$  only involves the edge  $vv'$ , the dual part is unique, which is the dual plaquette that cuts  $vv'$ . We choose the direct part as an infinitesimal direct plaquette  $vvvv$  here. However, the choice of the direct part is not unique and we can choose another plaquette  $p$  with finite area as the direct part, as long as  $v \in p$ .

part, and we start by acting  $L_{v_0v'_0}^h$  on  $v_0v'_0$ . We construct the operator  $L_{M_\alpha}^h$  by using a recursive procedure as follows. The  $L_{M_1}^h$  only acts on one edge  $v_0v'_0$  and is simply given by

$$L_{M_1}^h = L_{v_0v'_0}^h. \quad (51)$$

To obtain  $L_{M_2}^h$ , we need to connect  $L_{M_1}^h$  and  $L_{v_1v'_1}^{\bar{g}_0h_{g_0}}$  as

$$L_{M_2}^h = \sum_{g_0} L_{v_1v'_1}^{\bar{g}_0h_{g_0}} T_{v_0v_1}^{g_0} L_{M_1}^h = \sum_{g_0} L_{v_1v'_1}^{\bar{g}_0h_{g_0}} T_{v_0v_1}^{g_0} L_{v_0v'_0}^h. \quad (52)$$

The  $T_{v_0v_1}^{g_0}$  term is introduced to ensure that the  $L_{M_2}^h$  does not violate the plaquette term on  $v'_0v_0v_1v'_1$ . Keep connecting  $L_{M_2}^h$  and  $L_{v_2v'_2}^{\bar{g}_1h_{g_1}}$  produce  $L_{M_3}^h$  as

$$\begin{aligned} L_{M_3}^h &= \sum_{g_1} L_{v_2v'_2}^{\bar{g}_1h_{g_1}} T_{v_0v_2}^{g_1} L_{M_2}^h \\ &= \sum_{g_0, g_1} L_{v_2v'_2}^{\bar{g}_1h_{g_1}} T_{v_1v_2}^{\bar{g}_0g_1} L_{v_1v'_1}^{\bar{g}_0h_{g_0}} T_{v_0v_1}^{g_0} L_{v_0v'_0}^h, \end{aligned} \quad (53)$$

where  $T_{v_0v_2}^{g_1}$  acts on an arbitrary string whose endpoints are denoted by  $v_0$  and  $v_2$ . We choose the string to be  $(v_0, v_1, v_2)$  and use the connecting rule Eq. (36) of  $T_L^g$  to obtain the second line in the above equation. We can keep constructing operators that involve more edges. Generally, the connecting rule of  $L_{M_\alpha}^h$  is given by

$$L_{M_\alpha}^h = \sum_g L_{v_pv'_p}^{\bar{g}hg} T_{v_0v_p}^g L_{M_{\alpha-1}}^h, \quad (54)$$

where  $M_\alpha$  is obtained by cutting one more edge  $v_pv'_p$  than  $M_{\alpha-1}$  and  $T_{v_0v_p}^g$  acts on an arbitrary string with endpoints  $v_0$  and  $v_p$ . The vertices  $v_0$  and  $v_p$  live on the

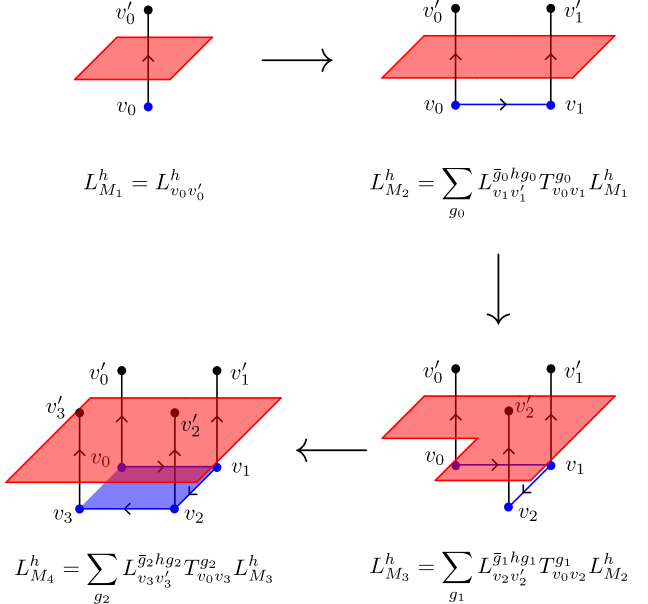


FIG. 12. Constructing the operator  $L_{M_\alpha}^h$ . We use red and blue to denote the dual part and the direct part respectively. Note that the choice of direct parts has some arbitrariness because we only demand that  $v_i$  lives on the direct part. Here, we choose infinitesimal direct plaquettes  $v_0v_0v_0v_0$ ,  $v_0v_0v_1v_1$ , and  $v_1v_1v_2v_2$  as the direct parts of  $M_1$ ,  $M_2 \setminus M_1$ , and  $M_3 \setminus M_2$ . The direct part of  $M_4 \setminus M_3$  is the plaquette  $v_0v_1v_2v_3$ , which has finite area. The loop-like excited state lives on the boundary of the thickened membrane  $M_\alpha$ , where  $\alpha$  indicates that the dual part cut  $\alpha$  edges.  $L_{M_\alpha}^h$  is obtained by using a recursive construction.

direct part, and the vertex  $v'_p$  lives on the dual part. If  $v_0 = v_p$ , then the term  $T_{v_0v_p}^g$  is defined as  $\delta_{g,e}$ , which means that Eq. (54) now becomes

$$L_{M_\alpha}^h = \sum_g L_{v_pv'_p}^{\bar{g}hg} \delta_{g,e} L_{M_{\alpha-1}}^h = L_{v_pv'_p}^h L_{M_{\alpha-1}}^h. \quad (55)$$

We further provide the connecting rule of two operators  $L_M^h$  and  $L_{M'}^{\bar{g}hg}$  from Eq. (54):

$$L_{M \cup M'}^h = \sum_g L_{M'}^{\bar{g}hg} T_{v_0v_p}^g L_M^h, \quad (56)$$

where  $M$  and  $M'$  are two membranes whose direct parts start at  $v_0$  and  $v_p$  respectively. The direct parts of the two membranes have no overlap, but the boundaries of dual parts have overlap. That is the case that the dual parts of  $M$  and  $M'$  do not cut the same edges. The direct parts of  $M$  and  $M'$  can always be chosen to satisfy that they share the common boundary and do not overlap in a finite area, see Fig. 12 as an example. To construct  $L_M^h$  and  $L_{M'}^h$ , we start by acting  $L_h^\pm$  on  $v_0v'_0$  and  $v_pv'_p$  respectively.

By using Eq. (56), we can create any open membrane operator that violates all plaquette terms along the boundary of the dual part of  $M$ . Besides the disk-like operator shown in Fig. 12, we can also construct a

cylinder-like operator as shown in Fig. 13. We consider four disk-like thickened membranes and label them as  $M_{0123}$ ,  $M_{0345}$ ,  $M_{4567}$ , and  $M_{1267}$ , where the subscripts imply which vertices are on the direct part. For example,  $M_{0123}$  means that the vertices  $v_0$ ,  $v_1$ ,  $v_2$ , and  $v_3$  are on the direct part and we construct the corresponding disk-like operators by acting  $L_h^{\pm}$  on the edge that contains the vertex  $v_0$  first. By using Eqs. (55) and (56), we connect operators  $L_{M_{0123}}^h$  and  $L_{M_{0345}}^h$  as

$$L_{M_{0123} \cup M_{0345}}^h = \sum_g L_{M_{0345}}^{\bar{g}hg} \delta_{g,e} L_{M_{0123}}^h = L_{M_{0345}}^h L_{M_{0123}}^h, \quad (57)$$

where both  $L_{M_{0123}}$  and  $L_{M_{0345}}$  start at the edge that contains vertex  $v_0$ , thus we have  $T_{v_0 v_p}^g = \delta_{g,e}$ . Continuing to connect the remaining operators, we have:

$$\begin{aligned} L_{M_{0123} \cup M_{0345} \cup M_{4567}}^h &= \sum_g L_{M_{4567}}^{\bar{g}hg} T_{v_0 v_4}^g L_{M_{0123} \cup M_{0345}}^h \\ &= \sum_g L_{M_{4567}}^{\bar{g}hg} T_{v_0 v_4}^g L_{M_{0123}}^h L_{M_{0345}}^h. \end{aligned} \quad (58)$$

Finally, we derive the cylinder-like operator

$$\begin{aligned} L_{M_{\text{cylinder}}}^h &= \sum_k L_{M_{1267}}^{\bar{k}hk} T_{v_0 v_1}^k L_{M_{0123} \cup M_{0345} \cup M_{4567}}^h \\ &= \sum_{g,k} L_{M_{1267}}^{\bar{k}hk} T_{v_0 v_1}^k L_{M_{4567}}^{\bar{g}hg} T_{v_0 v_4}^g L_{M_{0345}}^h L_{M_{0123}}^h, \end{aligned} \quad (59)$$

where  $M_{\text{cylinder}}$  is defined as  $M_{\text{cylinder}} = M_{0123} \cup M_{0345} \cup M_{4567} \cup M_{1267}$ . The plaquette terms are violated along the two boundaries of the dual part of the cylinder.

As shown in Appendix B, the connecting rule Eq. (54) ensures that the plaquette terms that live in the bulk of  $M$  are not violated by  $L_M^h$ . As for vertex terms, when  $G$  is non-Abelian, only  $A_{v_0}$  and  $A_{v'_0}$  are violated by  $L_M^h$ .

In the quantum double model, loops are characterized by a pair of data  $(C, R)$ , where  $C$  is the conjugacy class and  $R$  is the irrep of the centralizer of  $C$ . We write a membrane operator for loops as

$$W_M(C, R; c, j; c', j') = \sum_{g \in Z_r} \Gamma_{jj'}^{R^*}(g) L_M^c T_P^{q_c g \bar{q}_{c'}}, \quad (60)$$

where  $M$  is the thickened membrane,  $R^*$  denotes complex conjugate representation,  $c \in C$ ,  $Z_r$  is the centralizer of the representative  $r$  of the conjugacy class  $C = \{q_c r \bar{q}_c \mid q_c \in G\}$ . Given a fixed  $r \in C$ , for an arbitrary element  $c \in C$ , there are generally different choices of  $q_c$  satisfying  $c = q_c r \bar{q}_c$ . Thus, we need to pre-select  $r$  and  $q_c$  for given  $C$  and  $c$ .  $j$  and  $j'$  are row and column indices of the matrix  $\Gamma_{jj'}^{R^*}(g)$ . In the later discussion, we will see that  $c$ ,  $c'$ ,  $j$  and  $j'$  are just some local degrees of freedom and they can be changed by local operators.  $P$  is an arbitrary open string that lives

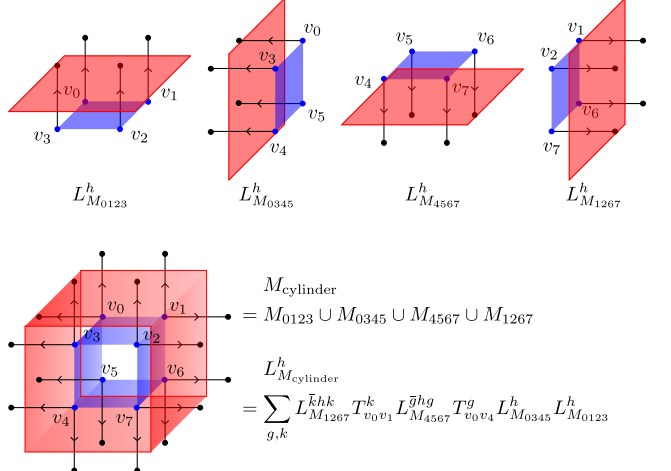


FIG. 13. Constructing the operator  $L_{M_{\text{cylinder}}}^h$ . We use red and blue to denote the dual part and the direct part respectively. We connect four disk-like operators to form a cylinder-like operator. For a disk-like membrane, the subscript implies which vertices are on the direct part, and the first number in the subscript implies the starting position of the corresponding operator.

on the direct part of the thickened membrane  $M$ . Besides,  $P$  ends on the boundary of the direct part of  $M$ . For example, consider the membrane  $M_4$  shown in the Fig. 12, where we use blue color to denote the direct part. The boundary of the direct part of  $M$  is a closed path  $(v_0, v_1, v_2, v_3, v_0)$ , so choices such as  $P = (v_0, v_1)$ ,  $P = (v_1, v_0, v_3)$ ,  $P = (v_0, v_1, v_2, v_3)$ , etc, are all legitimate. If we consider a cylinder-like membrane shown in the Fig. 13, the boundaries of the direct part consist of two closed paths  $(v_0, v_1, v_5, v_6, v_0)$  and  $(v_2, v_3, v_4, v_7, v_2)$ . We are allowed to choose  $P = (v_0, v_3)$ , or  $P = (v_0, v_3, v_2)$ , or  $P = (v_3, v_2, v_7, v_6)$ , etc, as long as the two endpoints of  $P$  are on the two closed paths respectively.

The conjugacy class  $C$  is viewed as the flux of the loop and it is related to the  $L_M^c$  term in Eq. (60). The irrep  $R$  is viewed as the charge decoration of the loop and is related to the  $T_P^{q_c g \bar{q}_{c'}}$  term in Eq. (60). Physically, the charge decoration is allowed to freely travel along the loop excitation. Thus, if we consider the thickened membrane  $M$  in Eq. (60) to be a disk-like membrane similar to those in Fig. 12, there will be a pair of charge and anti-charge decorations on a loop excitation. We can move the decorations and annihilate them, which results in a pure loop (i.e., without charge decorations). To encompass the decorated loops, we need to consider the  $M$  to be a cylinder-like membrane as shown in Fig. 13, and let the two endpoints of the string  $P$  live on the two boundaries of the direct part of the cylinder membrane. In this case, we create a pair of loop and anti-loop, and they carry the charge decoration and the anti-charge decoration respectively. Besides, the operator Eq. (60) automatically becomes a string operator Eq. (43) for a pair of particle and anti-particle when we set  $c = e$ . In the following

discussion, we only consider  $M$  to be a cylinder-like membrane.

For the operator  $W_M(C, R; c, j; c', j')$ , we denote the two boundaries of  $M$  as  $\partial_0 M$  and  $\partial_1 M$ . Without loss of generality, we consider that the  $L_M^c$  term acts on the edge  $v_0 v'_0 \ni p_0$  first, and the last edge acted on by the  $L_M^c$  term is denoted by  $v_1 v'_1 \ni p_1$ , where plaquettes  $p_0$  and  $p_1$  are violated. We set  $\partial_0 P = v_0$ ,  $\partial_1 P = v_1$ , and demand that  $v_0$  and  $p_0$  form a site  $s_0 = (v_0, p_0)$ ,  $v_1$  and  $p_1$  form a site  $s_1 = (v_1, p_1)$ . A state for a pair of loops is written as  $W_M(C, R; c, j; c', j') |GS\rangle$ . As shown in Appendix B, all local actions on the boundary  $\partial_0 M$  ( $\partial_1 M$ ) can be derived by considering the actions of  $A_{v_0}^g$  ( $A_{v_1}^g$ ) and  $B_{p_0, s_0}^h$  ( $B_{p_1, s_1}^h$ ) on the site  $s_0$  ( $s_1$ ). On the site  $s_0 \in \partial_0 M$ , the actions of local operators are given by

$$A_{v_0}^g W_M(C, R; c, j; c', j') |GS\rangle = \sum_i \Gamma_{ij}^R (\bar{q}_{gc\bar{g}} g q_c) W_M(C, R; gc\bar{g}, i; c', j') |GS\rangle, \quad (61)$$

$$B_{p_0, s_0}^h W_M(C, R; c, j; c', j') |GS\rangle = \delta_{c, h} W_M(C, R; c, j; c', j') |GS\rangle. \quad (62)$$

On the site  $s_1 \in \partial_1 M$ , we have

$$A_{v_1}^g W_M(C, R; c, j; c', j') |GS\rangle = \sum_i \Gamma_{ij'}^{R^*} (\bar{q}_{gc'\bar{g}} g q_{c'}) W_M(C, R; c, j; gc'\bar{g}, i) |GS\rangle, \quad (63)$$

$$B_{p_1, s_1}^h W_M(C, R; c, j; c', j') |GS\rangle = \delta_{c', h} W_M(C, R; c, j; c', j') |GS\rangle. \quad (64)$$

The label  $(C, R)$  is conserved under the actions of local operators, which justifies the statement: a topological excitation is characterized by a pair of data  $(C, R)$ . The local degrees of freedom  $c$  ( $c'$ ) and  $j$  ( $j'$ ) can be changed by the local operators on the site  $s_0$  ( $s_1$ ), leading to the conclusion that  $c$  ( $c'$ ) and  $j$  ( $j'$ ) label the internal degrees of freedom of the loop living on the boundary  $\partial_0 M$  ( $\partial_1 M$ ).

## IV. FUSION RULES

### A. General consideration

Now we consider the process of fusing topological excitations in the 3d quantum double model. In Sec. III B and III C, we have introduced the operators for excitations and the corresponding connecting rules of these operators, which allow us to create, move, and deform excitations. To encompass both pure loops and decorated loops, we choose the thickened membrane  $M$  in Eq. (60) to be cylinder-like and write the state for a pair of loops living on the two boundaries of  $M$  as  $W_M(C, R; c, j; c', j') |GS\rangle$ . Thus, the Hilbert space  $\mathcal{H}_{(C, R)}$  of the two loops is spanned by the set of basis

$$\{W_M(C, R; c, j; c', j') |GS\rangle \mid c, c' \in C; j, j' = 1, \dots, n_R\}, \quad (65)$$

where  $n_R$  is the dimension of the irrep  $R$ . We call  $\mathcal{H}_{(C, R)}$  an invariant space under the local actions Eq. (44) because for any vector  $|w\rangle \in \mathcal{H}_{(C, R)}$ , we have  $(\sum_{h, g \in G} n_{h, g} B_{p, s}^h A_v^g) |w\rangle \in \mathcal{H}_{(C, R)}$ .

The dimension of the space  $\mathcal{H}_{(C, R)}$  is given by  $|C|^2 \dim(R)^2$ . If we consider all possible conjugacy classes  $C$  and irreps  $R$  of the centralizer subgroup of  $C$ , the total dimension becomes

$$\sum_{C, R} |C|^2 \dim(R)^2 = \sum_C |C|^2 \frac{|G|}{|C|} = |G| \sum_C |C| = |G|^2. \quad (66)$$

It follows that for  $\bigoplus_{(C, R)} \mathcal{H}_{(C, R)}$ , a factor of  $|G|$  in the local dimension is carried by the two boundaries of  $M$ .

Eqs. (61) and (62) (Eqs. (63) and (64)) show that local operators on the boundaries  $\partial_0 M$  ( $\partial_1 M$ ) only change the labels  $c$  and  $j$  ( $c'$  and  $j'$ ). Thus, under the local actions, the Hilbert space  $\mathcal{H}_{(C, R)}$  can be written as

$$\mathcal{H}_{(C, R)} = V_{(C, R)} \otimes V_{(\bar{C}, R^*)}, \quad (67)$$

where  $\otimes$  means tensor product,  $\bar{C} = \{g\bar{c}\bar{g} \mid g \in G\}$ ,  $R^*$  denotes the complex conjugate representation.  $V_{(C, R)}$  and  $V_{(\bar{C}, R^*)}$  are local spaces of the loop  $[C, R]$  and the anti-loop  $[\bar{C}, R^*]$  living on  $\partial_0 M$  and  $\partial_1 M$  respectively. When we focus on the area nearby the boundary  $\partial_0 M$ , we denote the state  $W_M(C, R; c, j; c', j') |GS\rangle$  in this area as  $|c, j\rangle_{(C, R)}$  because  $c'$  and  $j'$  are invariant under the local actions.  $|c, j\rangle_{(C, R)}$  only labels the local internal degrees of freedom  $c$  and  $j$  of the loop  $[C, R]$  living on  $\partial_0 M$ . Thus, by exhausting all  $c$  and  $j$  with fixed  $c'$  and  $j'$ , we obtain a set of basis

$$\{|c, j\rangle_{(C, R)} \mid c \in C, j = 1, \dots, n_R\}, \quad (68)$$

which spans the local space  $V_{(C, R)}$  of the loop  $[C, R]$ . The local space  $V_{(C, R)}$  is invariant under the local actions nearby the boundary  $\partial_0 M$ . Similarly, the invariant local space  $V_{(\bar{C}, R^*)}$  is spanned by

$$\{|c', j'\rangle_{(\bar{C}, R^*)} \mid c' \in \bar{C}, j' = 1, \dots, n_R\}, \quad (69)$$

where  $|c', j'\rangle_{(\bar{C}, R^*)}$  labels the local internal degrees of freedom  $c', j'$  of the anti-loop  $[\bar{C}, R^*]$  living on  $\partial_1 M$  and is understood as the state  $W_M(C, R; c, j; c', j') |GS\rangle$  in the area nearby the boundary  $\partial_1 M$ .

The notations above also apply to the particles because Eq. (60) automatically becomes a string operator for a pair of particle and anti-particle when we set  $c = e$ . In this case,  $|c, j\rangle_{(C, R)}$  and  $|c', j'\rangle_{(\bar{C}, R^*)}$  are simplified as  $|j\rangle_{(R)}$  and  $|j'\rangle_{(R^*)}$  and they label the internal degrees of freedom on vertices  $\partial_0 P$  and  $\partial_1 P$ .

Consider a site  $s = (v_0, p_0)$  on the boundary  $\partial_0 M$  and we demand that the string  $P$  starts at  $v_0$ , then all possible

local actions on excitation  $[C, R]$  are given by Eq. (44), which form the quantum double algebra  $DG$  with basis  $\{D_{(h,g)} = B_{p,s}^h A_g^s\}$ . An irrep of the quantum double  $DG$  is also characterized by the pair  $(C, R)$ , and the action of  $DG$  on the corresponding representation space is given by Eqs. (C13) and (C14). By comparing Eqs. (61), (62) and Eqs. (C14), (C13), we can see that the local space  $V_{(C,R)}$  of the excitation  $[C, R]$  can be regarded as the representation space of the irrep. The action of  $DG$  on  $V_{(C,R)}$  is given by

$$\begin{aligned} & \Pi^{(C,R)} (D_{(h,g)}) |c, j\rangle_{(C,R)} \\ &= \sum_i \Gamma_{ij}^R (\bar{q}_{gc\bar{g}} g q_c) \delta_{h,gc\bar{g}} |gc\bar{g}, i\rangle_{(C,R)}, \end{aligned} \quad (70)$$

where  $\Pi^{(C,R)}$  is the irrep of  $DG$ . Details about the irreps of  $DG$  are shown in Appendix C. For  $V_{(\bar{C}, R^*)}$ , one can similarly regard it as the representation space of the irrep of  $DG$  labeled by  $(\bar{C}, R^*)$ . In the following discussion, we only need to focus on the local space  $V_{(C,R)}$  of the excitation  $[C, R]$  because mathematically,  $V_{(\bar{C}, R^*)}$  is just the dual space of  $V_{(C,R)}$ . The fusion and shrinking rules derived from  $V_{(\bar{C}, R^*)}$  are consistent with those derived from  $V_{(C,R)}$ .

If we move two excitations  $[C_1, R_1]$  and  $[C_2, R_2]$  to the same position  $\partial_0 M_1 = \partial_0 M_2$  as shown in Fig. 14, then the space on  $\partial_0 M_1$  is given by  $V_{(C_1, R_1)} \otimes V_{(C_2, R_2)}$ , which forms a representation space of a tensor product representation  $\Pi^{(C_1, R_1)} \otimes \Pi^{(C_2, R_2)}$ . Generally, the tensor product representation decomposes as

$$\Pi^{(C_1, R_1)} \otimes \Pi^{(C_2, R_2)} = \bigoplus_{(C, R)} N_{(C, R)}^{(C_1, R_1)(C_2, R_2)} \Pi^{(C, R)},$$

$$V_{(C_1, R_1)} \otimes V_{(C_2, R_2)} = \bigoplus_{(C, R)} N_{(C, R)}^{(C_1, R_1)(C_2, R_2)} V_{(C, R)}, \quad (71)$$

where  $\oplus$  is the direct sum that exhausts all possible choices of  $(C, R)$ . The equation above is deemed as the fusion rules Eq. (1) of the quantum double, with the fusion coefficient  $N_{(C, R)}^{(C_1, R_1)(C_2, R_2)}$  given by

$$\begin{aligned} & N_{(C, R)}^{(C_1, R_1)(C_2, R_2)} \\ &= \frac{1}{|G|} \sum_{h,g} \text{tr} [\Pi^{(C_1, R_1)} \otimes \Pi^{(C_2, R_2)} (\Delta (D_{(h,g)}))] \\ & \times \{ \text{tr} [\Pi^{(C, R)} (D_{(h,g)})] \}^*, \end{aligned} \quad (72)$$

where  $*$  means complex conjugate and we define

$$\Delta (D_{(h,g)}) = \sum_{k \in G} D_{(h\bar{k}, g)} \otimes D_{(k, g)}. \quad (73)$$

If  $N_{(C, R)}^{(C_1, R_1)(C_2, R_2)}$  does not vanish, then there are  $N_{(C, R)}^{(C_1, R_1)(C_2, R_2)}$  channels to fuse  $[C_1, R_1]$  and  $[C_2, R_2]$  to  $[C, R]$ . We use the fusion diagram shown in Fig. 1 to represent these fusion channels.

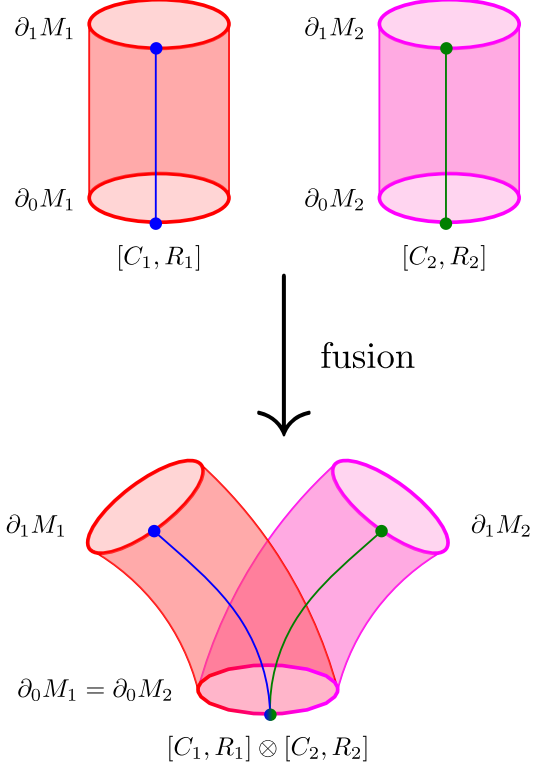


FIG. 14. Fusing two excitations. As shown on the top, we consider the excitations  $[C_1, R_1]$  and  $[C_2, R_2]$  living on the two boundaries  $\partial_1 M_1$  and  $\partial_1 M_2$  respectively. The red and purple denote the operators  $L_{M_1}^{c_1 \in \bar{C}_1}$  and  $L_{M_2}^{c_2 \in \bar{C}_2}$  in Eq. (60) respectively and the blue and green denote the operators  $T_{P_1}^{q_{c_1} g \bar{q}_{c_1'}}$  and  $T_{P_2}^{q_{c_2} g \bar{q}_{c_2'}}$  in Eq. (60) respectively. We bring  $[C_1, R_1]$  and  $[C_2, R_2]$  to a common position  $\partial_0 M_1 = \partial_0 M_2$  to implement the fusion process.

## B. Example of Abelian fusion rules

Here, we provide an example of Abelian fusion rules in the 3d quantum double model. Consider an Abelian group  $G = \mathbb{Z}_N$  and denote the generator of  $\mathbb{Z}_N$  by  $g$ . A group element can be written as  $g^\alpha$ , and  $g^\alpha$  itself forms a conjugacy class. Since the corresponding centralizer is  $Z_{g^\alpha} = G$ , and  $G$  has  $|G|$  one-dimensional irreps, we find  $|G| \times |G|$  excitations labeled by  $[g^\alpha, R^{(\beta)}]$ , where  $\alpha, \beta = 0, 1, 2, \dots, |G| - 1$  and  $R^{(\beta)}$  labels an irrep. We write  $\Gamma^{R^{(\beta)}} (g^\alpha) = \omega^{\alpha\beta}$  with  $\omega = \exp(2\pi i/N)$ . Since  $G$  is an Abelian group, the tensor product representation is directly given by

$$\begin{aligned} & \Pi^{(g^{\alpha_1}, R^{(\beta_1)})} \otimes \Pi^{(g^{\alpha_2}, R^{(\beta_2)})} \\ &= \Pi^{(g^{(\alpha_1 + \alpha_2 \bmod N)}, R^{(\beta_1 + \beta_2 \bmod N)})}, \end{aligned} \quad (74)$$

which leads to the fusion rules:

$$\begin{aligned} & \left[ g^{\alpha_1}, R^{(\beta_1)} \right] \otimes \left[ g^{\alpha_2}, R^{(\beta_2)} \right] \\ &= \left[ g^{(\alpha_1+\alpha_2 \bmod N)}, R^{(\beta_1+\beta_2 \bmod N)} \right]. \end{aligned} \quad (75)$$

The corresponding fusion diagram can be obtained by writing  $\mathbf{a}$ ,  $\mathbf{b}$ , and  $\mathbf{c}$  as  $[g^{\alpha_1}, R^{(\beta_1)}]$ ,  $[g^{\alpha_2}, R^{(\beta_2)}]$ , and  $[g^{(\alpha_1+\alpha_2 \bmod N)}, R^{(\beta_1+\beta_2 \bmod N)}]$  respectively, and writing  $\mu = 1$  in Fig. 1.

### C. Example of non-Abelian fusion rules

From Eq. (70) we see that when the group  $G$  is Abelian, the irrep of the quantum double  $DG$  is one-dimensional, which indicates that there are only Abelian fusion rules. To obtain non-Abelian fusion rules, we need to consider a non-Abelian group. Here, we take the simplest non-Abelian group  $G = \mathbb{D}_3$  as an example. The  $\mathbb{D}_3$  group has two generators  $r$  and  $t$ , which satisfy  $r^3 = t^2 = e$ ,  $rt = tr^2$ . We label the three conjugacy classes in  $\mathbb{D}_3$  as

$$C_e = \{e\}, \quad C_r = \{r, r^2\}, \quad C_t = \{t, tr, tr^2\}, \quad (76)$$

where  $e$ ,  $r$ , and  $t$  serve as the representatives of the classes  $C_e$ ,  $C_r$ , and  $C_t$  respectively. Their corresponding centralizers are

$$Z_e = \mathbb{D}_3, \quad Z_r = \{e, r, r^2\} \simeq \mathbb{Z}_3, \quad Z_t = \{e, t\} \simeq \mathbb{Z}_2, \quad (77)$$

where  $\simeq$  denotes isomorphism. To choose a set of  $q_c$  in Eq. (60), we need to consider  $Q_g = G/Z_g$  as follows

$$Q_e = \{e\}, \quad Q_r = \{e, t\}, \quad Q_t = \{e, r, r^2\}. \quad (78)$$

A natural choice for  $\mathbb{D}_3$  is  $q_e = q_r = q_t = e$ ,  $q_{r^2} = t$ ,  $q_{tr} = r$ , and  $q_{tr^2} = r^2$ . Thus, there are eight topological excitations and we label them as

$$\begin{aligned} & [Id], \quad [A], \quad [B], \quad [C_r, Id], \\ & [C_r, \omega], \quad [C_r, \omega^2], \quad [C_t, Id], \quad [C_t, -], \end{aligned} \quad (79)$$

where we write the particles  $[C_e, Id]$ ,  $[C_e, A]$ , and  $[C_e, B]$  as  $[Id]$ ,  $[A]$ , and  $[B]$  respectively for simplicity.  $Id$  is the 1d trivial representation,  $A$  and  $B$  are the nontrivial 1d and 2d representations of  $\mathbb{D}_3$  respectively.  $\omega$  and  $\omega^2$  are two nontrivial 1d representations of  $\mathbb{Z}_3$  respectively.  $-$  is the nontrivial 1d representation of  $\mathbb{Z}_2$ . We choose the representation matrices of the generators of  $\mathbb{D}_3$  to be

$$\begin{aligned} \Gamma^A(t^n r^m) &= (-1)^n, & \Gamma^-(t) &= -1, \\ \Gamma^B(t) &= \begin{pmatrix} 0 & 1 \\ 1 & 0 \end{pmatrix}, & \Gamma^B(r) &= \begin{pmatrix} \omega & 0 \\ 0 & \omega^2 \end{pmatrix}, \\ \Gamma^\omega(r^m) &= \omega^m, & \Gamma^{\omega^2}(r^m) &= \omega^{2m}, \end{aligned} \quad (80)$$

where  $\omega = \exp(2\pi i/3)$ . By using Eq. (72), we derive all fusion rules as shown in Table I. For an excitation  $\mathbf{a}$ , we

can define a matrix  $N_{\mathbf{a}}$  with matrix elements  $(N_{\mathbf{a}})_{bc} = N_{\mathbf{c}}^{ab}$ . The greatest eigenvalue  $d_{\mathbf{a}}$  of the matrix  $N_{\mathbf{a}}$  is called the quantum dimension of  $\mathbf{a}$ . All quantum dimensions of excitations in the  $G = \mathbb{D}_3$  quantum double model are shown in Table II.

## V. SHRINKING RULES AND FUSION-SHRINKING CONSISTENCY

### A. General consideration

The presence of the loop excitations in the 3d topological orders leads to nontrivial shrinking rules, which determine how loops are shrunk into particles. Consider a cylinder-like membrane  $M$  that creates a pair of loop and anti-loop as shown in Fig. 15. The red membrane supports the  $L_M^c$  operator and the blue string supports the  $T_P^{q_c g \bar{q}_{c'}}$  operators. Recall the connecting rule Eq. (56), since the operator  $L_c^\pm$  has the inverse  $L_{\bar{c}}^\pm$ , we can shrink a membrane  $M \cup M'$  to a smaller one  $M$  (by smaller we mean  $M$  cuts fewer edges) as

$$L_M^c = L_{M'}^{g \bar{c} \bar{q}} L_{M \cup M'}^c. \quad (81)$$

When the dual parts of  $M'$  and  $M \cup M'$  cut the same edges, Eq. (81) allows us to shrink a cylinder-like membrane to an infinitesimal thin cylinder, which behaves as a string operator. In Fig. 15, this shrinking process shrinks the flux of the loop to the vacuum, but the blue string is not affected. Even if we consider a loop without any charge decoration, after such a shrinking process, the end of the blue string may still behave as nontrivial particles. To be more specific, after the shrinking process, the operator in Eq. (60) becomes

$$\begin{aligned} \mathcal{S}(W_M(C, R; c, j; c', j')) &= \mathcal{S} \left( \sum_{g \in Z_r} \Gamma_{jj'}^{R^*}(g) L_M^c T_P^{q_c g \bar{q}_{c'}} \right) \\ &= \sum_{g \in Z_r} \Gamma_{jj'}^{R^*}(g) T_P^{q_c g \bar{q}_{c'}}. \end{aligned} \quad (82)$$

If we choose the irrep  $R$  to be the trivial representation which corresponds to zero charge decoration, the operator on the right hand side is

$$\sum_{g \in Z_r} \Gamma^{Id}(g) T_P^{q_c g \bar{q}_{c'}} = \sum_{g \in Z_r} T_P^{q_c g \bar{q}_{c'}}, \quad (83)$$

where  $Id^* = Id$ . This operator generally does not commute with the vertex terms  $A_{v_0=\partial_0 P}$  and  $A_{v_1=\partial_1 P}$ . Thus, acting this operator on the ground state creates excited vertices  $v_0 = \partial_0 P$  and  $v_1 = \partial_1 P$ .

In Sec. IV, we have shown that the set of basis  $\{W_M(C, R; c, j; c', j') | GS\}$  spans the Hilbert space  $\mathcal{H}_{(C,R)}$  of a pair of excitations on the two boundaries  $\partial_0 M$  and  $\partial_1 M$  of the cylinder  $M$ . After the shrinking process, the set of basis becomes

$$\{\mathcal{S}(W_M(C, R; c, j; c', j')) | GS\} \mid c, c' \in C; j, j' = 1, \dots, n_R\}, \quad (84)$$

TABLE I. Fusion table for the  $\mathbb{D}_3$  quantum double model. There are eight excitations in the  $\mathbb{D}_3$  quantum double model.  $[Id]$  and  $[A]$  are Abelian particles.  $[B]$  is a non-Abelian particle.  $[C_r, Id]$ ,  $[C_r, \omega]$ ,  $[C_r, \omega^2]$ ,  $[C_t, Id]$ , and  $[C_t, -]$  are non-Abelian loops.

$\otimes$	$[Id]$	$[A]$	$[B]$	$[C_r, Id]$	$[C_r, \omega]$	$[C_r, \omega^2]$	$[C_t, Id]$	$[C_t, -]$
$[Id]$	$[Id]$	$[A]$	$[B]$	$[C_r, Id]$	$[C_r, \omega]$	$[C_r, \omega^2]$	$[C_t, Id]$	$[C_t, -]$
$[A]$	$[A]$	$[Id]$	$[B]$	$[C_r, Id]$	$[C_r, \omega]$	$[C_r, \omega^2]$	$[C_t, -]$	$[C_t, Id]$
$[B]$	$[B]$	$[B]$	$\oplus [A]$ $\oplus [B]$	$[Id]$ $\oplus [C_r, \omega]$ $\oplus [C_r, \omega^2]$	$[C_r, \omega]$ $\oplus [C_r, \omega^2]$	$[C_r, Id]$ $\oplus [C_r, \omega^2]$	$[C_r, Id]$ $\oplus [C_r, \omega]$	$[C_t, Id]$ $\oplus [C_t, -]$ $\oplus [C_t, -]$
$[C_r, Id]$	$[C_r, Id]$	$[C_r, Id]$	$\oplus [C_r, \omega]$ $\oplus [C_r, \omega^2]$	$[C_r, Id]$ $\oplus [A]$ $\oplus [Id]$	$[C_r, \omega^2]$ $\oplus [B]$	$[C_r, \omega]$ $\oplus [B]$	$[C_t, Id]$ $\oplus [C_t, -]$	$[C_t, Id]$ $\oplus [C_t, -]$
$[C_r, \omega]$	$[C_r, \omega]$	$[C_r, \omega]$	$\oplus [C_r, \omega^2]$	$[C_r, Id]$ $\oplus [B]$	$[C_r, \omega^2]$ $\oplus [A]$ $\oplus [Id]$	$[C_r, \omega]$ $\oplus [B]$	$[C_t, Id]$ $\oplus [C_t, -]$	$[C_t, Id]$ $\oplus [C_t, -]$
$[C_r, \omega^2]$	$[C_r, \omega^2]$	$[C_r, \omega^2]$	$\oplus [C_r, \omega]$	$[C_r, Id]$ $\oplus [B]$	$[C_r, \omega]$ $\oplus [B]$	$[C_r, Id]$ $\oplus [B]$	$[C_t, Id]$ $\oplus [C_t, -]$	$[C_t, Id]$ $\oplus [C_t, -]$
$[C_t, Id]$	$[C_t, Id]$	$[C_t, -]$	$\oplus [C_t, -]$	$[C_t, Id]$ $\oplus [C_t, -]$	$[C_t, Id]$ $\oplus [C_t, -]$	$[C_t, Id]$ $\oplus [C_t, -]$	$[Id]$ $\oplus [B]$ $\oplus [C_r, Id]$ $\oplus [C_r, \omega]$ $\oplus [C_r, \omega^2]$ $[A]$ $[Id]$	$[A]$ $\oplus [B]$ $\oplus [C_r, Id]$ $\oplus [C_r, \omega]$ $\oplus [C_r, \omega^2]$
$[C_t, -]$	$[C_t, -]$	$[C_t, Id]$	$\oplus [C_t, -]$	$[C_t, Id]$ $\oplus [C_t, -]$	$[C_t, Id]$ $\oplus [C_t, -]$	$[C_t, Id]$ $\oplus [C_t, -]$	$\oplus [B]$ $\oplus [C_r, Id]$ $\oplus [C_r, \omega]$ $\oplus [C_r, \omega^2]$	$\oplus [B]$ $\oplus [C_r, Id]$ $\oplus [C_r, \omega]$ $\oplus [C_r, \omega^2]$

TABLE II. Quantum dimension table for the  $\mathbb{D}_3$  quantum double model. The quantum dimension of  $\mathbf{a}$  is defined as the greatest eigenvalue of the matrix  $N_{\mathbf{a}}$ , whose elements are given by  $(N_{\mathbf{a}})_{bc} = N_c^{\mathbf{a}b}$ . We can obtain all the fusion coefficients in Table I.

Excitation	$[Id]$	$[A]$	$[B]$	$[C_r, Id]$	$[C_r, \omega]$	$[C_r, \omega^2]$	$[C_t, Id]$	$[C_t, -]$
Quantum dimension	1	1	2	2	2	2	3	3

which spans the Hilbert space

$$\mathcal{S}(\mathcal{H}_{(C,R)}) = \mathcal{S}(V_{(C,R)}) \otimes \mathcal{S}(V_{(\bar{C},R^*)}). \quad (85)$$

On the boundary  $\partial_0 M$ , the local space denoted by  $\mathcal{S}(V_{(C,R)})$  is spanned by

$$\left\{ \mathcal{S}(|c, j\rangle_{(C,R)}) \mid c \in C, j = 1, \dots, n_R \right\}. \quad (86)$$

Under the action of the quantum double  $DG$  (i.e., the local action Eq. (44)), the space  $\mathcal{S}(V_{(C,R)})$  decomposes as a direct sum of its invariant subspace:

$$\mathcal{S}(V_{(C,R)}) = \bigoplus_{R'} S_{(C_e, R')}^{(C,R)} V_{(C_e, R')}, \quad (87)$$

where  $S_{(C_e, R')}^{(C,R)}$  is the shrinking coefficient,  $C_e = \{e\}$ ,  $R'$  denotes an irrep of  $G$ . The equation above is understood as the shrinking rules Eq. (2).

To derive the explicit form of the shrinking coefficient, we express the membrane operator  $\mathcal{S}(W_M(C, R; c, j; c', j'))$  as a linear combination of

the operators for particles:

$$\mathcal{S}(W_M(C, R; c, j; c', j')) = \sum_{R', i, i'} x(R', i, i') W_P(R; i, i'), \quad (88)$$

where  $x(R', i, i')$  is the undetermined coefficient, and  $R$  and  $R'$  denote irreps of the centralizer  $Z_r$  and the full group  $G$ , respectively. Substituting the explicit forms of  $W_M$  and  $W_P$  yields

$$\sum_{h \in Z_r} \Gamma_{jj'}^{R^*}(h) T_P^{q_c h \bar{q}_{c'}} = \sum_{R', i, i'} x(R', i, i') \sum_{g \in G} \Gamma_{ii'}^{R'^*}(g) T_P^g, \quad (89)$$

Substituting  $h = \bar{q}_c g q_{c'}$  into the left-hand side of the above equation, we obtain

$$\sum_{g \in q_c Z_r \bar{q}_{c'}} \Gamma_{jj'}^{R^*}(\bar{q}_c g q_{c'}) T_P^g = \sum_{R', i, i'} x(R', i, i') \sum_{g \in G} \Gamma_{ii'}^{R'^*}(g) T_P^g. \quad (90)$$

By comparing the coefficients in the front of  $T_P^g$  operator,

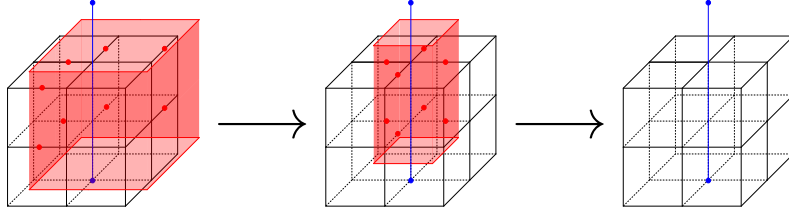


FIG. 15. The red denotes the dual part of  $M$  and all edges cut by the dual part are acted by operator  $L_M^c$ . We omit the direct part and only draw the blue string to represent the action of  $T_P^{q_c g \bar{q}_{c'}}$  because other edges on the direct part will not be acted by  $T_P^{q_c g \bar{q}_{c'}}$ . The flux of the loop lives on the boundaries of the direct part (red membrane) and we can shrink it to the vacuum. Yet, the blue string cannot be shrunk. After such a shrinking process, the end of the blue string generally behaves as a superposition of particles.

we obtain the equation

$$\delta_{g \in q_c Z_r \bar{q}_{c'}} \Gamma_{jj'}^{R^*} (\bar{q}_c g q_{c'}) = \sum_{R', i, i'} x(R', i, i') \Gamma_{ii'}^{R'^*} (g), \quad (91)$$

where  $\delta_{g \in q_c Z_r \bar{q}_{c'}}$  is defined to be 1 if  $g \in q_c Z_r \bar{q}_{c'}$  and 0 otherwise. Using the Schur orthogonality:

$$\frac{1}{|G|} \sum_g \Gamma_{ii'}^{R'^*} (g) \Gamma_{jj'}^{R''} (g) = \frac{1}{\dim(R')} \delta_{R', R''} \delta_{ij} \delta_{i'j'}, \quad (92)$$

we find the expression of  $x(R', i, i')$  as

$$\begin{aligned} & \sum_{g \in G} \sum_{R'', j, j'} x(R'', j, j') \Gamma_{jj'}^{R''*} (g) \Gamma_{ii'}^{R'} (g) \\ &= \sum_{R'', j, j'} x(R'', j, j') \frac{|G| \delta_{R'', R'} \delta_{ij} \delta_{i'j'}}{\dim(R'')} \\ &= \frac{|G|}{\dim(R')} x(R', i, i'). \end{aligned} \quad (93)$$

Using Eqs. (91) and (93), we have

$$\begin{aligned} x(R', i, i') &= \frac{\dim(R')}{|G|} \sum_{g \in G} \delta_{g \in q_c Z_r \bar{q}_{c'}} \Gamma_{jj'}^{R^*} (\bar{q}_c g q_{c'}) \Gamma_{ii'}^{R'} (g) \\ &= \frac{\dim(R')}{|G|} \sum_{h \in Z_r} \Gamma_{jj'}^{R^*} (h) \Gamma_{ii'}^{R'} (q_c h \bar{q}_{c'}), \end{aligned} \quad (94)$$

where we have used  $h = \bar{q}_c g q_{c'}$  to obtain the second line. By decomposing  $\Gamma_{ii'}^{R'} (q_c h \bar{q}_{c'})$  as

$$\Gamma_{ii'}^{R'} (q_c h \bar{q}_{c'}) = \sum_{k, l} \Gamma_{ik}^{R'} (q_c) \Gamma_{kl}^{R'} (h) \Gamma_{li'}^{R'} (\bar{q}_{c'}), \quad (95)$$

we finally obtain the explicit form of  $x(R', i, i')$ :

$$\begin{aligned} & x(R', i, i') \\ &= \frac{\dim(R')}{|G|} \sum_{k, l} \Gamma_{ik}^{R'} (q_c) \Gamma_{li'}^{R'} (\bar{q}_{c'}) \sum_{h \in Z_r} \Gamma_{jj'}^{R^*} (h) \Gamma_{kl}^{R'} (h). \end{aligned} \quad (96)$$

This gives the unique solution for the coefficient in the shrinking rule Eq. (88).

Let us now examine which particle excitation  $R' \in \text{Rep}(G)$  can appear after shrinking a loop excitation  $[C, R]$  in Eq. (88), where  $C$  is a conjugacy class of  $G$  and  $R \in \text{Rep}(Z_r)$ . The shrinking of a loop excitation forgets the conjugacy class  $C$  that labels its flux. Therefore, we need to understand how a representation  $R \in \text{Rep}(Z_r)$  decomposes into representations  $R' \in \text{Rep}(G)$ . In other words, we should view representation  $R$  of the subgroup  $Z_r$  as representation  $R'$  of the full group  $G$ .

A natural candidate is the *induction functor*  $\text{Ind}_{Z_r}^G$ , which maps an irrep  $R$  of the subgroup  $Z_r$  to a direct sum of irreps  $R'$  of  $G$ . The induction functor is adjoint to the restriction functor. It implies that a particle excitation  $R'$  appears after shrinking the loop excitation  $[C, R]$  if the representation  $R'$  of  $G$  restricts to  $R$  on the subgroup  $Z_r$ .

This is indeed confirmed by the last summation  $\sum_{h \in Z_r} \Gamma_{jj'}^{R^*} (h) \Gamma_{kl}^{R'} (h)$  in Eq. (96). We can first decompose  $R' \in \text{Rep}(G)$  into irreps of  $Z_r$ ; applying Eq. (92) then yields a delta function. We therefore conclude that  $x(R', i, i')$  vanishes unless  $R$  is contained in  $\text{Res}_{Z_r}^G(R')$ . Consequently, the loop excitation  $[C, R]$  can shrink to the particle excitation  $R'$  if and only if  $R$  is a subrepresentation of  $\text{Res}_{Z_r}^G(R')$ , or equivalently, by Frobenius reciprocity, if  $R'$  is a subrepresentation of  $\text{Ind}_{Z_r}^G(R)$ .

This result yields the direct sum decomposition of the space  $\mathcal{S}(V_{(C, R)})$  into the particle excitations  $[C_e, R']$ , where the irrep  $R'$  of  $G$  appears with the multiplicity given by its occurrence in the induced representation  $\text{Ind}_{Z_r}^G(R)$ . Explicitly, we have

$$\mathcal{S}(V_{(C, R)}) = \bigoplus_{R' \in \text{Irr}(G)} m_R(R') \cdot V_{(C_e, R')}, \quad (97)$$

where the multiplicity can be calculated from the inner product of the characters:  $m_R(R') = \langle \chi_{R'}, \text{Ind}_{Z_r}^G(\chi_R) \rangle_G = \langle \text{Res}_{Z_r}^G(\chi_{R'}), \chi_R \rangle_{Z_r}$ . This decomposition corresponds to the shrinking rule

$$\mathcal{S}([C, R]) = \bigoplus_{R' \in \text{Irr}(G)} m_R(R') \cdot [C_e, R']. \quad (98)$$

## B. Example of Abelian shrinking rules

To illustrate the shrinking rules more specifically, we take  $G = \mathbb{Z}_N$  and  $G = \mathbb{D}_3$  as two examples. We first consider  $G = \mathbb{Z}_N$ . As mentioned in Sec. IV B, an excitation can be labeled by  $[g^\alpha, R^{(\beta)}]$ , where  $g$  is the generator of the group  $G = \mathbb{Z}_N$ ,  $\alpha, \beta = 0, 1, 2, \dots, |G| - 1$  and  $R^{(\beta)}$  labels an irrep of  $G = \mathbb{Z}_N$ . The representation matrix is given by  $\Gamma^{R^{(\beta)}}(g^\alpha) = \omega^{\alpha\beta}$ , where  $\omega = \exp(2\pi i/N)$ . Thus, the operator for excitation  $[g^\alpha, R^{(\beta)}]$  is given by

$$\begin{aligned} W_M(g^\alpha, R^{(\beta)}) &= \sum_{\gamma=0}^{N-1} \omega^{-\beta\gamma} L_M^{g^\alpha} T_P^{g^\gamma} \\ &= \sum_{\gamma=0}^{N-1} \exp\left(\frac{-i2\pi\beta\gamma}{N}\right) L_M^{g^\alpha} T_P^{g^\gamma}. \end{aligned} \quad (99)$$

Since  $c, j, c', j'$  only have one possible choice, we omit these labels and simply write  $W_M(g^\alpha, R^{(\beta)}; g^\alpha, 1; g^\alpha, 1)$  as  $W_M(g^\alpha, R^{(\beta)})$  in the above equation. We use the procedure shown in Fig. 15 to shrink the flux part of  $[g^\alpha, R^{(\beta)}]$  and we obtain

$$\begin{aligned} \mathcal{S}(W_M(g^\alpha, R^{(\beta)})) &= \sum_{\gamma=0}^{N-1} \exp\left(\frac{-i2\pi\beta\gamma}{N}\right) T_P^{g^\gamma} \\ &= W_M(e, R^{(\beta)}), \end{aligned} \quad (100)$$

where  $W_M(e, R^{(\beta)})$  is exactly the operator for the particle  $[e, R^{(\beta)}]$ . From the above equation, we directly conclude that all shrinking rules in the 3d  $G = \mathbb{Z}_N$  quantum double model are Abelian and take the form

$$\mathcal{S}([g^\alpha, R^{(\beta)}]) = [e, R^{(\beta)}]. \quad (101)$$

The corresponding shrinking diagram is obtained by writing  $\mathbf{a}$  and  $\mathbf{b}$  as  $[g^\alpha, R^{(\beta)}]$  and  $[e, R^{(\beta)}]$  respectively, and writing  $\mu = 1$  in Fig. 2.

## C. Example of non-Abelian shrinking rules

Now we consider the shrinking rules when  $G = \mathbb{D}_3$ . Unlike the Abelian case, some excitations in the 3d  $G = \mathbb{D}_3$  quantum double model are non-Abelian, which means that there are some internal degrees of freedom in the corresponding operator. For example, according to Eq. (60) and the data about  $\mathbb{D}_3$  shown in Sec. IV C, the operators with different degrees of freedom for a pure loop (i.e.,

without charge decoration)  $[C_r, Id]$  are given by

$$\begin{aligned} W_M(C_r, Id; r; r) &= \sum_{g \in Z_r} \Gamma^{Id}(g) L_M^r T_P^g \\ &= L_M^r T_P^e + L_M^r T_P^r + L_M^r T_P^{r^2}, \end{aligned} \quad (102)$$

$$\begin{aligned} W_M(C_r, Id; r^2; r) &= \sum_{g \in Z_r} \Gamma^{Id}(g) L_M^{r^2} T_P^{tg} \\ &= L_M^{r^2} T_P^t + L_M^{r^2} T_P^{tr} + L_M^{r^2} T_P^{tr^2}, \end{aligned} \quad (103)$$

$$\begin{aligned} W_M(C_r, Id; r^2; r^2) &= \sum_{g \in Z_r} \Gamma^{Id}(g) L_M^{r^2} T_P^{tgt} \\ &= L_M^{r^2} T_P^e + L_M^{r^2} T_P^{r^2} + L_M^{r^2} T_P^r, \end{aligned} \quad (104)$$

$$\begin{aligned} W_M(C_r, Id; r; r^2) &= \sum_{g \in Z_r} \Gamma^{Id}(g) L_M^r T_P^{gt} \\ &= L_M^r T_P^t + L_M^r T_P^{tr^2} + L_M^r T_P^{tr}, \end{aligned} \quad (105)$$

where we omit the row and column indices  $j = j' = 1$  of the one-dimensional matrix. The internal degrees of freedom of the operator are labeled by the elements in the conjugacy class  $C_r = \{r, r^2\}$ .

Although  $[C_r, Id]$  does not carry any charge decoration, after the shrinking process, the remaining operator may still violate the vertex terms at the two ends of the string  $P$ . Focus on the local space on  $\partial_0 M$ , we fix  $c' = r$  and exhaust  $c \in C_r$  to obtain a set of basis in  $V_{(C_r, Id)}$ . When  $c = r$ , after the shrinking process as shown in Fig. 15, the flux part of  $[C_r, Id]$  vanishes and the operator shown in Eq. (102) becomes

$$\mathcal{S}(W_M(C_r, Id; r, r)) = T_P^e + T_P^r + T_P^{r^2}. \quad (106)$$

Notice that the operators for particles  $[Id]$  and  $[A]$  are given by

$$W_P(Id) = T_P^e + T_P^r + T_P^{r^2} + T_P^t + T_P^{tr} + T_P^{tr^2}, \quad (107)$$

$$W_P(A) = T_P^e + T_P^r + T_P^{r^2} - T_P^t - T_P^{tr} - T_P^{tr^2}, \quad (108)$$

where  $W_M(Id)$  and  $W_M(A)$  are the simplified notations of  $W_M(C_e, Id; e, 1; e, 1)$  and  $W_M(C_e, A; e, 1; e, 1)$ . Comparing the above equations, we have

$$\mathcal{S}(W_M(C_r, Id; r, r)) = \frac{1}{2} [W_P(Id) + W_P(A)]. \quad (109)$$

On the other hand, when  $c = r^2$ , after the shrinking process, the operator shown in Eq. (103) is given by

$$\mathcal{S}(W_M(C_r, Id; r^2, r)) = \frac{1}{2} [W_P(Id) - W_P(A)]. \quad (110)$$

To interpret these results as shrinking rules, we note that before the shrinking process, the space  $V_{(C_r, Id)}$  of  $[C_r, Id]$  is spanned by  $\{|r\rangle_{(C_r, Id)}, |r^2\rangle_{(C_r, Id)}\}$ , where we omit  $j = j' = 1$ . According to the discussion

in Sec. IV,  $|r\rangle_{(C_r, Id)}$  and  $|r^2\rangle_{(C_r, Id)}$  correspond to the states  $W_M(C_r, Id; r, r)|GS\rangle$  and  $W_M(C_r, Id; r^2, r)|GS\rangle$  nearby  $\partial_0 M$ . Eqs. (109) and (110) indicate that after the shrinking process, the set of basis transforms as

$$\mathcal{S}(|r\rangle_{(C_r, Id)}) = \frac{1}{2} \left[ |1\rangle_{(Id)} + |1\rangle_{(A)} \right], \quad (111)$$

$$\mathcal{S}(|r^2\rangle_{(C_r, Id)}) = \frac{1}{2} \left[ |1\rangle_{(Id)} - |1\rangle_{(A)} \right], \quad (112)$$

where we omit  $c = e$  and  $C_e$  for simplicity,  $|1\rangle_{(Id)}$  and  $|1\rangle_{(A)}$  correspond to the states  $W_P(Id)|GS\rangle$  and  $W_P(A)|GS\rangle$  nearby  $\partial_0 M$ . Now the space  $V_{(C_r, Id)}$  becomes  $\mathcal{S}(V_{(C_r, Id)})$ , which is spanned by

$$\left\{ \frac{1}{2} \left[ |1\rangle_{(Id)} + |1\rangle_{(A)} \right], \frac{1}{2} \left[ |1\rangle_{(Id)} - |1\rangle_{(A)} \right] \right\}. \quad (113)$$

Since the sets of basis  $\{|1\rangle_{(Id)}\}$  and  $\{|1\rangle_{(A)}\}$  span one-dimensional local spaces  $V_{(Id)}$  and  $V_{(A)}$  that are invariant under the action of the quantum double  $DG$ , the space  $\mathcal{S}(V_{(C_r, Id)})$  decomposes as

$$\mathcal{S}(V_{(C_r, Id)}) = V_{(Id)} \oplus V_{(A)}, \quad (114)$$

which gives the shrinking rule

$$\mathcal{S}([C_r, Id]) = [Id] \oplus [A]. \quad (115)$$

This result is consistent with Eq. (98) since  $\text{Ind}_{Z_r}^{\mathbb{D}_3}(Id)$  can be decomposed as

$$\text{Ind}_{Z_r}^{\mathbb{D}_3}(Id) = Id \oplus A. \quad (116)$$

One can also fix  $c' = r^2$  and exhaust  $c \in C_r$  to obtain the basis in  $V_{(C_r, Id)}$ , i.e., consider the operators shown in Eqs. (104) and (105), because physically the local actions nearby  $\partial_0 M$  cannot distinguish  $W_M(C, R; c, j; c', j')$  and  $W_M(C, R; c, j; c'', j'')$ . By using the same method, we will derive the same shrinking rule Eq. (115).

Similarly, we can derive all the shrinking rules in the 3d  $\mathbb{D}_3$  quantum double model. For simplicity, we omit  $C_e$  for particles,  $c$  and  $j$  labels when they only have one possible value in the following discussion. For  $[C_r, \omega]$ , the operators are given by

$$\begin{aligned} W_M(C_r, \omega; r, r) &= \sum_{g \in Z_r} \Gamma^{\omega^*}(g) L_M^r T_P^g \\ &= L_M^r T_P^e + \omega^2 L_M^r T_P^r + \omega L_M^r T_P^{r^2}, \end{aligned} \quad (117)$$

$$\begin{aligned} W_M(C_r, \omega; r^2, r) &= \sum_{g \in Z_r} \Gamma^{\omega^*}(g) L_M^{r^2} T_P^{tg} \\ &= L_M^{r^2} T_P^t + \omega^2 L_M^{r^2} T_P^{tr} + \omega L_M^{r^2} T_P^{tr^2}, \end{aligned} \quad (118)$$

where  $\omega = \exp(\frac{2\pi i}{3})$  and  $\omega^* = \omega^2$ . Note that only the first degree of freedom, i.e.,  $c$  in Eq. (60), is related to

the local space  $V_{(C, R)}$  on the boundary  $\partial_0 M$ . Thus, we need to exhaust the first degree of freedom. Here we fix the second degree of freedom as  $c' = r$ . One can also consider  $c' = r^2$ , which does not affect the final result. After the shrinking process, we have

$$\begin{aligned} \mathcal{S}(W_M(C_r, \omega; r, r)) &= T_P^e + \omega^2 T_P^r + \omega T_P^{r^2} \\ &= W_P(B; 1, 1), \end{aligned} \quad (119)$$

$$\begin{aligned} \mathcal{S}(W_M(C_r, \omega; r^2, r)) &= T_P^t + \omega^2 T_P^{tr} + \omega T_P^{tr^2} \\ &= W_P(B; 2, 1), \end{aligned} \quad (120)$$

where the operators for particle  $[B]$  are given by

$$\begin{aligned} W_P(B; 1; 1) &= \sum_{g \in G} \Gamma_{11}^{B^*}(g) L_M^e T_P^g \\ &= T_P^e + \omega^2 T_P^r + \omega T_P^{r^2}, \end{aligned} \quad (121)$$

$$\begin{aligned} W_P(B; 2; 2) &= \sum_{g \in G} \Gamma_{22}^{B^*}(g) L_M^e T_P^g \\ &= T_P^e + \omega T_P^r + \omega^2 T_P^{r^2}, \end{aligned} \quad (122)$$

$$\begin{aligned} W_P(B; 1; 2) &= \sum_{g \in G} \Gamma_{12}^{B^*}(g) L_M^e T_P^g \\ &= T_P^t + \omega T_P^{tr} + \omega^2 T_P^{tr^2}, \end{aligned} \quad (123)$$

$$\begin{aligned} W_P(B; 2; 1) &= \sum_{g \in G} \Gamma_{21}^{B^*}(g) L_M^e T_P^g \\ &= T_P^t + \omega^2 T_P^{tr} + \omega T_P^{tr^2}. \end{aligned} \quad (124)$$

The two operators  $W_P(B; 1, 1)$  and  $W_P(B; 2, 1)$  are related to the vectors  $|1\rangle_{(B)}$  and  $|2\rangle_{(B)}$ , which span the space  $V_{(B)}$ . Thus, we have

$$\mathcal{S}(V_{(C_r, \omega)}) = V_{(B)}, \quad (125)$$

which gives the Abelian shrinking rule

$$\mathcal{S}([C_r, \omega]) = [B]. \quad (126)$$

For  $[C_r, \omega^2]$ , we consider

$$\begin{aligned} W_M(C_r, \omega^2; r, r) &= \sum_{g \in Z_r} \Gamma^\omega(g) L_M^r T_P^g \\ &= L_M^r T_P^e + \omega L_M^r T_P^r + \omega^2 L_M^r T_P^{r^2}, \end{aligned} \quad (127)$$

$$\begin{aligned} W_M(C_r, \omega^2; r^2, r) &= \sum_{g \in Z_r} \Gamma^\omega(g) L_M^{r^2} T_P^{tg} \\ &= L_M^{r^2} T_P^t + \omega L_M^{r^2} T_P^{tr} + \omega^2 L_M^{r^2} T_P^{tr^2}. \end{aligned} \quad (128)$$

After the shrinking process, we have

$$\begin{aligned} \mathcal{S}(W_M(C_r, \omega^2; r, r)) &= T_P^e + \omega T_P^r + \omega^2 T_P^{r^2} \\ &= W_P(B; 2, 2), \end{aligned} \quad (129)$$

$$\begin{aligned} \mathcal{S}(W_M(C_r, \omega^2; r^2, r)) &= T_P^t + \omega T_P^{tr} + \omega^2 T_P^{tr^2} \\ &= W_P(B; 1, 2). \end{aligned} \quad (130)$$

The two operators  $W_P(B; 2, 2)$  and  $W_P(B; 1, 2)$  are also related to the vectors  $|2\rangle_{(B)}$  and  $|1\rangle_{(B)}$ . Thus, we have

$$\mathcal{S}(V_{(C_r, \omega^2)}) = V_{(B)}, \quad (131)$$

which leads to the shrinking rule

$$\mathcal{S}([C_r, \omega^2]) = [B]. \quad (132)$$

For  $[C_t, Id]$ , consider

$$\begin{aligned} W_M(C_t, Id; t, t) &= \sum_{g \in Z_t} \Gamma^{Id}(g) L_M^t T_P^g \\ &= L_M^t T_P^e + L_M^t T_P^t, \end{aligned} \quad (133)$$

$$\begin{aligned} W_M(C_t, Id; tr, t) &= \sum_{g \in Z_t} \Gamma^{Id}(g) L_M^{tr} T_P^{rg} \\ &= L_M^{tr} T_P^r + L_M^{tr} T_P^{tr^2}, \end{aligned} \quad (134)$$

$$\begin{aligned} W_M(C_t, Id; tr^2, t) &= \sum_{g \in Z_t} \Gamma^{Id}(g) L_M^{tr^2} T_P^{r^2g} \\ &= L_M^{tr^2} T_P^{r^2} + L_M^{tr^2} T_P^{tr}. \end{aligned} \quad (135)$$

After the shrinking process, we have

$$\begin{aligned} \mathcal{S}(W_M(C_t, Id; t, t)) &= T_P^e + T_P^t \\ &= \frac{1}{3} (W_P(B; 1, 1) + W_P(B; 1, 2) + W_P(B; 2, 1) \\ &\quad + W_P(B; 2, 2) + W_P(Id)), \end{aligned} \quad (136)$$

$$\begin{aligned} \mathcal{S}(W_M(C_t, Id; tr, t)) &= T_P^r + T_P^{tr^2} \\ &= \frac{1}{3} (\omega W_P(B; 1, 1) + \omega W_P(B; 1, 2) + \omega^2 W_P(B; 2, 1) \\ &\quad + \omega^2 W_P(B; 2, 2) + W_P(Id)), \end{aligned} \quad (137)$$

$$\begin{aligned} \mathcal{S}(W_M(C_t, Id; tr^2, t)) &= T_P^{r^2} + T_P^{tr} \\ &= \frac{1}{3} (\omega^2 W_P(B; 1, 1) + \omega^2 W_P(B; 1, 2) + \omega W_P(B; 2, 1) \\ &\quad + \omega W_P(B; 2, 2) + W_P(Id)). \end{aligned} \quad (138)$$

Thus,  $\mathcal{S}(V_{(C_t, Id)})$  has two invariant subspaces  $V_{(Id)}$  and  $V_{(B)}$ , which leads to the decomposition

$$\mathcal{S}(V_{(C_t, Id)}) = V_{(Id)} \oplus V_{(B)}, \quad (139)$$

and the shrinking rule

$$\mathcal{S}([C_t, Id]) = [Id] \oplus [B]. \quad (140)$$

TABLE III. Shrinking table for the 3d  $\mathbb{D}_3$  quantum double model. One can also use Eq. (98) to directly obtain these results.

Loop	$[C_r, Id]$	$[C_r, \omega]$	$[C_r, \omega^2]$	$[C_t, Id]$	$[C_t, -]$
$\mathcal{S}(\text{Loop})$	$[Id] \oplus [A]$	$[B]$	$[B]$	$[Id] \oplus [B]$	$[A] \oplus [B]$

For  $[C_t, -]$ , consider

$$\begin{aligned} W_M(C_t, -; t, t) &= \sum_{g \in Z_t} \Gamma^{-*}(g) L_M^t T_P^g \\ &= L_M^t T_P^e - L_M^t T_P^t, \end{aligned} \quad (141)$$

$$\begin{aligned} W_M(C_t, -; tr, t) &= \sum_{g \in Z_t} \Gamma^{-*}(g) L_M^{tr} T_P^{rg} \\ &= L_M^{tr} T_P^r - L_M^{tr} T_P^{tr^2}, \end{aligned} \quad (142)$$

$$\begin{aligned} W_M(C_t, -; tr^2, t) &= \sum_{g \in Z_t} \Gamma^{-*}(g) L_M^{tr^2} T_P^{r^2g} \\ &= L_M^{tr^2} T_P^{r^2} - L_M^{tr^2} T_P^{tr}. \end{aligned} \quad (143)$$

After the shrinking process, we have

$$\begin{aligned} \mathcal{S}(W_M(C_t, -; t, t)) &= T_P^e - T_P^t \\ &= \frac{1}{3} (W_P(B; 1, 1) - W_P(B; 1, 2) - W_P(B; 2, 1) \\ &\quad + W_P(B; 2, 2) + W_P(A)), \end{aligned} \quad (144)$$

$$\begin{aligned} \mathcal{S}(W_M(C_t, -; tr, t)) &= T_P^r - T_P^{tr^2} \\ &= \frac{1}{3} (\omega W_P(B; 1, 1) - \omega W_P(B; 1, 2) - \omega^2 W_P(B; 2, 1) \\ &\quad + \omega^2 W_P(B; 2, 2) + W_P(A)), \end{aligned} \quad (145)$$

$$\begin{aligned} \mathcal{S}(W_M(C_t, -; tr^2, t)) &= T_P^{r^2} - T_P^{tr} \\ &= \frac{1}{3} (\omega^2 W_P(B; 1, 1) - \omega^2 W_P(B; 1, 2) - \omega W_P(B; 2, 1) \\ &\quad + \omega W_P(B; 2, 2) + W_P(A)). \end{aligned} \quad (146)$$

The space  $\mathcal{S}(V_{(C_t, -)})$  decomposes as

$$\mathcal{S}(V_{(C_t, -)}) = V_{(A)} \oplus V_{(B)}, \quad (147)$$

which leads to the shrinking rule

$$\mathcal{S}([C_t, -]) = [A] \oplus [B]. \quad (148)$$

We collect all the shrinking rules in the 3d  $\mathbb{D}_3$  quantum double model in Table III. Although the five loops in the  $\mathbb{D}_3$  quantum double model are all non-Abelian excitations, only  $[C_r, Id]$ ,  $[C_t, Id]$ , and  $[C_t, -]$  have non-Abelian shrinking rules, while  $[C_r, \omega]$  and  $[C_r, \omega^2]$  have Abelian shrinking rules.

#### D. Controlling non-Abelian shrinking channels

Table III only shows us what shrinking channels are possible. For a non-Abelian loop, we can choose differ-

ent internal degrees of freedom to obtain different operators, which allows us to further control the loop to pick a determined shrinking channel in a shrinking process. For  $[C_r, Id]$ , we linearly combine the two operators  $W_M(C_r, Id; r, r)$  and  $W_M(C_r, Id; r^2, r)$  as

$$\begin{aligned} & [W_M(C_r, Id; r, r) \pm W_M(C_r, Id; r^2, r)] \\ &= \left[ \sum_{g \in Z_r} \Gamma^{Id}(g) L_M^r T_P^g \pm \sum_{g \in Z_r} \Gamma^{Id}(g) L_M^r T_P^{tg} \right] \\ &= L_M^r T_P^e + L_M^r T_P^r + L_M^r T_P^{r^2} \pm L_M^r T_P^t \pm L_M^r T_P^{tr} \\ &\quad \pm L_M^r T_P^{tr^2}. \end{aligned} \quad (149)$$

The operator above still corresponds to a vector  $|r\rangle_{(C_r, Id)} \pm |r^2\rangle_{(C_r, Id)}$  in the space  $V_{(C_r, Id)}$  and thus is a legitimate operator for excitation  $[C_r, Id]$ . The shrinking process will remove the flux part, i.e.,

$$\begin{aligned} & \mathcal{S}([W_M(C_r, Id; r, r) \pm W_M(C_r, Id; r^2, r)]) \quad (150) \\ &= T_P^e + T_P^r + T_P^{r^2} \pm T_P^t \pm T_P^{tr} \pm T_P^{tr^2} = \begin{cases} W_P(Id) & + \\ W_P(A) & - \end{cases}. \end{aligned}$$

The result above means that by choosing certain degrees of freedom, we can choose the shrinking channel to  $[Id]$  or  $[A]$ . We can use the shrinking diagram shown in Fig. 2 to describe these different channels. When we choose  $+$  in Eq. (149), we write **a** and **b** as  $[C_r, Id]$  and  $[Id]$  respectively in Fig. 2. When we choose  $-$  in Eq. (149), we write **a** and **b** as  $[C_r, Id]$  and  $[A]$  respectively in Fig. 2.

Similarly, we illustrate how to control other non-Abelian shrinking channels. For  $[C_t, Id]$ , notice that  $1 + \omega + \omega^2 = 0$ , we linearly combine the operators as follows to control the shrinking channel to  $[Id]$ :

$$\begin{aligned} & \mathcal{S}(W_M(C_t, Id; t, t) + W_M(C_t, Id; tr, t) \\ & \quad + W_M(C_t, Id; tr^2, t)) \\ &= W_P(Id). \end{aligned} \quad (151)$$

We can also linearly combine the operators as follows to control the shrinking channel to  $[B]$ :

$$\begin{aligned} & \mathcal{S}(3W_M(C_t, Id; t, t) - 3W_M(C_t, Id; tr, t)) \\ &= (1 - \omega) W_P(B; 1, 1) + (1 - \omega) W_P(B; 1, 2) \\ & \quad + (1 - \omega^2) W_P(B; 2, 1) + (1 - \omega^2) W_P(B; 2, 2). \end{aligned} \quad (152)$$

For  $[C_t, -]$ , we linearly combine the operators as follows to control the shrinking channel to  $[A]$ :

$$\begin{aligned} W_P(A) &= \mathcal{S}(W_M(C_t, -; t, t) + W_M(C_t, -; tr, t) \\ & \quad + W_M(C_t, -; tr^2, t)) \end{aligned} \quad (153)$$

We can also linearly combine the operators as follows to

control the shrinking channel to  $[B]$ :

$$\begin{aligned} & \mathcal{S}(3W_M(C_t, -; t, t) - 3W_M(C_t, -; tr, t)) \\ &= (1 - \omega) W_P(B; 1, 1) - (1 - \omega) W_P(B; 1, 2) \\ & \quad - (1 - \omega^2) W_P(B; 2, 1) + (1 - \omega^2) W_P(B; 2, 2). \end{aligned} \quad (154)$$

## E. Microscopic verification of consistency relations between fusion and shrinking

A systematic check using the fusion Table I and the shrinking Table III demonstrates that all fusion and shrinking processes satisfy the consistency condition Eq. (10) derived from the continuum topological field theory. For example, if we consider shrinking two excitations  $[C_r, Id]$  and  $[C_t, -]$  followed by fusion in the  $\mathbb{D}_3$  quantum double model, we have

$$\begin{aligned} \mathcal{S}([C_r, Id]) \otimes \mathcal{S}([C_t, -]) &= ([Id] \oplus [A]) \otimes ([A] \oplus [B]) \\ &= [Id] \oplus [A] \oplus 2 \cdot [B]. \end{aligned} \quad (155)$$

If we first fuse  $[C_r, Id]$  and  $[C_t, -]$ , and then perform the shrinking process, we have

$$\begin{aligned} \mathcal{S}([C_r, Id] \otimes [C_t, -]) &= \mathcal{S}([C_t, Id] \oplus [C_t, -]) \\ &= [Id] \oplus [A] \oplus 2 \cdot [B] \\ &= \mathcal{S}([C_r, Id]) \otimes \mathcal{S}([C_t, -]). \end{aligned} \quad (156)$$

We can similarly verify the consistency condition for other excitations. We conclude that Eq. (10) applies to the 3d quantum double model with arbitrary finite group  $G$ .

Another important property of the shrinking rules obtained from the continuum topological field theory is that the shrinking process preserves the quantum dimensions of the excitations, i.e.,

$$d_a = \sum_b S_b^a d_b, \quad (157)$$

where  $d_a$  and  $d_b$  are quantum dimensions of excitations **a** and **b** respectively. By using Tables II and III, we verify that Eq. (157) holds in our 3d quantum double model. As an illustration, consider the excitation  $[C_r, Id]$  in the  $\mathbb{D}_3$  quantum double model, which has  $d_{[C_r, Id]} = 2$ . Its shrinking rule yields  $[Id] \oplus [A]$ , where  $d_{[Id]} = d_{[A]} = 1$ , thus satisfying Eq. (157).

## VI. MICROSCOPIC CONSTRUCTION OF THE BF FIELD THEORY WITH AN AAB TWIST

### A. Overview

Within the framework of continuum field theory, the (3+1)D BF field theory with an *AAB* twist unveils a hidden layer of quantum statistical behavior in 3d topological phases. Unlike conventional particle-loop braiding,

where a phase arises from the direct winding of a particle around a loop, this theory supports braiding processes in which a particle moves around two unlinked loops without winding around either [25]. The resulting trajectory, together with the loops, forms intricate Brunnian structures such as the Borromean rings, i.e., a configuration in which all three components are pairwise unlinked yet collectively linked. Remarkably, the non-trivial Borromean rings braiding indicates that this theory exhibits non-Abelian topological order, despite the underlying gauge group  $G = \prod_i \mathbb{Z}_{N_i}$  being Abelian. It is important to note that Borromean rings braiding is not compatible with all multi-loop braiding processes, because a legitimate topological action cannot be written down to describe certain combinations of these processes [26]. This incompatibility stems from the requirement that the action for the twisted  $BF$  theory must be gauge invariant. Building on these results, Ref. [53] systematically computes all fusion and shrinking rules in the  $BF$  theory with an  $AAB$  twist and confirm the presence of non-Abelian fusion and shrinking rules. Moreover, these rules are shown to satisfy the consistency condition Eq. (10), which strongly constrains the associated fusion and shrinking coefficients.

In this section, we present the 3d  $\mathbb{D}_4$  quantum double model as a microscopic construction of the  $BF$  theory with an  $AAB$  twist. The fact that all nontrivial fusion and shrinking rules in the  $BF$  theory with an  $AAB$  twist are captured by the  $\mathbb{D}_4$  quantum double model allows us to establish a concrete correspondence between these two theories. This result not only confirms the data derived from the continuum field theory but also demonstrates how these data are encoded in the microscopic lattice model.

## B. Microscopic construction

Here, we present the basic data of the group  $G = \mathbb{D}_4$  and derive the fusion and shrinking rules in the  $\mathbb{D}_4$  quantum double model. Denote the two generators of  $G = \mathbb{D}_4$  by  $r$  and  $t$ , then we have  $r^4 = t^2 = e$  and  $rt = t\bar{r} = tr^3$ . We label the five conjugacy classes as

$$\begin{aligned} C_e &= \{e\}, \\ C_r &= \{r, r^3\}, \\ C_t &= \{t, tr^2\}, \\ C_{tr} &= \{tr, tr^3\}, \\ C_{r^2} &= \{r^2\}, \end{aligned} \quad (158)$$

where  $e$ ,  $r$ ,  $t$ ,  $tr$ , and  $r^2$  serve as the representative of the classes  $C_e$ ,  $C_r$ ,  $C_t$ ,  $C_{tr}$  and  $C_{r^2}$  respectively. Their

corresponding centralizers are

$$\begin{aligned} Z_e &= \mathbb{D}_4, \\ Z_r &= \{e, r, r^2, r^3\} \simeq \mathbb{Z}_4, \\ Z_t &= \{e, t, r^2, tr^2\} \simeq \mathbb{Z}_2 \times \mathbb{Z}_2, \\ Z_{tr} &= \{e, r^2, tr, tr^3\} \simeq \mathbb{Z}_2 \times \mathbb{Z}_2, \\ Z_{r^2} &= \mathbb{D}_4, \end{aligned} \quad (159)$$

where  $\simeq$  denotes isomorphism. Consider  $Q_g = G/Z_g$ , we have

$$\begin{aligned} Q_e &= \{e\}, \\ Q_r &= \{e, t\}, \\ Q_t &= \{e, r\}, \\ Q_{tr} &= \{e, r\}, \\ Q_{r^2} &= \{e\}. \end{aligned} \quad (160)$$

We choose  $q_e = q_r = q_t = q_{tr} = q_{r^2} = e$ ,  $q_{r^3} = t$ , and  $q_{tr^2} = q_{tr^3} = r$ . We label the five irreps of  $\mathbb{D}_4$  as  $Id$ ,  $\mathcal{R}$ ,  $\mathcal{T}$ ,  $\mathcal{RT}$ , and  $\mathcal{B}$ , where  $\mathcal{B}$  is a 2d irrep, others are 1d irreps. The representation matrices of the generators are given by

$$\begin{aligned} \Gamma^{Id}(g) &= 1, & \Gamma^{\mathcal{R}}(r) &= -1, \\ \Gamma^{\mathcal{R}}(t) &= 1, & \Gamma^{\mathcal{T}}(r) &= 1, \\ \Gamma^{\mathcal{T}}(t) &= -1, & \Gamma^{\mathcal{RT}}(r) &= \Gamma^{\mathcal{RT}}(t) = -1, \\ \Gamma^{\mathcal{B}}(r) &= \begin{pmatrix} 0 & -1 \\ 1 & 0 \end{pmatrix}, & \Gamma^{\mathcal{B}}(t) &= \begin{pmatrix} 1 & 0 \\ 0 & -1 \end{pmatrix}. \end{aligned} \quad (161)$$

The four 1d irreps of  $\mathbb{Z}_4 = \{e, r, r^2, r^3\}$  are labeled by  $Id$ ,  $\omega$ ,  $\omega^2$ , and  $\omega^3$ . The representation matrices of the generator are given by

$$\Gamma^{Id}(g) = 1, \quad \Gamma^{\omega^n}(r) = \omega^n, \quad (162)$$

where  $n = 1, 2, 3$  and  $\omega = \exp(\pi i/2) = i$ . The four 1d irreps of  $\mathbb{Z}_2 \times \mathbb{Z}_2 = \{e, a, b, ab\}$  are labeled by  $Id$ ,  $a$ ,  $b$ , and  $ab$ . The representation matrices of the generator are given by

$$\begin{aligned} \Gamma^{Id}(g) &= \Gamma^a(b) = \Gamma^b(a) = 1, \\ \Gamma^a(a) &= \Gamma^b(b) = \Gamma^{ab}(a) = \Gamma^{ab}(b) = -1. \end{aligned} \quad (163)$$

Thus, there are 22 excitations in the  $\mathbb{D}_4$  quantum double model. We label the 5 particles as

$$[Id], \quad [\mathcal{R}], \quad [\mathcal{T}], \quad [\mathcal{RT}], \quad [\mathcal{B}]. \quad (164)$$

The 17 loops are labeled by

$$\begin{aligned} [C_r, Id], \quad [C_r, \omega], \quad [C_r, \omega^2], \quad [C_r, \omega^3], \\ [C_t, Id], \quad [C_t, a], \quad [C_t, b], \quad [C_t, ab], \\ [C_{tr}, Id], \quad [C_{tr}, a], \quad [C_{tr}, b], \quad [C_{tr}, ab], \\ [C_{r^2}, Id], \quad [C_{r^2}, \mathcal{R}], \quad [C_{r^2}, \mathcal{T}], \quad [C_{r^2}, \mathcal{RT}], \\ [C_{r^2}, \mathcal{B}]. \end{aligned} \quad (165)$$

Using the same strategy shown in Sec. IV and Sec. V, we derive all the fusion rules (Tables IV and V) as well as the shrinking rules (Table VI).

TABLE IV. The first part of fusion table for the  $D_4$  quantum double model. The complete fusion table is a  $22 \times 22$  table. This table shows columns 1 to 11 and columns 12 to 22 are shown in Table V.

TABLE V. The second part of fusion table for the  $D_4$  quantum double model. The complete fusion table is a  $22 \times 22$  table. This table shows columns 12 to 22.

---

TABLE VI. Shrinking table for the 3d  $\mathbb{D}_4$  quantum double model.

Loop	$[C_r, Id]$	$[C_r, \omega]$	$[C_r, \omega^2]$	$[C_r, \omega^3]$	$[C_t, Id]$	$[C_t, a]$	$[C_t, b]$	$[C_t, ab]$	$[C_{tr}, Id]$
$\mathcal{S}$ (Loop)	$[Id] \oplus [\mathcal{T}]$	$[\mathcal{B}]$	$[\mathcal{R}] \oplus [\mathcal{RT}]$	$[\mathcal{B}]$	$[Id] \oplus [\mathcal{R}]$	$[\mathcal{B}]$	$[\mathcal{T}] \oplus [\mathcal{RT}]$	$[\mathcal{B}]$	$[Id] \oplus [\mathcal{RT}]$
Loop	$[C_{tr}, a]$	$[C_{tr}, b]$	$[C_{tr}, ab]$	$[C_{r^2}, Id]$	$[C_{r^2}, \mathcal{R}]$	$[C_{r^2}, \mathcal{T}]$	$[C_{r^2}, \mathcal{RT}]$	$[C_{r^2}, \mathcal{B}]$	
$\mathcal{S}$ (Loop)	$[\mathcal{B}]$	$[\mathcal{R}] \oplus [\mathcal{T}]$	$[\mathcal{B}]$	$[Id]$	$[\mathcal{R}]$	$[\mathcal{T}]$	$[\mathcal{RT}]$	$[\mathcal{B}]$	

### C. $BF$ field theory with $AAB$ twisted term as a Borromean-Rings topological order

Now we briefly review the  $BF$  field theory with an  $AAB$  twist. Consider gauge group  $G = \prod_{i=1}^3 \mathbb{Z}_{N_i} = (\mathbb{Z}_2)^3$ , the topological action is given by

$$S = \int \sum_{i=1}^3 \frac{N_i}{2\pi} B^i dA^i + q A^1 A^2 B^3, \quad (166)$$

where  $A^i$  and  $B^i$  are 1- and 2-form  $U(1)$  gauge fields respectively.  $q = \frac{pN_1N_2N_3}{(2\pi)^2N_{123}}$  is a quantized coefficient due to the large gauge invariance, where  $p \in \mathbb{Z}_{N_{123}}$ ,  $N_{123}$  is the greatest common divisor of  $N_1$ ,  $N_2$  and  $N_3$ . Lagrange multipliers  $B^1$ ,  $B^2$ , and  $A^3$  enforce the flat-connection conditions:  $dA^1 = 0$ ,  $dA^2 = 0$ , and  $dB^3 = 0$ . The gauge transformations are given by

$$\begin{aligned} A^1 &\rightarrow A^1 + d\chi^1, \\ A^2 &\rightarrow A^2 + d\chi^2, \\ B^3 &\rightarrow B^3 + dV^3, \\ A^3 &\rightarrow A^3 + d\chi^3 \\ &+ \frac{2\pi q}{N_3} \left( \chi^2 A^1 - \chi^1 A^2 + \frac{1}{2} \chi^2 d\chi^1 - \frac{1}{2} \chi^1 d\chi^2 \right), \\ B^1 &\rightarrow B^1 + dV^1 \\ &- \frac{2\pi q}{N_1} \left( \chi^2 B^3 - A^2 V^3 + \chi^2 dV^3 \right), \\ B^2 &\rightarrow B^2 + dV^2 \\ &+ \frac{2\pi q}{N_2} \left( \chi^1 B^3 - A^1 V^3 + \chi^1 dV^3 \right), \end{aligned} \quad (167)$$

where  $\chi^i$  and  $V^i$  are 0- and 1-form gauge parameters with  $\int d\chi^i \in 2\pi\mathbb{Z}$  and  $\int dV^i \in 2\pi\mathbb{Z}$ .

A particle in the  $BF$  field theory with an  $AAB$  twist with  $G = (\mathbb{Z}_2)^3$  can carry gauge charges that are minimally coupled to 1-form fields  $A^i$  and we generally denote such a particle by  $\mathcal{P}_{n_1 n_2 n_3}$ , where  $n_1, n_2, n_3 = 0, 1$ . The subscript  $n_1 n_2 n_3$  denotes  $n_1$ ,  $n_2$ , and  $n_3$  units of  $\mathbb{Z}_{N_1}$ ,  $\mathbb{Z}_{N_2}$ , and  $\mathbb{Z}_{N_3}$  gauge charge. A typical example of an Abelian particle is  $\mathcal{P}_{100}$ , whose corresponding gauge invariant Wilson operator is given by

$$\mathcal{O}_{\mathcal{P}_{100}} = \exp \left( i \int_{\gamma} A^1 \right), \quad (168)$$

where the  $\gamma = S^1$  is the world-line of the particle. A typical non-Abelian particle in the  $BF$  field theory with an  $AAB$  twist with  $G = (\mathbb{Z}_2)^3$  is  $\mathcal{P}_{001}$ , whose gauge invariant Wilson operator is given by

$$\begin{aligned} \mathcal{O}_{\mathcal{P}_{001}} = & 2 \exp \left[ i \int_{\gamma} A^3 + \frac{1}{2} \frac{2\pi q}{N_3} (d^{-1} A^1 A^2 - d^{-1} A^2 A^1) \right] \\ & \times \delta \left( \int_{\gamma} A^1 \right) \delta \left( \int_{\gamma} A^2 \right), \end{aligned} \quad (169)$$

where the normalization factor 2 in the front of  $\mathcal{O}_{\mathcal{P}_{001}}$  ensures that all fusion and shrinking coefficients are integers. The nontrivial terms  $\frac{1}{2} \frac{2\pi q}{N_3} (d^{-1} A^1 A^2 - d^{-1} A^2 A^1)$  guarantee that the Wilson operator is gauge invariant, where  $d^{-1} A^1$  and  $d^{-1} A^2$  are defined as  $d^{-1} A^1 = \alpha^1$  and  $d^{-1} A^2 = \alpha^2$  such that  $d\alpha^1 = A^1$  and  $d\alpha^2 = A^2$ . The two delta functions

$$\delta \left( \int_{\gamma} A^1 \right) = \begin{cases} 1, & \int_{\gamma} A^1 = 0 \pmod{2\pi} \\ 0, & \text{else} \end{cases} \quad (170)$$

$$\delta \left( \int_{\gamma} A^2 \right) = \begin{cases} 1, & \int_{\gamma} A^2 = 0 \pmod{2\pi} \\ 0, & \text{else} \end{cases} \quad (171)$$

are introduced to ensure that  $d^{-1} A^1$  and  $d^{-1} A^2$  are well-defined.

A loop can carry gauge fluxes that are minimally coupled to 2-form fields  $B^i$  and decorated by gauge charges that are minimally coupled to 1-form fields  $A^i$ . We generally use  $\mathcal{L}_{n_1 n_2 n_3}^{m_1 m_2 m_3}$  to represent the loop, where  $n_i, m_i = 0, 1$ . The subscript  $n_1 n_2 n_3$  denotes  $n_1$ ,  $n_2$ , and  $n_3$  units of  $\mathbb{Z}_{N_1}$ ,  $\mathbb{Z}_{N_2}$ , and  $\mathbb{Z}_{N_3}$  gauge flux. The superscript  $m_1 m_2 m_3$  denotes  $m_1$ ,  $m_2$ , and  $m_3$  units of  $\mathbb{Z}_{N_1}$ ,  $\mathbb{Z}_{N_2}$ , and  $\mathbb{Z}_{N_3}$  gauge charge decoration. As an example, we write the gauge invariant Wilson operator for the Abelian loop  $\mathcal{L}_{001}^{000}$  as

$$\mathcal{O}_{\mathcal{L}_{001}^{000}} = \exp \left( i \int_{\sigma} B^3 \right), \quad (172)$$

where  $\mathcal{L}_{001}^{000}$  is the abbreviation for  $\mathcal{L}_{001}^{000}$ .  $\sigma = S^1 \times S^1$  is the world-sheet of the loop. Analogous to the non-Abelian particle  $\mathcal{P}_{001}$ , the gauge invariant Wilson operator for a non-Abelian loop must contain additional nontrivial terms and delta function constraints. For instance, the Wilson operator for non-Abelian decorated loop  $\mathcal{L}_{100}^{001}$  is

given by

$$\begin{aligned} \mathcal{O}_{L_{100}^{001}} = & 2 \exp \left[ i \int_{\sigma} B^1 + \frac{1}{2} \frac{2\pi q}{N_1} (d^{-1} A^2 B^3 + d^{-1} B^3 A^2) \right. \\ & + i \int_{\gamma} A^3 + \frac{1}{2} \frac{2\pi q}{N_3} (d^{-1} A^1 A^2 - d^{-1} A^2 A^1) \left. \right] \\ & \times \delta \left( \int_{\gamma} A^2 \right) \delta \left( \int_{\sigma} B^3 - \int_{\gamma} A^1 \right), \end{aligned} \quad (173)$$

where the normalization factor 2 ensures that all fusion and shrinking coefficients are integers.  $d^{-1} B^3$  is defined as  $d^{-1} B^3 = \beta^3$  such that  $d\beta^3 = B^3$ . In Ref. [53], the delta function constraints in Eq. (173) are originally written as  $\delta \left( \int_{\gamma} A^2 \right) \delta \left( \int_{\sigma} B^3 \right) \delta \left( \int_{\gamma} A^1 \right)$ . This set of conditions, however, is stronger than necessary and can be relaxed to  $\delta \left( \int_{\gamma} A^2 \right) \delta \left( \int_{\sigma} B^3 - \int_{\gamma} A^1 \right)$  while preserving the gauge invariance of Eq. (173). The delta function  $\delta \left( \int_{\sigma} B^3 - \int_{\gamma} A^1 \right)$  is defined as

$$\delta \left( \int_{\sigma} B^3 - \int_{\gamma} A^1 \right) = \begin{cases} 1, & \int_{\sigma} B^3 - \int_{\gamma} A^1 = 0 \pmod{2\pi} \\ 0, & \text{else} \end{cases} \quad (174)$$

By computing the correlation functions of the Wilson operators as in Eqs. (8) and (9), we find that the *BF* field theory with an *AAB* twist with  $G = (\mathbb{Z}_2)^3$  admits 22 distinct Wilson operators for excitations. This count differs from the 19 excitations originally reported in Ref. [53]. The discrepancy arises because the delta function constraints in the Wilson operators for the loops  $L_{100}^{001}$ ,  $L_{010}^{001}$ , and  $L_{110}^{001}$  were overly restrictive. By relaxing these constraints as demonstrated for  $L_{100}^{001}$  in Eq. (173), we obtain the 22 excitations. Having identified the complete set, we then compute their correlation functions to derive all fusion and shrinking rules.

#### D. Matching between microscopic construction and continuum field theory

We establish that the  $\mathbb{D}_4$  quantum double model matches the *BF* field theory with an *AAB* twist with  $G = (\mathbb{Z}_2)^3$ , by constructing an explicit isomorphism between their excitations. A direct comparison of the fusion and shrinking tables of these two theories confirms that the isomorphism  $f : a \mapsto [C, R]$  preserves the fusion and shrinking structures, satisfying

$$f(a) \otimes f(b) = f(a \otimes b), \quad (175)$$

$$f(\mathcal{S}(a)) = \mathcal{S}(f(a)), \quad (176)$$

where  $a$  and  $b$  denote excitations in the *BF* field theory with an *AAB* twist with  $G = (\mathbb{Z}_2)^3$ , and  $[C, R]$  denotes an excitation in the  $\mathbb{D}_4$  quantum double model. The explicit form of an isomorphism  $f$  is presented in Table VII. Note that the choice of isomorphism from the *BF* field

theory with an *AAB* twist with  $G = (\mathbb{Z}_2)^3$  to the  $\mathbb{D}_4$  quantum double model is not unique. An alternative isomorphism  $\tilde{f} : a \mapsto [C, R]$  can be constructed by  $\tilde{f} = f \circ F$ , where  $F$  permutes excitations in the *BF* field theory with an *AAB* twist with  $G = (\mathbb{Z}_2)^3$  as

$$\begin{aligned} F(P_{n_1 n_2 n_3}) &= P_{n_2 n_1 n_3}, \\ F(L_{n_1 n_2 n_3}^{m_1 m_2 m_3}) &= L_{n_2 n_1 n_3}^{m_2 m_1 m_3}. \end{aligned} \quad (177)$$

The isomorphism  $f$  ( $\tilde{f}$ ) relates the gauge fluxes that are minimally coupled to 2-form fields  $B^1$  ( $B^2$ ),  $B^2$  ( $B^1$ ) and  $B^3$  to conjugacy classes  $C_r$ ,  $C_t$  and  $C_{r^2}$ . Gauge charges that are minimally coupled to 1-form fields  $A^1$  ( $A^2$ ),  $A^2$  ( $A^1$ ) and  $A^3$  are related to the irreps  $\mathcal{R}$ ,  $\mathcal{T}$ , and  $\mathcal{B}$ .

Eqs. (175) and (176) demonstrate that the  $\mathbb{D}_4$  quantum double model and the *BF* field theory with an *AAB* twist with  $G = (\mathbb{Z}_2)^3$  share identical fusion and shrinking structures. The isomorphism  $f$  establishes the  $\mathbb{D}_4$  quantum double model as the microscopic construction of the *BF* field theory with an *AAB* twist with  $G = (\mathbb{Z}_2)^3$ . This correspondence bridges two complementary approaches to topological order: the long wavelength continuum field theory and the microscopic lattice model. The agreement of their topological data not only provides strong support for the field-theoretic derivation of the fusion and shrinking rules but also reveals how these rules are encoded in the microscopic degrees of freedom of a local lattice Hamiltonian.

## VII. SUMMARY AND OUTLOOK

### A. Summary

Understanding higher-dimensional non-Abelian topological orders requires a unified framework that connects continuum topological field theories with explicit microscopic constructions. In this work, we have established such a connection in three dimensions by constructing a concrete microscopic foundation for excitations, fusion, shrinking, and their mutual consistency, thereby placing field-theoretical principles of three-dimensional topological order on a firm lattice footing.

More concretely, we have explicitly constructed creation operators for topological excitations and established the corresponding connecting rules that allow excitations to be moved or deformed in the 3d quantum double model. These operators enable us to implement both fusion and shrinking processes directly on the lattice. The fusion of two excitations is described as taking the tensor product of their local Hilbert spaces, with the coefficients appearing in the resulting direct-sum decomposition defining the fusion coefficients. Likewise, shrinking rules correspond to the direct-sum decomposition of the local Hilbert space after the shrinking process.

We have calculated all fusion and shrinking rules in the 3d  $\mathbb{D}_3$  and  $\mathbb{D}_4$  quantum double models and shown that the  $\mathbb{D}_4$  quantum double model exhibits the same fusion and

TABLE VII. Mapping table of  $f$ . We write  $L_{n_1 n_2 n_3}^{000}$  as  $L_{n_1 n_2 n_3}$  for simplicity.

a	1	$P_{100}$	$P_{010}$	$P_{110}$	$P_{001}$	$L_{100}$	$L_{100}^{001}$	$L_{100}^{100}$	$L_{100}^{101}$	$L_{010}$	$L_{010}^{001}$
$f(a)$	$[Id]$	$[\mathcal{R}]$	$[\mathcal{T}]$	$[\mathcal{RT}]$	$[\mathcal{B}]$	$[C_r, Id]$	$[C_r, \omega]$	$[C_r, \omega^2]$	$[C_r, \omega^3]$	$[C_t, Id]$	$[C_t, a]$
a	$L_{010}^{010}$	$L_{010}^{011}$	$L_{110}^{011}$	$L_{110}^{001}$	$L_{110}^{100}$	$L_{110}^{101}$	$L_{001}^{001}$	$L_{001}^{100}$	$L_{001}^{010}$	$L_{001}^{110}$	$L_{001}^{001}$
$f(a)$	$[C_t, b]$	$[C_t, ab]$	$[C_{tr}, Id]$	$[C_{tr}, a]$	$[C_{tr}, b]$	$[C_{tr}, ab]$	$[C_{r^2}, Id]$	$[C_{r^2}, \mathcal{R}]$	$[C_{r^2}, \mathcal{T}]$	$[C_{r^2}, \mathcal{RT}]$	$[C_{r^2}, \mathcal{B}]$

shrinking rules as the  $BF$  field theory with an  $AAB$  twist and gauge group  $G = (\mathbb{Z}_2)^3$ . We therefore conclude that the  $\mathbb{D}_4$  quantum double model provides a microscopic construction of the  $BF$  field theory with an  $AAB$  twist and  $G = (\mathbb{Z}_2)^3$ , which is a continuum topological field theory initiated in Ref. [25]. We conjecture that this correspondence originates from an underlying algebraic relationship between the group  $\mathbb{D}_4$  of the quantum double model and the gauge group  $(\mathbb{Z}_2)^3$  of the  $BF$  field theory with an  $AAB$  twist. Specifically, the  $AAB$  twist involves two 1-form gauge fields  $A$  and one 2-form gauge field  $B$ , which naturally correspond to a  $(\mathbb{Z}_2)^2$  subgroup and a  $\mathbb{Z}_2$  subgroup, respectively. The potential connection to the group  $\mathbb{D}_4$  can be obtained from  $(\mathbb{Z}_2)^2$  and  $\mathbb{Z}_2$  via a nontrivial central extension,  $1 \rightarrow \mathbb{Z}_2 \rightarrow \mathbb{D}_4 \rightarrow (\mathbb{Z}_2)^2 \rightarrow 1$ . This connection may be helpful to find microscopic counterparts of the  $BF$  field theory with an  $AAB$  twist and general gauge group  $\mathbb{Z}_{N_1} \times \mathbb{Z}_{N_2} \times \mathbb{Z}_{N_3}$ .

Our explicit construction of particle creation operators on the lattice allows us to deterministically control which shrinking channel occurs in a non-Abelian shrinking process by selecting the internal degrees of freedom of a non-Abelian loop operator. Moreover, by analyzing the fusion and shrinking tables of the quantum double model, we have verified that the shrinking rules are consistent with the fusion rules: performing fusion followed by shrinking yields the same result as shrinking first and then fusing. This consistency condition, previously derived within field-theoretical analyses [53, 55, 56], is here demonstrated concretely on the lattice for the first time. We conjecture that all anomaly-free 3d topological orders must satisfy this fusion–shrinking consistency, which thus serves as a nontrivial criterion for topological self-consistency.

The coexistence and compatibility of fusion and shrinking rules naturally lead to the diagrammatic framework developed in Ref. [56], in which these processes are represented by fusion and shrinking diagrams subject to algebraic constraints such as the pentagon equation and the (hierarchical) shrinking–fusion hexagon equation. Our microscopic construction not only confirms the validity of this framework but also provides an explicit microscopic foundation for its abstract structures. These algebraic relations play an essential role in ensuring the anomaly-free nature of higher-dimensional topological orders and may serve as an alternative, computationally friendly route toward a systematic categorical classification [8, 57–61].

## B. Outlook

Several promising research directions emerge from this study. First, the interplay among braiding, fusion, and shrinking constitutes a more complete set of topological data characterizing higher-dimensional topological orders. While this work verifies the consistency between fusion and shrinking, it remains an open question whether similar relations also involving braiding statistics exist, such as multi-loop and particle–loop–loop braiding in the 3d quantum double model or within the Hamiltonian formulation of  $(3+1)$ D Dijkgraaf–Witten theory [62, 63]. Constructing combined braiding–fusion–shrinking processes may reveal deeper topological consistency conditions. Within such an extended framework, topics including hole dynamics in topological spin backgrounds [64–69], external-field-induced global phase diagrams [70–72], and parton constructions [73–77] constitute interesting future directions.

Building on this perspective, extending the existing diagrammatic framework offers another fruitful avenue. The fusion–shrinking consistency gives rise to a hierarchy of diagrammatic representations [56]. Elementary fusion and shrinking diagrams correspond to vectors in fusion and shrinking spaces, while more complicated diagrams arise through stacking and tensoring these elements. Transformations among diagrams are mediated by unitary  $F$ -symbols and  $\Delta$ -symbols, constrained by the pentagon and shrinking–fusion hexagon equations. Incorporating braiding into this formalism would likely generate a richer set of algebraic constraints, potentially illuminating the deeper categorical structure underlying 3d topological orders.

Another exciting direction is to deepen our understanding of generalized symmetries [78–84] in microscopic constructions of 3d topological orders. The 1-form and 2-form invertible and non-invertible symmetries in 3d topological orders encode information about their algebraic structures, boundary theories, and phase transitions. As a first step, we have initiated investigations of generalized symmetries in a 3d non-Abelian topological order from the continuum-field-theoretical perspective [85]. Future steps include constructing generalized symmetry operators on the lattice, with careful attention to onsite realizability and higher-form anomaly structures [86, 87].

As all topological orders considered in this work are bosonic, an important future direction is the microscopic construction of 3d topological orders with fermions,

which can be described by  $BF$  theories with a  $BB$  twist [22, 27, 43, 44]. bridging microscopic construction and continuum field theory with fermions are an important topic, which will further extends the diagrammatic representation of higher-dimensional topological orders in Ref. [56] by involving fermions. Recently, Ref. [88] showed that the thermal states of the 3d fermionic toric code remain long-range entangled below a finite temperature. Such finite-temperature topological order in fewer than four spatial dimensions originates from an anomalous two-form symmetry associated with emergent fermionic particle excitations. Further study of such phenomena in broader microscopic construction as well as field theoretical analysis is promising.

Finally, these theoretical advances naturally point toward the prospect of topological quantum computation in three dimensions. In two dimensions, the creation and manipulation of anyons underpin topological quantum computation. Experimentally, programmable quantum processors based on trapped ions and superconducting qubits have enabled the preparation of non-Abelian topologically ordered states, together with the manipulation of anyon fusion and braiding [89–91]. Recent progress using sequential quantum circuits [92–99] has led to concrete protocols for implementing *ribbon operators* of non-Abelian anyons [100], providing a pathway toward universal topological quantum computation in the 2d quantum double model [101]. Extending these ideas to three dimensions, one may design quantum circuits or higher-order cellular automata [102, 103] to create, braid, fuse, and shrink membrane and loop excitations, thereby exploring the computational power encoded in their non-Abelian fusion and shrinking dynamics.

In summary, this work bridges the gap between continuum field-theoretical descriptions of higher-dimensional topological orders and their concrete microscopic constructions. By establishing the fusion–shrinking correspondence in an exactly solvable 3d model, we provide both a microscopic verification and a new conceptual tool set for exploring the algebraic and computational structures of topological matter beyond two spatial dimensions.

## ACKNOWLEDGMENTS

This work was in part supported by National Natural Science Foundation of China (NSFC) under Grants No. 12474149 and No. 12274250, Research Center for Magnetoelectric Physics of Guangdong Province under Grant No. 2024B0303390001, and Guangdong Provincial Key Laboratory of Magnetoelectric Physics and Devices under Grant No. 2022B1212010008.

## Appendix A: Diagrammatics, pentagon and hexagon equations

In this appendix, we introduce unitary  $F$ - and  $\Delta$ -symbols to transform diagrams. They satisfy a series of stringent algebraic equations known as the pentagon equation and the shrinking-fusion hexagon equation [56]. Any violation of these equations indicates quantum anomaly in 3d topological orders.

In Sec. II B, we illustrate how to construct more complicated diagrams by stacking basic diagrams. Besides Fig. 3, we can also construct the diagram that describes the fusion of three excitations as shown in Fig. 16. The difference between the diagrams shown in Figs. 3 and 16 is the order of the fusion process. Physically, fusion rules satisfy associativity, i.e., fusing  $b$  and  $c$  first should give the same final output as fusing  $a$  and  $b$  first. Therefore, the diagram shown in Fig. 16 also represents a set of basis vectors that span the same space  $V_d^{abc}$ . The two different bases represented by Fig. 3 and Fig. 16 can be transformed to each other by a unitary matrix known as the  $F$ -symbol, which is defined in Fig. 17. We can express the equation in Fig. 17 as:

$$\begin{aligned} & |(a, b); e, \mu\rangle \otimes |e, c; d, \nu\rangle \\ &= \sum_{f, \lambda, \eta} [F_d^{abc}]_{e\mu\nu, f\lambda\eta} |a, f; d, \eta\rangle \otimes |(b, c); f, \lambda\rangle. \end{aligned} \quad (A1)$$

The summation over  $f$  exhausts all excitations in the set  $\Phi_0^{3+1}$ ,  $\lambda = \{1, 2, \dots, N_f^{bc}\}$  and  $\eta = \{1, 2, \dots, N_d^{af}\}$ . Since the  $F$ -symbol is unitary, we have

$$\sum_{f, \lambda, \eta} [F_d^{abc}]_{e\mu\nu, f\lambda\eta} \left( [F_d^{abc}]_{e'\mu'\nu', f\lambda\eta} \right)^* = \delta_{ee'} \delta_{\mu\mu'} \delta_{\nu\nu'} \quad (A2)$$

which allow us to implement the inverse transformation. Since the total space  $V_d^{abc}$  is isomorphic to  $\bigoplus_f V_d^{af} \otimes V_f^{bc}$  in Fig. 16, the dimension of the total space is given by

$$\dim(V_d^{abc}) = \sum_f N_d^{af} N_f^{bc}. \quad (A3)$$

By comparing Eq. (17) and Eq. (A3), we obtain a constraint on fusion coefficients:

$$\sum_e N_e^{ab} N_d^{ec} = \sum_f N_d^{af} N_f^{bc}. \quad (A4)$$

We employ a similar tensor product approach to construct fusion diagrams that involve more excitations. Applying the  $F$ -symbols inside these diagrams leads to a basis transformation. For example, consider fusing four excitations, we have two different ways to transform the far left diagram to the far right diagram as shown in Fig. 18, which gives a very strong algebraic constraint on

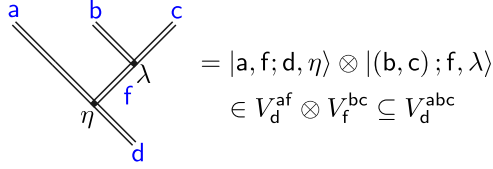


FIG. 16. A different diagram of fusing three excitations in 3d. The associativity of fusion rules guarantees that this diagram describes the same physics as the diagram shown in Fig. 3. The only difference between them is just a change of basis.

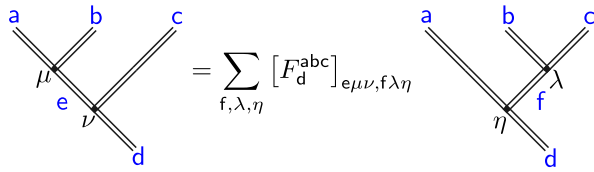


FIG. 17. Definition of the  $F$ -symbol in 3d. The left and right diagrams represent different bases for the same space  $V_d^{abc}$ , and we use the unitary  $F$ -symbol to change the basis. Transforming these diagrams to each other does not change any physics.

the  $F$ -symbols, known as the pentagon equation:

$$\begin{aligned} & \sum_{\sigma=1}^{N_e^{\text{fh}}} [F_e^{\text{fc}}]_{g\nu\lambda, h\gamma\sigma} [F_e^{\text{ab}}]_{f\mu\sigma, i\rho\delta} \\ &= \sum_j \sum_{\omega=1}^{N_g^{\text{aj}}} \sum_{\theta=1}^{N_j^{\text{bc}}} \sum_{\tau=1}^{N_i^{\text{jd}}} [F_g^{\text{ab}}]_{f\mu\nu, j\theta\omega} [F_e^{\text{aj}}]_{g\omega\lambda, i\tau\delta} [F_i^{\text{bc}}]_{j\theta\tau, h\gamma\rho}. \end{aligned} \quad (\text{A5})$$

A similar pentagon equation can also be derived in the diagrammatic representations of 2d anyons. Actually, if we draw all previous fusion diagrams in a single-line fashion, our fusion diagrams automatically reduce to 2d anyonic fusion diagrams. Considering fusion diagrams for more excitations does not give any independent constraint beyond the pentagon equation.

Now we construct diagrams that incorporate both fusion and shrinking processes. Consider  $\mathcal{S}(a) \otimes \mathcal{S}(b)$  and  $\mathcal{S}(a \otimes b)$ , their corresponding diagrams are shown in Figs. 4 and 19 respectively. Since we have the consistency condition Eq. (10), these two processes have the same final output and we consider them as different bases in the same space. The diagram in Fig. 4 is defined as  $|d, e; c, \lambda\rangle \otimes |b; e, \nu\rangle \otimes |a; d, \mu\rangle$ , where different  $d, e, \mu, \nu$ , and  $\lambda$  label different orthogonal vectors. This set of orthogonal vectors spans the space denoted as  $V_c^{\mathcal{S}(a) \otimes \mathcal{S}(b)}$ , which is isomorphic to  $\bigoplus_{d,e} V_e^{\text{de}} \otimes V_e^b \otimes V_d^a$  due to our tensor product construction. Similarly, the diagram shown in Fig. 19 is defined as  $|f; c, \gamma\rangle \otimes |a, b; f, \delta\rangle$ , where  $f, \delta$ , and  $\gamma$  label different orthogonal vectors. The corresponding space  $V_c^{\mathcal{S}(a \otimes b)} = V_c^{\mathcal{S}(a) \otimes \mathcal{S}(b)}$  is isomorphic to  $\bigoplus_f V_f^f \otimes V_f^{ab}$ ,

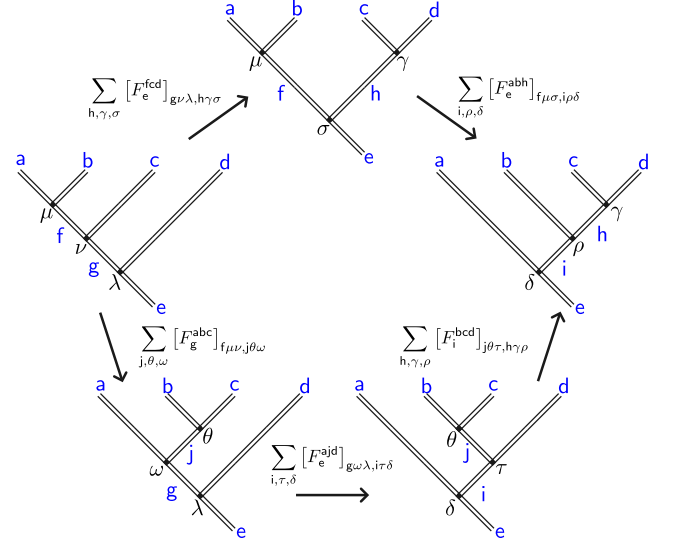


FIG. 18. Diagrammatic representation of the pentagon equation (A5). Starting from the far left diagram, we can go to the far right diagram through either the upper path or the lower path. Comparing these two different paths, we derive the pentagon equation.

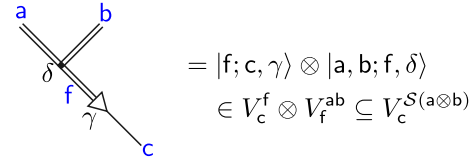


FIG. 19. The diagram describing  $\mathcal{S}(a \otimes b)$  in 3d. This diagram is constructed by stacking a basic fusion diagram and a basic shrinking diagram. The corresponding vector is obtained by tensor product construction.

which recovers the constraint in Eq. (14):

$$\begin{aligned} & \dim(V_c^{\mathcal{S}(a) \otimes \mathcal{S}(b)}) = \dim(V_c^{\mathcal{S}(a \otimes b)}) \\ &= \sum_{d,e} N_c^{\text{de}} S_e^b S_d^a = \sum_f S_c^f N_f^{ab}. \end{aligned} \quad (\text{A6})$$

The two sets of vectors shown in Fig. 19 correspond to two different bases of the total space  $V_c^{\mathcal{S}(a) \otimes \mathcal{S}(b)} = V_c^{\mathcal{S}(a \otimes b)}$ . We expect that these two bases can transform to each other by a unitary matrix, called the  $\Delta$ -symbol. The definition of the  $\Delta$ -symbol is shown in Fig. 20. We

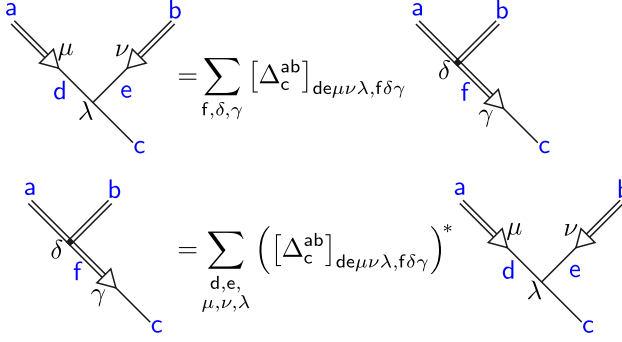


FIG. 20. Definition of the  $\Delta$ -symbol in 3d. The left diagram and the right diagram describe the same physics in different bases. Similar to the  $F$ -symbol, the  $\Delta$ -symbol is also unitary and we use it to change bases.

explicitly write down the transformations in Fig. 20 as:

$$\begin{aligned}
 & |d, e; c, \lambda\rangle \otimes |b; e, \nu\rangle \otimes |a; d, \mu\rangle \\
 &= \sum_{f, \delta, \gamma} [\Delta_c^{ab}]_{de\mu\nu\lambda, f\delta\gamma} |f; c, \gamma\rangle \otimes |a, b; f, \delta\rangle, \quad (A7) \\
 & |f; c, \gamma\rangle \otimes |a, b; f, \delta\rangle \\
 &= \sum_{\substack{d, e, \\ \mu, \nu, \lambda}} \left( [\Delta_c^{ab}]_{de\mu\nu\lambda, f\delta\gamma} \right)^* |d, e; c, \lambda\rangle \otimes |b; e, \nu\rangle \otimes |a; d, \mu\rangle. \quad (A8)
 \end{aligned}$$

Unitarity of the  $\Delta$ -symbol demands:

$$\begin{aligned}
 & \sum_{f, \delta, \gamma} [\Delta_c^{ab}]_{de\mu\nu\lambda, f\delta\gamma} \left( [\Delta_c^{ab}]_{d'e'\mu'\nu'\lambda', f\delta\gamma} \right)^* \\
 &= \delta_{dd'} \delta_{ee'} \delta_{\mu\mu'} \delta_{\nu\nu'} \delta_{\lambda\lambda'}, \quad (A9) \\
 & \sum_{\substack{d, e, \\ \mu, \nu, \lambda}} [\Delta_c^{ab}]_{de\mu\nu\lambda, f\delta\gamma} \left( [\Delta_c^{ab}]_{de\mu\nu\lambda, f'\delta'\gamma'} \right)^* \\
 &= \delta_{ff'} \delta_{\delta\delta'} \delta_{\gamma\gamma'}.
 \end{aligned} \quad (A10)$$

The consistency condition between the fusion and shrinking rules further leads to a strong constraint on both  $F$ -symbols and  $\Delta$ -symbols called the shrinking-fusion hexagon equation. Consider three excitations going through fusion and shrinking processes as shown in Fig. 21. By applying the  $F$ -symbols and  $\Delta$ -symbols inside of the diagrams, we find two paths to transform the far left diagram to the far right diagram. By comparing the coefficients calculated from the upper and lower paths in Fig. 21, we obtain the shrinking-fusion hexagon equation:

$$\begin{aligned}
 & \sum_i \sum_{\alpha=1}^{N_i^{fg}} \sum_{\beta=1}^{N_d^{ei}} \sum_{\xi=1}^{S_i^j} \left[ F_d^{efg} \right]_{h\delta\gamma, i\alpha\beta} [\Delta_i^{bc}]_{fg\nu\lambda\alpha, j\tau\xi} [\Delta_d^{aj}]_{ei\mu\xi\beta, k\theta\epsilon} \\
 &= \sum_t \sum_{\sigma=1}^{N_t^{ab}} \sum_{\rho=1}^{S_h^t} \sum_{\omega=1}^{N_k^{tc}} [\Delta_h^{ab}]_{ef\mu\nu\delta, t\sigma\rho} [\Delta_d^{tc}]_{hg\rho\lambda\gamma, kw\epsilon} [F_k^{abc}]_{t\sigma\omega, j\tau\theta}.
 \end{aligned} \quad (A11)$$

The shrinking-fusion hexagon equation is understood as the consistency relation between  $F$ -symbols and  $\Delta$ -symbols. We can further consider applying  $F$ -symbols and  $\Delta$ -symbols to transform diagrams that involve more excitations, such as  $\mathcal{S}(a) \otimes \mathcal{S}(b) \otimes \mathcal{S}(c) \otimes \mathcal{S}(d)$ . However, no more independent equations are obtained from these more complicated diagrams.

Since being able to use the  $F$ -symbols and  $\Delta$ -symbols to change basis indicates the constraints on fusion and shrinking coefficients (i.e., Eq. (14) and Eq. (A4) hold), we conclude that the pentagon Eq. (A5) and shrinking-fusion hexagon Eq. (A11) are stronger constraints. These equations describe not only the behavior of fusion and shrinking coefficients but also the transformations of bases. We conjecture that the pentagon equation and shrinking-fusion hexagon equation are universal for all anomaly-free 3d topological orders. Our construction of the diagrammatics for 3d topological orders can be generalized to higher dimensions, and the details can be found in Ref. [56].

## Appendix B: Details about basic operators

In this appendix, we provide some technical details about basic operators in Sec. III.

### 1. Proof of Eq. (37)

Consider a string  $L = L_1 \cup L_2 \cup L_3$ , if we connect  $L_2$  and  $L_3$  first, by using Eq. (36), we have

$$T_{L_1 \cup (L_2 \cup L_3)}^g = \sum_h T_{L_2 \cup L_3}^{\bar{h}g} T_{L_1}^h = \sum_{h, m} T_{L_3}^{\bar{m}h} T_{L_2}^m T_{L_1}^h, \quad (B1)$$

where the bracket  $(L_2 \cup L_3)$  is introduced to emphasize that  $L_2$  and  $L_3$  are connected first. If we connect  $L_1$  and  $L_2$  first, then we have

$$T_{(L_1 \cup L_2) \cup L_3}^g = \sum_m T_{L_3}^{\bar{m}g} T_{L_1 \cup L_2}^m = \sum_{h, m} T_{L_3}^{\bar{m}g} T_{L_2}^{\bar{h}m} T_{L_1}^h. \quad (B2)$$

Rewrite  $T_{L_3}^{\bar{m}g}$  and  $T_{L_2}^{\bar{h}m}$  as  $T_{L_3}^{\bar{m}h\bar{h}g}$  and  $T_{L_2}^{\bar{h}h\bar{h}m}$  respectively, then replace the sum over  $m$  with the sum over  $\bar{h}m$ , we have

$$\begin{aligned}
 T_{(L_1 \cup L_2) \cup L_3}^g &= \sum_h \sum_{\bar{h}m} T_{L_3}^{(\bar{h}m)\bar{h}g} T_{L_2}^{\bar{h}h(\bar{h}m)} T_{L_1}^h \\
 &= \sum_{h, m'} T_{L_3}^{\bar{m}'\bar{h}g} T_{L_2}^{m'} T_{L_1}^h = T_{L_1 \cup (L_2 \cup L_3)}^g.
 \end{aligned} \quad (B3)$$

Thus, we conclude that the order of connection is irrelevant.

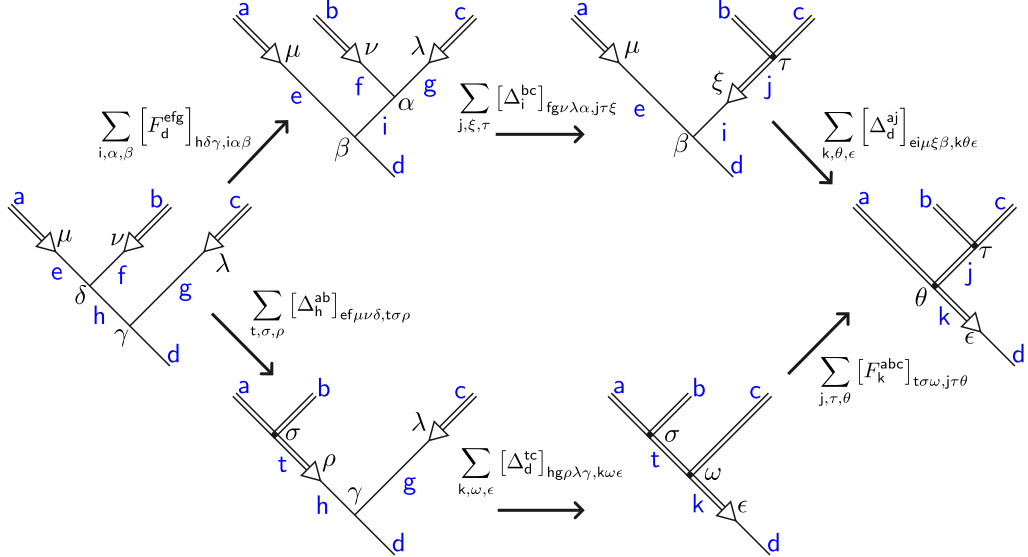


FIG. 21. Diagrammatic representations of the shrinking-fusion hexagon equation (A11). Two different paths can be constructed to transform the far left diagram to the far right diagram. Comparing these two different paths, we obtain the shrinking-fusion hexagon equation.

## 2. Proof of Eqs. (38), (39) and (40)

Thus, we have

Suppose  $L = (v_0, v_1, \dots, v_n)$  starts at the vertex  $v_0$ , goes through  $n$  edges denoted by  $v_i v_{i+1}$  and finally ends at  $v_n$ . We set the arrow of  $v_i v_{i+1}$  points from  $v_i$  to  $v_{i+1}$ . Then we write  $T_L^g$  as

$$T_L^g = \sum_{h_1, h_2, \dots, h_{n-1}} T_{v_{n-1} v_n}^{\bar{h}_{n-1} g} \dots T_{v_i v_{i+1}}^{\bar{h}_i h_{i+1}} \dots T_{v_1 v_2}^{\bar{h}_1 h_2} T_{v_0 v_1}^{h_1}. \quad (\text{B4})$$

Notice that the vertex operator  $A_{v_i}^k$  commutes with all  $T_{v_j v_{j+1}}^g$  when  $j \neq i-1, i$  because they act on different edges. Since the action of  $A_{v_i}^k$  on the edges  $v_{i-1} v_i$  and  $v_i v_{i+1}$  is given by  $L_{v_{i-1} v_i}^k = L_k^-$  and  $L_{v_i v_{i+1}}^k = L_k^+$ , from Eq. (21) we can see

$$A_{v_i}^k T_{v_i v_{i+1}}^{\bar{h}_i h_{i+1}} = T_{v_i v_{i+1}}^{k \bar{h}_i h_{i+1}} A_{v_i}^k, \quad (\text{B5})$$

$$A_{v_i}^k T_{v_{i-1} v_i}^{\bar{h}_{i-1} h_i} = T_{v_{i-1} v_i}^{\bar{h}_{i-1} h_i \bar{k}} A_{v_i}^k. \quad (\text{B6})$$

$$\begin{aligned} & A_{v_i}^k T_L^g \\ &= \sum_{h_1, \dots, h_i, \dots, h_{n-1}} T_{v_{n-1} v_n}^{\bar{h}_{n-1} g} \dots A_{v_i}^k T_{v_i v_{i+1}}^{\bar{h}_i h_{i+1}} T_{v_{i-1} v_i}^{\bar{h}_{i-1} h_i} \dots T_{v_0 v_1}^{h_1} \\ &= \sum_{h_1, \dots, h_i, \dots, h_{n-1}} T_{v_{n-1} v_n}^{\bar{h}_{n-1} g} \dots T_{v_i v_{i+1}}^{k \bar{h}_i h_{i+1}} T_{v_{i-1} v_i}^{\bar{h}_{i-1} h_i \bar{k}} A_{v_i}^k \dots T_{v_0 v_1}^{h_1} \\ &= \left[ \sum_{h_1, \dots, (h_i \bar{k}), \dots, h_{n-1}} T_{v_{n-1} v_n}^{\bar{h}_{n-1} g} \dots T_{v_i v_{i+1}}^{k \bar{h}_i h_{i+1}} T_{v_{i-1} v_i}^{\bar{h}_{i-1} h_i \bar{k}} \dots T_{v_0 v_1}^{h_1} \right] A_{v_i}^k \\ &= T_L^g A_{v_i}^k, \end{aligned} \quad (\text{B7})$$

where  $i \neq 0, n$ . When  $i = 0$  or  $i = n$ , similar to Eq. (B6), we obtain

$$A_{v_0}^k T_{v_0 v_1}^{h_1} = T_{v_0 v_1}^{k h_1} A_{v_0}^k, \quad (\text{B8})$$

$$A_{v_n}^k T_{v_{n-1} v_n}^{\bar{h}_{n-1} g} = T_{v_{n-1} v_n}^{\bar{h}_{n-1} g \bar{k}} A_{v_n}^k. \quad (\text{B9})$$

Thus, we have

$$\begin{aligned}
& A_{v_0}^k T_L^g \\
&= \sum_{\substack{h_1, \dots, h_j, \\ \dots, h_{n-1}}} T_{v_{n-1}v_n}^{\bar{h}_{n-1}g} \dots T_{v_1v_2}^{\bar{h}_1h_2} A_{v_0}^k T_{v_0v_1}^{h_1} \\
&= \sum_{\substack{h_1, \dots, h_j, \\ \dots, h_{n-1}}} T_{v_{n-1}v_n}^{\bar{h}_{n-1}g} \dots T_{v_1v_2}^{\bar{h}_1h_2} T_{v_iv_{i+1}}^{kh_1} A_{v_0}^k \\
&= \left[ \sum_{\substack{(kh_1), \dots, (kh_j), \\ \dots, (kh_{n-1})}} T_{v_{n-1}v_n}^{\bar{kh}_{n-1}kg} \dots T_{v_iv_{i+1}}^{\bar{kh}_i kh_{i+1}} \dots T_{v_0v_1}^{kh_1} \right] A_{v_0}^k \\
&= T_L^{kg} A_{v_0}^k, \tag{B10}
\end{aligned}$$

and

$$\begin{aligned}
A_{v_n}^k T_L^g &= \sum_{h_1, \dots, h_j, \dots, h_{n-1}} A_{v_n}^k T_{v_{n-1}v_n}^{\bar{h}_{n-1}g} \dots T_{v_0v_1}^{h_1} \\
&= \sum_{h_1, \dots, h_j, \dots, h_{n-1}} T_{v_{n-1}v_n}^{\bar{h}_{n-1}g\bar{k}} \dots T_{v_0v_1}^{h_1} A_{v_n}^k \\
&= T_L^{g\bar{k}} A_{v_n}^k. \tag{B11}
\end{aligned}$$

### 3. Proof of Eqs. (46), (47) and (48)

We consider Eq. (46) first. Using Eq. (43), we have

$$\begin{aligned}
A_{v=\partial_0 L}^g |R; i, j\rangle &= A_{v=\partial_0 L}^g W_L(R; i, j) |GS\rangle \\
&= A_{v=\partial_0 L}^g \sum_{h \in G} \Gamma_{ij}^{R^*}(h) T_L^h |GS\rangle. \tag{B12}
\end{aligned}$$

Notice Eq. (39), we obtain

$$\begin{aligned}
A_{v=\partial_0 L}^g |R; i, j\rangle &= \sum_{h \in G} \Gamma_{ij}^{R^*}(h) T_L^{gh} A_{v=\partial_0 L}^g |GS\rangle \\
&= \sum_{h \in G} \Gamma_{ij}^{R^*}(h) T_L^{gh} |GS\rangle, \tag{B13}
\end{aligned}$$

where we absorb the  $A_{v=\partial_0 L}^g$  into the ground state in the last step. By writing the matrix element  $\Gamma_{ij}^{R^*}(g)$  as  $\sum_k \Gamma_{ik}^{R^*}(\bar{g}) \Gamma_{kj}^{R^*}(gh)$ , we can finally prove Eq. (46):

$$\begin{aligned}
A_{v=\partial_0 L}^g |R; i, j\rangle &= \sum_k \Gamma_{ik}^{R^*}(\bar{g}) \sum_{h \in G} \Gamma_{kj}^{R^*}(gh) T_L^{gh} |GS\rangle \\
&= \sum_k \Gamma_{ik}^{R^*}(\bar{g}) W_L(R; k, j) |GS\rangle \\
&= \sum_k \Gamma_{ki}^R(g) |R; k, j\rangle, \tag{B14}
\end{aligned}$$

where we have used  $\Gamma_{ik}^{R^*}(\bar{g}) = \Gamma_{ki}^R(g)$ . Similarly, we prove Eq. (47) as follows:

$$\begin{aligned}
A_{v=\partial_1 L}^g |R; i, j\rangle &= A_{v=\partial_1 L}^g \sum_{h \in G} \Gamma_{ij}^{R^*}(h) T_L^h |GS\rangle \\
&= \sum_{h \in G} \Gamma_{ij}^{R^*}(h) T_L^{h\bar{g}} A_{v=\partial_1 L}^g |GS\rangle \\
&= \sum_k \sum_{h \in G} \Gamma_{kj}^{R^*}(g) \Gamma_{ik}^{R^*}(h\bar{g}) T_L^{h\bar{g}} |GS\rangle \\
&= \sum_k \Gamma_{kj}^{R^*}(g) W_L(R; i, k) |GS\rangle \\
&= \sum_k \Gamma_{kj}^{R^*}(g) |R; i, k\rangle. \tag{B15}
\end{aligned}$$

As for Eq. (48), notice that the plaquette operator  $B_{p,s}^h$  is a projector, while the  $T_L^h$  term does not change any group element. Thus, the plaquette operator  $B_{p,s}^h$  automatically commutes with the string operator  $W_L(R; i, j)$  for all  $(p, s)$ . We can directly absorb the plaquette operator  $B_{p,s}^h$  into the ground state and have

$$\begin{aligned}
B_{p,s}^h |R; i, j\rangle &= B_{p,s}^h W_L(R; i, j) |GS\rangle \\
&= W_L(R; i, j) \delta_{h,e} |GS\rangle \\
&= \delta_{h,e} |R; i, j\rangle. \tag{B16}
\end{aligned}$$

### 4. Proof of Eq. (49)

Consider

$$\begin{aligned}
& \sum_k W_{L_2}(R; k, j) W_{L_1}(R; i, k) \\
&= \sum_k \sum_{g, h \in G} \Gamma_{kj}^{R^*}(h) T_{L_2}^h \Gamma_{ik}^{R^*}(g) T_{L_1}^g \\
&= \sum_{g, h} \Gamma_{ij}^{R^*}(gh) T_{L_2}^h T_{L_1}^g \\
&= \sum_m \sum_g \Gamma_{ij}^{R^*}(m) T_{L_2}^{\bar{g}m} T_{L_1}^g. \tag{B17}
\end{aligned}$$

By using Eq. (36), we have

$$\begin{aligned}
\sum_m \sum_g \Gamma_{ij}^{R^*}(m) T_{L_2}^{\bar{g}m} T_{L_1}^g &= \sum_m \Gamma_{ij}^{R^*}(m) T_{L_1 \cup L_2}^m \\
&= W_{L=L_1 \cup L_2}(R; i, j). \tag{B18}
\end{aligned}$$

Thus, we obtain the connecting rule of  $W_{L=L_1 \cup L_2}(R; i, j)$ :

$$W_{L_1 \cup L_2}(R; i, j) = \sum_k W_{L_2}(R; k, j) W_{L_1}(R; i, k). \tag{B19}$$

### 5. The commutation relations between $B_p$ and $L_M^c$

When  $p$  lives in the bulk of the membrane  $M$ , we have  $[B_p, L_M^c] = 0$ . For simplicity, we consider the plaquette  $v_0v_1v'_1v'_0$  shown in Fig. 12. Suppose the edges  $v_0v'_0$ ,

$v_0v_1$ , and  $v_1v'_1$  are assigned with group elements  $g_1$ ,  $g_2$ , and  $g_3$  respectively, then we label this configuration as  $|g_1, g_2, g_3\rangle$ . Before the action of the operator  $L_{M_2}^h$ , the ordered product on the path  $v'_0v_0v_1v'_1$  is  $\bar{g}_1g_2g_3$ . After the action of the operator  $L_{M_2}^h$ , the configuration becomes

$$\begin{aligned} L_{M_2}^h |g_1, g_2, g_3\rangle &= \sum_{g_0} L_{v_1v'_1}^{\bar{g}_0h} T_{v_0v_1}^{g_0} L_{v_0v'_0}^h |g_1, g_2, g_3\rangle \\ &= \sum_{g_0} \delta_{g_0, g_2} |hg_1, g_0, \bar{g}_0hg_0g_3\rangle \\ &= |hg_1, g_2, \bar{g}_2hg_2g_3\rangle. \end{aligned} \quad (\text{B20})$$

Now, the ordered product becomes

$$\overline{hg_1}g_2\bar{g}_2hg_2g_3 = \bar{g}_1\bar{h}g_2\bar{g}_2hg_2g_3 = \bar{g}_1g_2g_3. \quad (\text{B21})$$

Since the operator  $L_{M_2}^h$  does not change the ordered product on the path  $v'_0v_0v_1v'_1$ , it automatically commutes with the plaquette term  $B_{p=v_0v_1v'_1v'_0}$ . For an arbitrary plaquette  $p$  living in the bulk of an membrane  $M$ , we can similarly prove that  $[B_p, L_M^c] = 0$ .

## 6. The commutation relations between $A_v$ and $L_M^c$

When  $v \neq v_0, v'_0$ , where  $L_M^c$  is constructed by acting  $L_h^\pm$  on  $v_0v'_0$  first, we have  $[A_v, L_M^c] = 0$ . From Eq. (54), we can see that any  $L_M^c$  has the form of

$$L_M^c = \sum \cdots \left( \sum_g L_{vv'}^{\bar{g}cg} T_{v_0v}^g \right) \cdots L_{v_0v'_0}^c, \quad (\text{B22})$$

where  $\cdots$  represents some terms that commute with  $A_v^h$  because they do not act on edges that contain vertex  $v$ .  $T_{v_0v}^g$  acts on an arbitrary string with endpoints denoted by  $v_0$  and  $v$ . Thus, we only need to consider the term  $\sum_g L_{vv'}^{\bar{g}cg} T_{v_0v}^g$ . By using Eq. (40) and  $L_{vv'}^g A_v^h = A_v^h L_{vv'}^{\bar{g}gh}$ , we have

$$\begin{aligned} &\sum_{g \in G} L_{vv'}^{\bar{g}cg} T_{v_0v}^g A_v^h \\ &= \sum_{g \in G} L_{vv'}^{\bar{g}cg} A_v^h T_{v_0v}^{gh} \\ &= A_v^h \sum_{g \in G} L_{vv'}^{\bar{h}\bar{g}cgh} T_{v_0v}^{gh} \\ &= A_v^h \sum_{gh \in G} L_{vv'}^{\bar{h}\bar{g}cgh} T_{v_0v}^{gh} \\ &= A_v^h \sum_{m \in G} L_{vv'}^{\bar{m}cm} T_{v_0v}^m, \end{aligned} \quad (\text{B23})$$

Thus, we have  $[A_v, L_M^c] = 0$ , where  $v \neq v_0, v'_0$ .

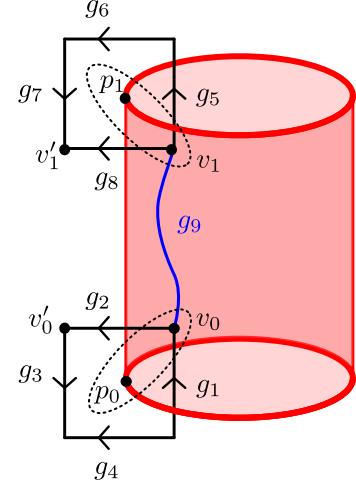


FIG. 22. Two sites  $s_0 = (v_0, p_0)$  and  $s_1 = (v_1, p_1)$  on the boundaries of  $M$ .  $v_0v_1$  denotes a string that starts and ends at  $v_0$  and  $v_1$ . The ordered product of elements along this string is labeled by  $g_9$ .

## 7. Proof of Eqs. (61), (62), (63) and (64)

First, we consider that when  $v_0v$  in Eq. (B22) is an edge, the  $L_M^c$  can be written as

$$L_M^c = \sum \cdots \left( \sum_{g_0} L_{vv'}^{\bar{g}_0cg_0} T_{v_0v}^{g_0} \right) L_{v_0v'_0}^c. \quad (\text{B24})$$

By using Eq. (39) and  $A_{v_0}^g L_{v_0v'_0}^c = L_{v_0v'_0}^{gc\bar{g}} A_{v_0}^g$ , we have

$$\begin{aligned} A_{v_0}^g L_M^c &= \sum \cdots \left( \sum_{g_0} L_{vv'}^{\bar{g}_0cg_0} A_{v_0}^g T_{v_0v}^{g_0} \right) L_{v_0v'_0}^c \\ &= \sum \cdots \left( \sum_{g_0} L_{vv'}^{\bar{g}_0cg_0} T_{v_0v}^{gg_0} \right) L_{v_0v'_0}^{gc\bar{g}} A_{v_0}^g \\ &= \left[ \sum \cdots \left( \sum_{gg_0} L_{vv'}^{\bar{g}_0\bar{g}gc\bar{g}gg_0} T_{v_0v}^{gg_0} \right) L_{v_0v'_0}^{gc\bar{g}} \right] A_{v_0}^g \\ &= L_M^{gc\bar{g}} A_{v_0}^g. \end{aligned} \quad (\text{B25})$$

As shown in Fig. 22, we consider a cylinder-like membrane  $M$  and construct the operator  $L_M^c$  as

$$L_M^c = \sum \left( \sum_{g_0} L_{v_1v'_1}^{\bar{g}_0cg_0} T_{v_0v_1}^{g_0} \right) \cdots L_{v_0v'_0}^c, \quad (\text{B26})$$

where the plaquette  $p_0$  ( $p_1$ ) and the vertex  $v_0$  ( $v_1$ ) form a site  $s_0$  ( $s_1$ ). Before we act the operator  $L_M^c$ , an arbitrary configuration on plaquettes  $p_0$  is labeled by  $|g_1, g_2, g_3, g_4\rangle$ , an arbitrary configuration on plaquettes  $p_1$  and the ordered product on the string with endpoints  $v_0$  and  $v_1$  are labeled by  $|g_5, g_6, g_7, g_8, g_9\rangle$ . Since  $L_M^c$  acts on  $|g_1, g_2, g_3, g_4\rangle$  as  $L_{v_0v'_0}^c$ , we consider acting  $B_{p_0, s_0}^h$  and

$L_M^c$  on  $|g_1, g_2, g_3, g_4\rangle$  as

$$\begin{aligned} B_{p_0, s_0}^h L_M^c |g_1, g_2, g_3, g_4\rangle &= B_{p_0, s_0}^h L_{v_0 v_0'}^c |g_1, g_2, g_3, g_4\rangle \\ &= B_{p_0, s_0}^h |cg_1, g_2, g_3, g_4\rangle \\ &= \delta_{h, cg_1 g_2 \bar{g}_3 g_4} |cg_1, g_2, g_3, g_4\rangle . \end{aligned} \quad (\text{B27})$$

Notice that

$$\begin{aligned} L_M^c B_{p_0, s_0}^{\bar{h}} |g_1, g_2, g_3, g_4\rangle &= L_M^c \delta_{\bar{h}, g_1 g_2 \bar{g}_3 g_4} |g_1, g_2, g_3, g_4\rangle \\ &= \delta_{\bar{h}, g_1 g_2 \bar{g}_3 g_4} L_{v_0 v_0'}^c |g_1, g_2, g_3, g_4\rangle \\ &= \delta_{\bar{h}, g_1 g_2 \bar{g}_3 g_4} |cg_1, g_2, g_3, g_4\rangle \\ &= \delta_{h, cg_1 g_2 \bar{g}_3 g_4} |cg_1, g_2, g_3, g_4\rangle , \end{aligned} \quad (\text{B28})$$

we conclude that

$$B_{p_0, s_0}^h L_M^c = L_M^c B_{p_0, s_0}^{\bar{h}} . \quad (\text{B29})$$

Now we consider acting  $B_{p_1, s_1}^h$  and  $L_M^c T_{v_0 v_1}^g$  on  $|g_5, g_6, g_7, g_8, g_9\rangle$ . Notice that  $L_M^c$  acts on  $|g_5, g_6, g_7, g_8, g_9\rangle$  as  $\sum_{g_0} L_{v_1 v_1'}^{\bar{g}_0 c g_0} T_{v_0 v_1}^g$ , we have

$$\begin{aligned} &B_{p_1, s_1}^h L_M^c T_{v_0 v_1}^g |g_5, g_6, g_7, g_8, g_9\rangle \\ &= B_{p_1, s_1}^h \sum_{g_0} L_{v_1 v_1'}^{\bar{g}_0 c g_0} T_{v_0 v_1}^g T_{v_0 v_1}^g |g_5, g_6, g_7, g_8, g_9\rangle \\ &= B_{p_1, s_1}^h \sum_{g_0} \delta_{g_0, g_9} \delta_{g_9, g} |g_5, g_6, g_7, \bar{g}_0 c g_0 g_8, g_0\rangle \\ &= \delta_{g_9, g} B_{p_1, s_1}^h |g_5, g_6, g_7, \bar{g}_9 c g_9 g_8, g_9\rangle \\ &= \delta_{g_9, g} \delta_{h, g_5 g_6 g_7 \bar{g}_9 c g_9 g_8} |g_5, g_6, g_7, \bar{g}_9 c g_9 g_8, g_9\rangle . \end{aligned} \quad (\text{B30})$$

Since

$$\begin{aligned} &L_M^c T_{v_0 v_1}^g B_{p_1, s_1}^{\bar{h} c g} |g_5, g_6, g_7, g_8, g_9\rangle \\ &= L_M^c \delta_{g_9, g} \delta_{h \bar{g} c g, g_5 g_6 g_7 \bar{g}_8} |g_5, g_6, g_7, g_8, g_9\rangle \\ &= \delta_{g_9, g} \delta_{h \bar{g} c g, g_5 g_6 g_7 \bar{g}_8} \sum_{g_0} L_{v_1 v_1'}^{\bar{g}_0 c g_0} T_{v_0 v_1}^g |g_5, g_6, g_7, g_8, g_9\rangle \\ &= \delta_{g_9, g} \delta_{h \bar{g} c g, g_5 g_6 g_7 \bar{g}_8} |g_5, g_6, g_7, \bar{g}_9 c g_9 g_8, g_9\rangle \\ &= \delta_{g_9, g} \delta_{h, g_5 g_6 g_7 \bar{g}_9 c g_9 g_8} |g_5, g_6, g_7, \bar{g}_9 c g_9 g_8, g_9\rangle , \end{aligned} \quad (\text{B31})$$

we conclude that

$$B_{p_1, s_1}^h L_M^c T_{v_0 v_1}^g = L_M^c T_{v_0 v_1}^g B_{p_1, s_1}^{\bar{h} c g} . \quad (\text{B32})$$

By using Eqs. (39) and (B25), we prove Eq. (61) as follows:

$$\begin{aligned} &A_{v_1}^g W_M (C, R; c, j; c', j') |GS\rangle \\ &= \sum_{h \in Z_r} \Gamma_{jj'}^R (h) A_{v_1}^g L_M^c T_P^{q_c h \bar{q}_{c'}} |GS\rangle \\ &= \sum_{h \in Z_r} \Gamma_{jj'}^R (h) L_M^{g \bar{c}} T_P^{g q_c h \bar{q}_{c'}} A_{v_1}^g |GS\rangle \\ &= \sum_{h \in Z_r} \Gamma_{jj'}^R (h) L_M^{g \bar{c}} T_P^{g q_c h \bar{q}_{c'}} |GS\rangle . \end{aligned} \quad (\text{B33})$$

We prove that for any  $g \in G$ ,  $\bar{q}_{gc \bar{g}} g q_c \in Z_r$  in Eq. (C10). Since  $h \in Z_r$ , we have  $\bar{q}_{gc \bar{g}} g q_c h \in Z_r$ . By writing  $T_P^{g q_c h \bar{q}_{c'}}$  as  $T_P^{q_{gc \bar{g}} \bar{q}_{gc \bar{g}} g q_c h \bar{q}_{c'}}$  and expanding  $\Gamma_{jj'}^R (h)$  as

$$\Gamma_{jj'}^R (h) = \sum_i \Gamma_{ji}^R (\bar{q}_{c \bar{g}} q_{gc \bar{g}}) \Gamma_{ij'}^R (\bar{q}_{gc \bar{g}} g q_c h) , \quad (\text{B34})$$

we have

$$\begin{aligned} &\sum_{h \in Z_r} \Gamma_{jj'}^R (h) L_M^{g \bar{c}} T_P^{g q_c h \bar{q}_{c'}} |GS\rangle \\ &= \sum_{h \in Z_r} \sum_i \Gamma_{ji}^R (\bar{q}_{c \bar{g}} q_{gc \bar{g}}) \Gamma_{ij'}^R (\bar{q}_{gc \bar{g}} g q_c h) \\ &\quad \times L_M^{g \bar{c}} T_P^{q_{gc \bar{g}} \bar{q}_{gc \bar{g}} g q_c h \bar{q}_{c'}} |GS\rangle \\ &= \sum_i \Gamma_{ji}^R (\bar{q}_{c \bar{g}} q_{gc \bar{g}}) \sum_{h' \in Z_r} \Gamma_{ij'}^R (h') L_M^{g \bar{c}} T_P^{q_{gc \bar{g}} h' \bar{q}_{c'}} |GS\rangle \\ &= \sum_i \Gamma_{ji}^R (\bar{q}_{c \bar{g}} q_{gc \bar{g}}) W_M (C, R; gc \bar{g}, i; c', j') |GS\rangle , \end{aligned} \quad (\text{B35})$$

where  $h'$  is defined as  $\bar{q}_{gc \bar{g}} g q_c h$ . Notice that  $\Gamma_{ji}^R (\bar{q}_{c \bar{g}} q_{gc \bar{g}}) = \Gamma_{ij}^R (\bar{q}_{gc \bar{g}} g q_c)$ , we obtain

$$\begin{aligned} &A_{v_1}^g W_M (C, R; c, j; c', j') |GS\rangle \\ &= \sum_i \Gamma_{ij}^R (\bar{q}_{gc \bar{g}} g q_c) W_M (C, R; gc \bar{g}, i; c', j') |GS\rangle . \end{aligned} \quad (\text{B36})$$

Now, by using Eq. (B29), we prove Eq. (62) as follows:

$$\begin{aligned} &B_{p_0, s_0}^h W_M (C, R; c, j; c', j') |GS\rangle \\ &= \sum_{g \in Z_r} \Gamma_{jj'}^R (g) B_{p_0, s_0}^h L_M^c T_P^{q_c g \bar{q}_{c'}} |GS\rangle \\ &= \sum_{g \in Z_r} \Gamma_{jj'}^R (g) L_M^c T_P^{q_c g \bar{q}_{c'}} B_{p_0, s_0}^{\bar{h}} |GS\rangle \\ &= \delta_{\bar{h}, e} \sum_{g \in Z_r} \Gamma_{jj'}^R (g) L_M^c T_P^{q_c g \bar{q}_{c'}} |GS\rangle \\ &= \delta_{c, h} W_M (C, R; c, j; c', j') |GS\rangle . \end{aligned} \quad (\text{B37})$$

Similarly, we use Eq. (40) to prove Eq. (63):

$$\begin{aligned} &A_{v_1}^g W_M (C, R; c, j; c', j') |GS\rangle \\ &= \sum_{h \in Z_r} \Gamma_{jj'}^R (h) A_{v_1}^g L_M^c T_P^{q_c h \bar{q}_{c'}} |GS\rangle \\ &= \sum_{h \in Z_r} \Gamma_{jj'}^R (h) L_M^c T_P^{q_c h \bar{q}_{c'}} A_{v_1}^g |GS\rangle \\ &= \sum_{h \in Z_r} \Gamma_{jj'}^R (h) L_M^c T_P^{q_c h \bar{q}_{c'}} \bar{g} |GS\rangle \\ &= \sum_{h \bar{q}_{c'} \bar{g} q_{gc' \bar{g}} \in Z_r} \sum_i \Gamma_{ji}^R (h \bar{q}_{c'} \bar{g} q_{gc' \bar{g}}) \Gamma_{ij'}^R (\bar{q}_{gc' \bar{g}} g q_{c'}) \\ &\quad \times L_M^c T_P^{q_c h \bar{q}_{c'}} \bar{g} q_{gc' \bar{g}} \bar{q}_{gc' \bar{g}} |GS\rangle \\ &= \sum_i \Gamma_{ij'}^R (\bar{q}_{gc' \bar{g}} g q_{c'}) W_M (C, R; c, j; gc' \bar{g}, i) |GS\rangle , \end{aligned} \quad (\text{B38})$$

As for Eq. (64), we use Eq. (B32) to obtain that

$$\begin{aligned}
& B_{p_1, s_1}^h W_M(C, R; c, j; c', j') |GS\rangle \\
&= \sum_{g \in Z_r} \Gamma_{jj'}^{R^*}(g) B_{p_1, s_1}^h L_M^c T_P^{q_c g \bar{q}_{c'}} |GS\rangle \\
&= \sum_{g \in Z_r} \Gamma_{jj'}^{R^*}(g) L_M^c T_P^{q_c g \bar{q}_{c'}} B_{p_1, s_1}^{h \bar{q}_c g \bar{q}_{c'}} |GS\rangle \\
&= \sum_{g \in Z_r} \Gamma_{jj'}^{R^*}(g) L_M^c T_P^{q_c g \bar{q}_{c'}} \delta_{h \bar{q}_c g \bar{q}_{c'}, e} |GS\rangle. \quad (B39)
\end{aligned}$$

Notice  $c = q_c r \bar{q}_c$  and  $g \in Z_r$ , we have

$$\begin{aligned}
\delta_{h q_{c'} \bar{g} \bar{q}_c c q_c g \bar{q}_{c'}, e} &= \delta_{h q_{c'} \bar{g} r g \bar{q}_{c'}, e} \\
&= \delta_{h q_{c'} r \bar{q}_{c'}, e} = \delta_{h c', e}. \quad (B40)
\end{aligned}$$

Thus, we conclude that

$$\begin{aligned}
& B_{p_1, s_1}^h W_M(C, R; c, j; c', j') |GS\rangle \\
&= \delta_{h, \bar{c}} W_M(C, R; c, j; c', j') |GS\rangle. \quad (B41)
\end{aligned}$$

### Appendix C: Irreducible Representations of Quantum Double

The quantum double  $DG$  of a finite group  $G$  is an algebra with two sets of generators  $\{A_g \mid g \in G\}$ ,  $\{B_h \mid h \in G\}$ , which satisfy:

$$\begin{aligned}
A_{g_1} A_{g_2} &= A_{g_1 g_2}, \\
B_{h_1} B_{h_2} &= \delta_{h_1, h_2} B_{h_2}, \\
A_g B_h &= B_{gh\bar{g}} A_g. \quad (C1)
\end{aligned}$$

A set of basis of  $DG$  is given by  $\{D_{(h, g)} = B_h A_g\}$ , which satisfies:

$$\begin{aligned}
D_{(h_1, g_1)} D_{(h_2, g_2)} &= B_{h_1} A_{g_1} B_{h_2} A_{g_2} = B_{h_1} B_{g_1 h_2 \bar{g}_1} A_{g_1} A_{g_2} \\
&= \delta_{h_1, g_1 h_2 \bar{g}_1} B_{h_1} A_{g_1 g_2} \\
&= \delta_{h_1, g_1 h_2 \bar{g}_1} D_{(h_1, g_1 g_2)}. \quad (C2)
\end{aligned}$$

The group  $G$  can be written as:

$$G = \bigcup_i C_i, \quad (C3)$$

where  $C_i$  is a conjugacy class. We can choose a representative  $r$  in the class and denote the class by  $C_r$ , then we have

$$r \in C_r = \{q_c r \bar{q}_c \mid q_c \in G\}. \quad (C4)$$

Any element  $c \in C_r$  can be written as  $q_c r \bar{q}_c$ ,  $q_c \in G$ . We choose a specific set of  $q_c$  and demand that  $q_r = e$  when  $c = r$ . The choices of  $q_c$  are not unique, if  $c = q_c r \bar{q}_c = q'_c r \bar{q}'_c$ , then

$$r = \bar{q}_c q'_c r \bar{q}'_c q_c = (\bar{q}_c q'_c) r \bar{q}_c q'_c, \quad (C5)$$

i.e.,

$$\bar{q}_c q'_c \in Z_r, \quad (C6)$$

where  $Z_r$  is the centralizer of  $r$ . We write  $\bar{q}_c q'_c = z \in Z_r$ , then

$$q'_c = q_c z \quad \text{for some } z \in Z_r. \quad (C7)$$

That is, for given  $c \in C_r$  and  $r$ , all  $q_c$  that satisfy  $c = q_c r \bar{q}_c$  form a coset of  $G$ :

$$\{q_c \mid q_c r \bar{q}_c = c \in C_r\} = q_c Z_r. \quad (C8)$$

Thus, we can rewrite the  $G$  as:

$$G = \bigcup_{c \in C_r} q_c Z_r, \quad (C9)$$

where  $r$  and  $q_c$  are preselected.

We prove that for any  $g \in G$ ,  $c \in C_r$ , we have  $\bar{q}_{gc\bar{g}} g q_c \in Z_r$ :

$$\begin{aligned}
(\bar{q}_{gc\bar{g}} g q_c) r (\bar{q}_{gc\bar{g}} g q_c) &= (\bar{q}_{gc\bar{g}} g q_c) r (\bar{q}_c \bar{g} q_{gc\bar{g}}) \\
&= \bar{q}_{gc\bar{g}} g c \bar{g} q_{gc\bar{g}} = r. \quad (C10)
\end{aligned}$$

In the last step, we use:

$$q_c r \bar{q}_c = c \implies r = \bar{q}_c c q_c, \quad \forall q_c \in G, \forall c \in C_r. \quad (C11)$$

Each irrep of  $DG$  is labeled by a pair  $(C, R)$ , where  $C$  is the conjugacy class,  $R$  is the irrep of the centralizer  $Z_r$ . The corresponding representation space is given by  $V^{(C, R)} = \mathbb{C}[C] \otimes V^R$ , where  $\mathbb{C}[C]$  is an algebra with the basis  $\{c \in C\}$  and  $V^R$  is the representation space of the irrep  $R$ . A set of basis of  $V^{(C, R)}$  is given by

$$\{|c\rangle \otimes |j\rangle \mid c \in C, j = 1, \dots, \dim(R)\}. \quad (C12)$$

Denote the irrep of  $DG$  as  $\Pi^{(C, R)}$ , then the action of  $DG$  on  $V^{(C, R)}$  is given by

$$\Pi^{(C, R)}(B_h)(|c\rangle \otimes |j\rangle) = \delta_{h, c} |c\rangle \otimes |j\rangle, \quad (C13)$$

$$\begin{aligned}
\Pi^{(C, R)}(A_g)(|c\rangle \otimes |j\rangle) &= |gc\bar{g}\rangle \otimes R(\bar{q}_{gc\bar{g}} g q_c) |j\rangle \\
&= |gc\bar{g}\rangle \otimes \left[ \sum_i \Gamma_{ij}^R (\bar{q}_{gc\bar{g}} g q_c) |i\rangle \right] \\
&= \sum_i \Gamma_{ij}^R (\bar{q}_{gc\bar{g}} g q_c) |gc\bar{g}\rangle \otimes |i\rangle. \quad (C14)
\end{aligned}$$

Obviously we have

$$\Pi^{(C, R)}(B_{h_1}) \Pi^{(C, R)}(B_{h_2}) = \delta_{h_1, h_2} \Pi^{(C, R)}(B_{h_2}), \quad (C15)$$

$$\Pi^{(C, R)}(A_g) \Pi^{(C, R)}(B_h) = \Pi^{(C, R)}(B_{gh\bar{g}}) \Pi^{(C, R)}(A_g), \quad (C16)$$

Then we verify that  $\Pi^{(C,R)}(A_{g_1})\Pi^{(C,R)}(A_{g_2}) = \Pi^{(C,R)}(A_{g_1g_2})$ : define

$$\begin{aligned}
& \Pi^{(C,R)}(A_{g_1})\Pi^{(C,R)}(A_{g_2})|c\rangle\otimes|j\rangle \\
&= \Pi^{(C,R)}(A_{g_1})\left[\sum_i\Gamma_{ij}^R(\bar{q}_{g_2c\bar{g}_2}g_2q_c)|g_2c\bar{g}_2\rangle\otimes|i\rangle\right] \\
&= \sum_i\Gamma_{ij}^R(\bar{q}_{g_2c\bar{g}_2}g_2q_c)\sum_k\Gamma_{ki}^R(\bar{q}_{g_1g_2c\bar{g}_2\bar{g}_1}g_1q_{g_2c\bar{g}_2}) \\
&\quad \times|g_1g_2c\bar{g}_2\bar{g}_1\rangle\otimes|k\rangle \\
&= \sum_{i,k}\Gamma_{ki}^R(\bar{q}_{g_1g_2c\bar{g}_2\bar{g}_1}g_1q_{g_2c\bar{g}_2})\Gamma_{ij}^R(\bar{q}_{g_2c\bar{g}_2}g_2q_c) \\
&\quad \times|g_1g_2c\bar{g}_2\bar{g}_1\rangle\otimes|k\rangle \\
&= \sum_k\Gamma_{kj}^R(\bar{q}_{g_1g_2c\bar{g}_2\bar{g}_1}g_1q_{g_2c\bar{g}_2})|g_1g_2c\bar{g}_2\bar{g}_1\rangle\otimes|k\rangle \\
&= \Pi^{(C,R)}(A_{g_1g_2})|c\rangle\otimes|j\rangle. \tag{C17}
\end{aligned}$$

Given two irreps and their corresponding representation spaces  $(\Pi^{(C_1,R_1)}, V^{(C_1,R_1)})$  and  $(\Pi^{(C_2,R_2)}, V^{(C_2,R_2)})$ , the tensor product representation and the corresponding representation space  $(\Pi^{(C_1,R_1)}\otimes\Pi^{(C_2,R_2)}, V^{(C_1,R_1)}\otimes V^{(C_2,R_2)})$  is constructed by means of the co-multiplication  $\Delta$ . Explicitly, we

$$\Delta(D_{(h,g)}) = \sum_{k\in G} D_{(h\bar{k},g)} \otimes D_{(k,g)}. \tag{C18}$$

Then for  $v \in V^{(C_1,R_1)}$  and  $w \in V^{(C_2,R_2)}$ , the action on  $v \otimes w$  is given by

$$\begin{aligned}
& \Pi^{(C_1,R_1)} \otimes \Pi^{(C_2,R_2)} (\Delta(D_{(h,g)})) v \otimes w \\
&= \sum_{k\in G} \Pi^{(C_1,R_1)}(D_{(h\bar{k},g)}) v \otimes \Pi^{(C_2,R_2)}(D_{(k,g)}) w. \tag{C19}
\end{aligned}$$

The tensor product representation is generally reducible and can be decomposed as

$$\Pi^{(C_1,R_1)} \otimes \Pi^{(C_2,R_2)} = \bigoplus_{(C_3,R_3)} N_{(C_3,R_3)}^{(C_1,R_1)(C_2,R_2)} \Pi^{(C_3,R_3)}, \tag{C20}$$

where the coefficient is given by

$$\begin{aligned}
& N_{(C_3,R_3)}^{(C_1,R_1)(C_2,R_2)} \\
&= \frac{1}{|G|} \sum_{h,g} \text{tr} \left[ \Pi^{(C_1,R_1)} \otimes \Pi^{(C_2,R_2)} (\Delta(D_{(h,g)})) \right] \\
&\quad \times \left\{ \text{tr} \left[ \Pi^{(C_3,R_3)}(D_{(h,g)}) \right] \right\}^*. \tag{C21}
\end{aligned}$$

---

[1] B. Zeng, X. Chen, D.-L. Zhou, and X.-G. Wen, Quantum information meets quantum matter – from quantum entanglement to topological phase in many-body systems (2018), [arXiv:1508.02595 \[cond-mat.str-el\]](#).

[2] A. Kitaev, Fault-tolerant quantum computation by anyons, *Annals of Physics* **303**, 2 (2003).

[3] S. Bravyi and A. Kitaev, Universal quantum computation with ideal clifford gates and noisy ancillas, *Phys. Rev. A* **71**, 022316 (2005).

[4] D. Horsman, A. G. Fowler, S. Devitt, and R. V. Meter, Surface code quantum computing by lattice surgery, *New Journal of Physics* **14**, 123011 (2012).

[5] C. Chamberland and E. T. Campbell, Universal quantum computing with twist-free and temporally encoded lattice surgery, *PRX Quantum* **3**, 010331 (2022).

[6] M. Barkeshli, C.-M. Jian, and X.-L. Qi, Twist defects and projective non-abelian braiding statistics, *Phys. Rev. B* **87**, 045130 (2013).

[7] M. S. Kesselring, F. Pastawski, J. Eisert, and B. J. Brown, The boundaries and twist defects of the color code and their applications to topological quantum computation, *Quantum* **2**, 101 (2018).

[8] M. A. Levin and X.-G. Wen, String-net condensation: A physical mechanism for topological phases, *Phys. Rev. B* **71**, 045110 (2005).

[9] E. Witten, Quantum field theory and the jones polynomial, *Commun. Math. Phys.* **121**, 351 (1989).

[10] V. G. Turaev, *Quantum Invariants of Knots and 3-Manifolds* (De Gruyter, Berlin, Boston, 2016).

[11] B. Blok and X. G. Wen, Effective theories of the fractional quantum hall effect at generic filling fractions, *Phys. Rev. B* **42**, 8133 (1990).

[12] C. Nayak, S. H. Simon, A. Stern, M. Freedman, and S. Das Sarma, Non-abelian anyons and topological quantum computation, *Rev. Mod. Phys.* **80**, 1083 (2008).

[13] X.-G. Wen, *Quantum field theory of many-body systems: from the origin of sound to an origin of light and electrons* (Oxford University Press, 2004).

[14] A. Kitaev, Anyons in an exactly solved model and beyond, *Annals of Physics* **321**, 2 (2006), january Special Issue.

[15] H. Bombin and M. A. Martin-Delgado, Family of non-abelian kitaev models on a lattice: Topological condensation and confinement, *Phys. Rev. B* **78**, 115421 (2008).

[16] M. Koch-Janusz, M. Levin, and A. Stern, Exactly soluble lattice models for non-abelian states of matter in two dimensions, *Phys. Rev. B* **88**, 115133 (2013).

[17] J. M. Leinaas and J. Myrheim, On the theory of identical particles, *Il Nuovo Cimento B (1971-1996)* **37**, 1 (1977).

[18] P. Ye, T. L. Hughes, J. Maciejko, and E. Fradkin, Composite particle theory of three-dimensional gapped fermionic phases: Fractional topological insulators and charge-loop excitation symmetry, *Phys. Rev. B* **94**,

115104 (2016).

[19] B. Moy, H. Goldman, R. Sohal, and E. Fradkin, Theory of oblique topological insulators, *SciPost Phys.* **14**, 023 (2023).

[20] P. Ye and X.-G. Wen, Constructing symmetric topological phases of bosons in three dimensions via fermionic projective construction and dyon condensation, *Phys. Rev. B* **89**, 045127 (2014).

[21] P. Putrov, J. Wang, and S.-T. Yau, Braiding statistics and link invariants of bosonic/fermionic topological quantum matter in 2+1 and 3+1 dimensions, *Annals of Physics* **384**, 254 (2017).

[22] Q.-R. Wang, M. Cheng, C. Wang, and Z.-C. Gu, Topological quantum field theory for abelian topological phases and loop braiding statistics in (3+1)-dimensions, *Phys. Rev. B* **99**, 235137 (2019).

[23] P. Ye and Z.-C. Gu, Topological quantum field theory of three-dimensional bosonic abelian-symmetry-protected topological phases, *Phys. Rev. B* **93**, 205157 (2016).

[24] X. Wen, H. He, A. Tiwari, Y. Zheng, and P. Ye, Entanglement entropy for (3+1)-dimensional topological order with excitations, *Phys. Rev. B* **97**, 085147 (2018).

[25] A. P. O. Chan, P. Ye, and S. Ryu, Braiding with borromean rings in (3+1)-dimensional spacetime, *Phys. Rev. Lett.* **121**, 061601 (2018).

[26] Z.-F. Zhang and P. Ye, Compatible braidings with hopf links, multiloop, and borromean rings in (3+1)-dimensional spacetime, *Phys. Rev. Res.* **3**, 023132 (2021).

[27] P. Ye and Z.-C. Gu, Vortex-line condensation in three dimensions: A physical mechanism for bosonic topological insulators, *Phys. Rev. X* **5**, 021029 (2015).

[28] P. Ye and J. Wang, Symmetry-protected topological phases with charge and spin symmetries: Response theory and dynamical gauge theory in two and three dimensions, *Phys. Rev. B* **88**, 235109 (2013).

[29] M. G. Alford and F. Wilczek, Aharonov-bohm interaction of cosmic strings with matter, *Phys. Rev. Lett.* **62**, 1071 (1989).

[30] L. M. Krauss and F. Wilczek, Discrete gauge symmetry in continuum theories, *Phys. Rev. Lett.* **62**, 1221 (1989).

[31] T. Hansson, V. Oganesyan, and S. Sondhi, Superconductors are topologically ordered, *Annals of Physics* **313**, 497 (2004).

[32] M. G. Alford, Kai-Ming Lee, J. March-Russell, and J. Preskill, Quantum field theory of non-abelian strings and vortices, *Nuclear Physics B* **384**, 251 (1992).

[33] J. Preskill and L. M. Krauss, Local discrete symmetry and quantum-mechanical hair, *Nuclear Physics B* **341**, 50 (1990).

[34] C. Wang and M. Levin, Braiding statistics of loop excitations in three dimensions, *Phys. Rev. Lett.* **113**, 080403 (2014).

[35] J. C. Wang, Z.-C. Gu, and X.-G. Wen, Field-theory representation of gauge-gravity symmetry-protected topological invariants, group cohomology, and beyond, *Phys. Rev. Lett.* **114**, 031601 (2015).

[36] J. C. Wang and X.-G. Wen, Non-abelian string and particle braiding in topological order: Modular  $SL(3, \mathbb{Z})$  representation and (3+1)-dimensional twisted gauge theory, *Phys. Rev. B* **91**, 035134 (2015).

[37] C.-M. Jian and X.-L. Qi, Layer construction of 3d topological states and string braiding statistics, *Phys. Rev. X* **4**, 041043 (2014).

[38] S. Jiang, A. Mesaros, and Y. Ran, Generalized modular transformations in (3+1)D topologically ordered phases and triple linking invariant of loop braiding, *Phys. Rev. X* **4**, 031048 (2014).

[39] C. Wang, C.-H. Lin, and M. Levin, Bulk-boundary correspondence for three-dimensional symmetry-protected topological phases, *Phys. Rev. X* **6**, 021015 (2016).

[40] A. Tiwari, X. Chen, and S. Ryu, Wilson operator algebras and ground states of coupled  $BF$  theories, *Phys. Rev. B* **95**, 245124 (2017).

[41] A. Kapustin and R. Thorngren, *Anomalies of discrete symmetries in various dimensions and group cohomology* (2014), arXiv:1404.3230 [hep-th].

[42] X. Chen, A. Tiwari, and S. Ryu, Bulk-boundary correspondence in (3+1)-dimensional topological phases, *Phys. Rev. B* **94**, 045113 (2016).

[43] A. Kapustin and N. Seiberg, Coupling a QFT to a TQFT and Duality, *JHEP* **04**, 001, arXiv:1401.0740 [hep-th].

[44] Z.-F. Zhang, Q.-R. Wang, and P. Ye, Continuum field theory of three-dimensional topological orders with emergent fermions and braiding statistics, *Phys. Rev. Res.* **5**, 043111 (2023).

[45] X.-L. Qi and S.-C. Zhang, Topological insulators and superconductors, *Rev. Mod. Phys.* **83**, 1057 (2011).

[46] M. F. Lapa, C.-M. Jian, P. Ye, and T. L. Hughes, Topological electromagnetic responses of bosonic quantum hall, topological insulator, and chiral semimetal phases in all dimensions, *Phys. Rev. B* **95**, 035149 (2017).

[47] P. Ye, M. Cheng, and E. Fradkin, Fractional  $s$ -duality, classification of fractional topological insulators, and surface topological order, *Phys. Rev. B* **96**, 085125 (2017).

[48] E. Witten, Fermion path integrals and topological phases, *Rev. Mod. Phys.* **88**, 035001 (2016).

[49] B. Han, H. Wang, and P. Ye, Generalized wen-zee terms, *Phys. Rev. B* **99**, 205120 (2019).

[50] S.-Q. Ning, Z.-X. Liu, and P. Ye, Fractionalizing global symmetry on looplike topological excitations, *Phys. Rev. B* **105**, 205137 (2022).

[51] S.-Q. Ning, Z.-X. Liu, and P. Ye, Symmetry enrichment in three-dimensional topological phases, *Phys. Rev. B* **94**, 245120 (2016).

[52] P. Ye, Three-dimensional anomalous twisted gauge theories with global symmetry: Implications for quantum spin liquids, *Phys. Rev. B* **97**, 125127 (2018).

[53] Z.-F. Zhang, Q.-R. Wang, and P. Ye, Non-abelian fusion, shrinking, and quantum dimensions of abelian gauge fluxes, *Phys. Rev. B* **107**, 165117 (2023).

[54] Z.-F. Zhang and P. Ye, Topological orders, braiding statistics, and mixture of two types of twisted BF theories in five dimensions, *JHEP* **04**, 138, arXiv:2104.07067 [hep-th].

[55] Y. Huang, Z.-F. Zhang, and P. Ye, Fusion rules and shrinking rules of topological orders in five dimensions, *JHEP* **11**, 210, arXiv:2306.14611 [hep-th].

[56] Y. Huang, Z.-F. Zhang, and P. Ye, Diagrammatics, pentagon equations, and hexagon equations of topological orders with loop- and membrane-like excitations, *JHEP* **2025** (6), 238, arXiv:2405.19077 [hep-th].

[57] L. Kong, T. Lan, X.-G. Wen, Z.-H. Zhang, and H. Zheng, Classification of topological phases with finite internal symmetries in all dimensions, *Journal of High Energy Physics* **2020**, 93 (2020).

[58] L. Kong and H. Zheng, Categories of quantum liquids i, *Journal of High Energy Physics* **2022**, 70 (2022).

[59] L. Kong and H. Zheng, Categories of quantum liquids ii, *Communications in Mathematical Physics* **405**, 203 (2024).

[60] C. Delcamp and A. Tiwari, From gauge to higher gauge models of topological phases, *Journal of High Energy Physics* **2018**, 1 (2018).

[61] C. Delcamp and A. Tiwari, On 2-form gauge models of topological phases, *Journal of High Energy Physics* **2019**, 1 (2019).

[62] Y. Wan, J. C. Wang, and H. He, Twisted gauge theory model of topological phases in three dimensions, *Phys. Rev. B* **92**, 045101 (2015).

[63] J. Huxford, D. X. Nguyen, and Y. B. Kim, Twisted lattice gauge theory: Membrane operators, three-loop braiding, and topological charge, *Phys. Rev. B* **110**, 035117 (2024).

[64] P. Ye, C.-S. Tian, X.-L. Qi, and Z.-Y. Weng, Confinement-deconfinement interplay in quantum phases of doped mott insulators, *Phys. Rev. Lett.* **106**, 147002 (2011).

[65] P. Ye and Q.-R. Wang, Monopoles, confinement and charge localization in the t-j model with dilute holes, *Nuclear Physics B* **874**, 386 (2013).

[66] Y. Ma, P. Ye, and Z.-Y. Weng, Low-temperature pseudogap phenomenon: precursor of high-*Tc* superconductivity, *New Journal of Physics* **16**, 083039 (2014).

[67] J.-W. Mei, Possible fermi liquid in the lightly doped kitaev spin liquid, *Phys. Rev. Lett.* **108**, 227207 (2012).

[68] X.-Y. Song, A. Vishwanath, and Y.-H. Zhang, Doping the chiral spin liquid: Topological superconductor or chiral metal, *Phys. Rev. B* **103**, 165138 (2021).

[69] Z.-T. Xu, Z.-C. Gu, and S. Yang, Global phase diagram of doped quantum spin liquid on the Kagome lattice, *arXiv e-prints*, arXiv:2404.05685 (2024), arXiv:2404.05685 [cond-mat.str-el].

[70] G.-Y. Zhu, J.-Y. Chen, P. Ye, and S. Trebst, Topological fracton quantum phase transitions by tuning exact tensor network states, *Phys. Rev. Lett.* **130**, 216704 (2023).

[71] C. Zhou, M.-Y. Li, Z. Yan, P. Ye, and Z. Y. Meng, Detecting subsystem symmetry protected topological order through strange correlators, *Phys. Rev. B* **106**, 214428 (2022).

[72] C. Zhou, M.-Y. Li, Z. Yan, P. Ye, and Z. Y. Meng, Evolution of dynamical signature in the x-cube fracton topological order, *Phys. Rev. Res.* **4**, 033111 (2022).

[73] X.-G. Wen, Mean-field theory of spin-liquid states with finite energy gap and topological orders, *Phys. Rev. B* **44**, 2664 (1991).

[74] P. Ye and X.-G. Wen, Projective construction of two-dimensional symmetry-protected topological phases with  $u(1)$ ,  $so(3)$ , or  $su(2)$  symmetries, *Phys. Rev. B* **87**, 195128 (2013).

[75] Y.-M. Lu and D.-H. Lee, Spin quantum hall effects in featureless nonfractionalized spin-1 magnets, *Phys. Rev. B* **89**, 184417 (2014).

[76] C. Wang, A. Nahum, and T. Senthil, Topological paramagnetism in frustrated spin-1 mott insulators, *Phys. Rev. B* **91**, 195131 (2015).

[77] M. Barkeshli and X.-G. Wen,  $u(1) \times u(1) \rtimes Z_2$  chern-simons theory and  $Z_4$  parafermion fractional quantum hall states, *Phys. Rev. B* **81**, 045323 (2010).

[78] D. Gaiotto, A. Kapustin, N. Seiberg, and B. Willett, Generalized global symmetries, *Journal of High Energy Physics* **2015**, 172 (2015).

[79] X.-G. Wen, Emergent anomalous higher symmetries from topological order and from dynamical electromagnetic field in condensed matter systems, *Phys. Rev. B* **99**, 205139 (2019).

[80] J. McGreevy, Generalized symmetries in condensed matter, *Annual Review of Condensed Matter Physics* **14**, 57 (2023).

[81] C. Cordova, T. T. Dumitrescu, K. Intriligator, and S.-H. Shao, Snowmass white paper: Generalized symmetries in quantum field theory and beyond, arXiv:2205.09545.

[82] S. Schafer-Nameki, ICTP lectures on (non-)invertible generalized symmetries, arXiv:2305.18296.

[83] L. Bhardwaj, L. E. Bottini, L. Fraser-Taliente, L. Gladden, D. S. W. Gould, A. Platschchorre, and H. Tillim, Lectures on generalized symmetries, arXiv:2307.07547.

[84] R. Luo, Q.-R. Wang, and Y.-N. Wang, Lecture notes on generalized symmetries and applications, *Physics Reports* **1065**, 1 (2024).

[85] Z.-F. Zhang, Y. Huang, Q.-R. Wang, and P. Ye, to appear.

[86] Y. Feng, Y.-A. Chen, P.-S. Hsin, and R. Kobayashi, Onsiteability of higher-form symmetries, (2025), arXiv:2510.23701.

[87] Y. Feng, R. Kobayashi, Y.-A. Chen, and S. Ryu, Higher-form anomalies on lattices, (2025), arXiv:2509.12304.

[88] S.-T. Zhou, M. Cheng, T. Rakovszky, C. von Keyserlingk, and T. D. Ellison, Finite-temperature quantum topological order in three dimensions, *Phys. Rev. Lett.* **135**, 040402 (2025).

[89] M. Iqbal, N. Tantivasadakarn, R. Verresen, S. L. Campbell, J. M. Dreiling, C. Figgatt, J. P. Gaebler, J. Johansen, M. Mills, S. A. Moses, J. M. Pino, A. Ransford, M. Rowe, P. Siegfried, R. P. Stutz, M. Foss-Feig, A. Vishwanath, and H. Dreyer, Non-abelian topological order and anyons on a trapped-ion processor, *Nature* **626**, 505 (2024), arXiv:2305.03766 [quant-ph].

[90] S. Xu, Z.-Z. Sun, K. Wang, H. Li, Z. Zhu, H. Dong, J. Deng, X. Zhang, J. Chen, Y. Wu, C. Zhang, F. Jin, X. Zhu, Y. Gao, A. Zhang, N. Wang, Y. Zou, Z. Tan, F. Shen, J. Zhong, Z. Bao, W. Li, W. Jiang, L.-W. Yu, Z. Song, P. Zhang, L. Xiang, Q. Guo, Z. Wang, C. Song, H. Wang, and D.-L. Deng, Non-abelian braiding of fibonacci anyons with a superconducting processor, *Nature Physics* **20**, 1469 (2024), arXiv:2404.00091 [quant-ph].

[91] Google Quantum AI and Collaborators, Non-abelian braiding of graph vertices in a superconducting processor, *Nature* **618**, 264 (2023), arXiv:2210.10255 [quant-ph].

[92] C. Schön, E. Solano, F. Verstraete, J. I. Cirac, and M. M. Wolf, Sequential generation of entangled multiqubit states, *Phys. Rev. Lett.* **95**, 110503 (2005).

[93] C. Schön, K. Hammerer, M. M. Wolf, J. I. Cirac, and E. Solano, Sequential generation of matrix-product states in cavity qed, *Phys. Rev. A* **75**, 032311 (2007).

[94] M. C. Bañuls, D. Pérez-García, M. M. Wolf, F. Verstraete, and J. I. Cirac, Sequentially generated states for the study of two-dimensional systems, *Phys. Rev. A* **77**, 052306 (2008).

[95] Y.-J. Liu, K. Shtengel, A. Smith, and F. Pollmann, Methods for simulating string-net states and anyons on a digital quantum computer, *PRX Quantum* **3**, 040315

(2022).

[96] Z.-Y. Wei, D. Malz, and J. I. Cirac, Sequential generation of projected entangled-pair states, *Phys. Rev. Lett.* **128**, 010607 (2022).

[97] S.-H. Lin, R. Dilip, A. G. Green, A. Smith, and F. Pollmann, Real- and imaginary-time evolution with compressed quantum circuits, *PRX Quantum* **2**, 010342 (2021).

[98] X. Chen, A. Dua, M. Hermele, D. T. Stephen, N. Tantivasadakarn, R. Vanhove, and J.-Y. Zhao, Sequential quantum circuits as maps between gapped phases, *Phys. Rev. B* **109**, 075116 (2024).

[99] Y.-T. Hu, M.-Y. Li, and P. Ye, Preparing code states via seed-entangler-enriched sequential quantum circuits: Application to tetradigit topological error-correcting codes, *Phys. Rev. B* **112**, 165139 (2025).

[100] A. Lyons, C. F. B. Lo, N. Tantivasadakarn, A. Vishwanath, and R. Verresen, Protocols for creating anyons and defects via gauging, *Phys. Rev. Lett.* **135**, 200405 (2025).

[101] C. F. B. Lo, A. Lyons, R. Verresen, A. Vishwanath, and N. Tantivasadakarn, *Universal quantum computation with the  $s_3$  quantum double: A pedagogical exposition* (2025), arXiv:2502.14974 [quant-ph].

[102] J.-Y. Zhang and P. Ye, Programmable anyon mobility through higher order cellular automata (2025), arXiv:2508.13961 [quant-ph].

[103] J.-Y. Zhang, M.-Y. Li, and P. Ye, Higher-order cellular automata generated symmetry-protected topological phases and detection through multi point strange correlators, *PRX Quantum* **5**, 030342 (2024).